NASA TECHNICAL MEMORANDUM

NASA TM X-3036

LOW-SPEED AERODYNAMIC CHARACTERISTICS OF A 42° SWEPT HIGH-WING MODEL HAVING A DOUBLE-SLOTTED FLAP SYSTEM AND A SUPERCRITICAL AIRFOIL

by Paul G. Fournier and Kenneth P. Gouatoo

Langley Research Center

Hampton, Va. 23665

NATIONAL AERONAUTICS AND SPACE ADMINISTRATION • WASHINGTON, D. C. • AUGUST 1982

[redacted]

1 Report No	2 Government Accession No	3 Recipient's Catalog No
NASA TM X-3036		

4 Title and Subtitle	5 Report Date
LOW-SPEED AERODYNAMIC CHARACTERISTICS OF A 42° SWEPT HIGH-WING MODEL HAVING A DOUBLE-SLOTTED FLAP SYSTEM AND A SUPERCRITICAL AIRFOIL [redacted]	August 1974
	6 Performing Organization Code
7 Author(s)	8. Performing Organization Report No
Paul G. Fournier and Kenneth W. Goodson	L-9233
	10 Work Unit No
9 Performing Organization Name and Address	760-64-60-04
NASA Langley Research Center Hampton, Va. 23665	11 Contract or Grant No
	13 Type of Report and Period Covered
12 Sponsoring Agency Name and Address	Technical Memorandum
National Aeronautics and Space Administration Washington, D.C. 20546	14 Sponsoring Agency Code

15 Supplementary Notes

16 Abstract

A low-speed investigation was conducted over an angle-of-attack range from about -4° to 20° in the Langley V/STOL tunnel to determine the effects of a double-slotted flap, high-lift system on the aerodynamic characteristics of a 42° swept high-wing model having a supercritical airfoil. The wing had an aspect ratio of 6.78 and a taper ratio of 0.36; the double-slotted flap consisted of a 35-percent-chord flap with a 15-percent-chord vane. The model was tested with a 15-percent-chord leading-edge slat.

17 Key Words (Suggested by Author(s))	18 Distribution Statement
High-lift flap system Supercritical wing Low-speed aerodynamic characteristics Swept wing	[redacted] – Available to U.S. Government Agencies and Their Contractors Only [redacted] Category 01

19 Security Classif (of this report)	20 Security Classif (of this page)	21. No of Pages	22 Price
[redacted]	Unclassified	105	

[redacted]

[redacted] CLASSIFIED BY [redacted] Classification Officer [redacted] LaRC SUBJECT TO GENERAL [redacted] CLASSIFICATION SCHEDULE OF EXECUTIVE ORDER 11652 AUTOMATICALLY DOWNGRADED AT [redacted] YEAR INTERVALS AND DECLASSIFIED ON DEC 31 1980

[redacted]

[redacted]

LOW-SPEED AERODYNAMIC CHARACTERISTICS OF A 42° SWEPT HIGH-WING MODEL HAVING A DOUBLE-SLOTTED FLAP SYSTEM AND A SUPERCRITICAL AIRFOIL*

By Paul G. Fournier and Kenneth W. Goodson
Langley Research Center

SUMMARY

A low-speed investigation was conducted over an angle-of-attack range from about -4° to 20° in the Langley V/STOL tunnel to determine the effects of a double-slotted flap, high-lift system on the aerodynamic characteristics of a 42° swept high-wing model having a supercritical airfoil. The wing had an aspect ratio of 6.78 and a taper ratio of 0.36; the double-slotted flap consisted of a 35-percent-chord flap with a 15-percent-chord vane. The model was tested with a 15-percent-chord leading-edge slat.

The results showed that a leading-edge slat delayed flow separation on both the plain and flapped wing at any flap deflection. The optimum slat deflection was about 50°. A maximum lift coefficient of 2.39 was obtained with the partial-span flap deflected 40° and with the leading-edge slat deflected 50°. Change in airfoil shape of the leading-edge slat as well as extension of the chord of the tip slat had no beneficial effect on maximum lift or stability characteristics. The complete model was longitudinally stable for all conditions (flaps off or deflected) up to angles of attack of about 12°. However, at higher angles of attack (for some flap deflections), there was a considerable loss in stability with a tendency to pitch-up. Differential flap deflection was not effective as a method of roll control and, in some cases, had an adverse effect. The addition of a 75° deflected partial-span spoiler on the right-wing upper surface was an effective lateral control device with a maximum incremental rolling-moment coefficient of 0.116 with flaps deflected 50°. The complete model was directionally stable (at small sideslip angles) throughout most of the angle-of-attack range. There was a large loss in directional stability for all model configurations for angles of attack above 16°, and the data trends indicate that directional instability would be expected for angles of attack somewhat above 20°.

*Title, Unclassified.

INTRODUCTION

Extensive research effort by NASA to improve the performance of subsonic aircraft has shown that the drag rise can be delayed to Mach numbers approaching unity by the use of supercritical airfoil sections. (See ref. 1.) Research has also been conducted at low speeds to develop high-lift systems for supercritical airfoils so that these configurations could land and take off at reasonable speeds and runway lengths. Some work has been reported in reference 2 on a rectangular wing with a slotted supercritical airfoil having several high-lift devices, and in references 3 to 5, for more recent adaptations of the supercritical airfoil.

The present investigation was conducted in the Langley V/STOL tunnel to provide high-lift data applicable to configurations similar to the F-8 supercritical-wing airplane. The model used was a general research model that was modified to simulate the F-8 supercritical-wing airplane configuration by the addition of a large glove over the inboard part of the wing and a dummy engine inlet attached to the underside of the fuselage at the nose. The present model had a wing with 42° sweep of the quarter-chord line, an aspect ratio of 6.78, and supercritical airfoil sections. The high-lift system consisted of a double-slotted flap which could be tested as a partial- or full-span flap and a leading-edge slat which extended from the outboard edge of the glove (32-percent wing semispan station) to the wing tip. Pressures were measured on the basic wing and on each segment of the high-lift system at the mean-aerodynamic-chord station of the basic wing.

SYMBOLS

The static longitudinal and lateral stability data are presented about the stability-axis system. The positive direction of forces, moments, and angles are indicated in figure 1. The model reference point was located longitudinally at the quarter chord of the wing mean aerodynamic chord (theoretical wing) and on the fuselage center line.

Measurements of this investigation are presented in the International System of Units (SI). Details concerning the use of the SI units, together with physical constants and conversion factors, are presented in reference 6.

b wing span, cm

C_D drag coefficient, $\frac{\text{Drag}}{qS}$

C_L lift coefficient, $\frac{\text{Lift}}{qS}$

$C_{L,max}$	maximum lift coefficient
C_l	rolling-moment coefficient, $\frac{\text{Rolling moment}}{qSb}$
ΔC_l	incremental rolling-moment coefficient
C_{l_β}	effective-dihedral parameter, $\frac{\Delta C_l}{\Delta \beta}$, per deg ($\pm 5^o$ β)
C_m	pitching-moment coefficient, $\frac{\text{Pitching moment}}{qS\bar{c}}$
C_n	yawing-moment coefficient, $\frac{\text{Yawing moment}}{qSb}$
ΔC_n	incremental yawing-moment coefficient
C_{n_β}	directional stability parameter, $\frac{\Delta C_n}{\Delta \beta}$, per deg ($\pm 5^o$ β)
C_Y	side-force coefficient, $\frac{\text{Side force}}{qS}$
ΔC_Y	incremental side-force coefficient
C_{Y_β}	side-force parameter, $\frac{\Delta C_Y}{\Delta \beta}$, per deg ($\pm 5^o$ β)
C_p	pressure coefficient, $\frac{p_l - p_\infty}{q}$
c	wing chord, cm
c_f	chord of flap, cm
c_r	wing root chord, cm
c_s	chord of leading-edge slat, cm
c_t	wing tip chord, cm
c_{th}	theoretical wing chord, cm
c_v	chord of vane, cm

c_{w_1} part (0.775c) of basic wing ahead of flap vane, cm

$\bar{c}$ mean aerodynamic chord of theoretical wing, cm

$\bar{c}_H$ mean aerodynamic chord of horizontal tail, cm

$\bar{c}_V$ mean aerodynamic chord of vertical tail, cm

i_t incidence of horizontal tail, positive trailing edge down (see fig. 1), deg

l_t tail length (distance from moment reference ($\bar{c}/4$) to $\bar{c}_{H/4}$), cm

p_l local static pressure, N/m^2

p_∞ free-stream static pressure, N/m^2

q free-stream dynamic pressure, N/m^2

R Reynolds number based on $\bar{c}$

r_{le} leading-edge radius of wing airfoil section, cm

S wing area (based on theoretical planform, glove not included), m^2

t_{max} maximum thickness of airfoil section, cm

t_{te} airfoil trailing-edge thickness, cm

x distance along chord of selected wing, slat, or flap-vane element (see tables and fig. 2(c)), cm

Δx_{le} distance from leading edge of glove to leading edge of theoretical wing planform at a given spanwise station, cm

y spanwise distance measured from fuselage center line, cm

z_l lower coordinate of airfoil section, cm

z_{le} vertical distance from wing reference line to chord line at leading edge, cm

z_{te} vertical distance from wing reference line to chord line at trailing edge, cm

z_u upper coordinate of airfoil section, cm

α angle of attack of wing chord line, deg

β angle of sideslip, deg

δ_a aileron deflection angle (left-right drooped aileron deflection), deg

δ_f flap deflection angle with respect to wing chord line, deg

δ_s leading-edge slat deflection angle with respect to wing chord line, deg

$\delta_{spoiler}$ wing upper surface spoiler deflection angle relative to wing surface, deg

δ_v vane deflection angle of double-slotted flap with respect to wing chord line, deg

ϕ wing twist (positive trailing edge down), deg

MODEL DESCRIPTION

The model used in the present investigation was a general research model that was modified to simulate the F-8 supercritical-wing airplane configuration by the addition of a large glove over the inboard part of the wing and a dummy inlet attached to the underside of the fuselage at the nose. A drawing of the complete model is presented in figure 2(a); details of the wing, glove, and high-lift system are shown in figures 2(b) and 2(c). A description of the upper surface spoiler that was installed on only the right wing is given in figure 2(d). Photographs of the model are presented in figure 3.

Wing

The basic wing planform was constructed to conform to the theoretical planform shown in figure 2(a); the wing reference area, aspect ratio, taper ratio, and sweep were defined for the theoretical planform. The aluminum wing had 42° sweep of the quarter-chord line, an aspect ratio of 6.78, and a taper ratio of 0.36. The basic wing was fitted with a fiber-glass—resin glove over the inboard part to simulate the planform of the F-8 airplane with the supercritical wing. The chord, twist, and maximum thickness variation with span for the glove and the wing are shown in figure 2(b). Detailed coordinates for

the wing are present in table I. The basic geometric characteristics are summarized in figure 2(a). The wing had a negative dihedral angle of 1.71°. Transition strips, 0.32 cm wide, of No. 80 carborundum were applied to the upper and lower surfaces of the wing 3.81 cm behind the leading edge.

Each component of the wing-slat-flap system had pressure orifice tubes installed in the left wing panel at the mean-aerodynamic-chord span station of the basic wing for measuring pressure contours through the use of scanner valve transducers. The chordwise locations of the pressure orifices are shown in tables II and III.

High-Lift System

The high-lift system of the model consisted of a double-slotted flap which extended from the wing-body juncture to the tip of the wing and a leading-edge slat which extended from the outboard edge of the glove (32-percent wing-semispan station) to the wing tip. The chord of the double-slotted flap was taken as the aft 35 percent of the basic supercritical airfoil, except at the trailing edge of the inboard part where the glove was located. The leading edge of the flap was rounded to the nose contour of a modified NASA 4415 airfoil in order to nest within the basic airfoil from 0.650c to 0.755c and to allow 0.159 cm for the upper-surface skin thickness of the airfoil at 0.755c. The chord of both the leading-edge slat and vane was 15 percent of the basic wing chord. Both of these elements had St. Cyr 156 airfoil sections modified in thickness ratio as shown at two stations (the inboard end and the tip) by the coordinates in tables IV and V.

The geometry of the flap, vane, and slat was defined in a reference deflection position of 50° for the flap and 40° for the slat. The spanwise extent of the partial-span flap was from $0.10\frac{y}{b/2}$ to $0.80\frac{y}{b/2}$ and the full-span flap extended from $0.10\frac{y}{b/2}$ to the wing tip. The coordinates for the full-span, double-slotted flap are presented in table VI. The angle between the vane and flap was fixed at 25°. Deflections of the flap-vane combination and the leading-edge slat were measured in the streamwise plane (fig. 2(c)) relative to their respective reference chord. Transition strips, 0.32 cm wide, of No. 60 carborundum were applied to the upper and lower surface of the leading-edge slat 2.54 cm behind the leading edge of the slat.

A modified airfoil leading-edge slat was designed and used for several tests. This slat was shaped as though it had evolved from the upper surface of the nose of the basic wing. The coordinates of this modified slat are presented in table VII. Several tests were made with the chord of the outboard section of the leading-edge slat $\left(0.80\frac{y}{b/2}\right.$ to $\left.1.00\frac{y}{b/2}\right)$, both the original and modified airfoil shape, increased to 20 percent of the wing chord. The coordinates of these extended chord slats are presented in table IV(b) for the original slat and table VII(b) for the modified slat.

Spoiler

A spoiler was attached to the upper surface of the right wing panel to investigate its effectiveness as a roll control. This spoiler was simulated by attaching a piece of 0.159-cm-thick metal along the 60-percent chord line of the wing from the 32- to 80-percent semispan stations (fig. 2(b)). On an aircraft equipped with this type of spoiler, the actual upper surface of the wing would move and provide a gap between the wing and the flap vane of the high-lift system. Some tests were made with part of the wing behind the spoiler removed (fig. 2(d)) when the high-lift system was deflected, and other tests were made with this part of the wing in place.

Fuselage

The fuselage of the model had a modified cylindrical cross section with circular bottom and top parts and flat sides. Overall dimensions of the fuselage are shown in figure 2(a). A fiber-glass—resin shell, 0.32 cm thick, formed the outer shape of the fuselage that was attached to a metal strongback which housed a six-component strain-gage balance. An electronic angle-of-attack sensor was mounted to the internal strongback to provide the measured geometric angle of attack of the model during the tests. A dummy inlet made of wood and covered with fiber-glass resin was attached to the underside of the fuselage at the nose to simulate the F-8 air inlet.

Tail Surfaces

The locations and principal dimensions of the horizontal and vertical tails are given in figure 2(a). These tail surfaces were made of aluminum and had a 45° quarter-chord-line sweep and NACA 65A006 airfoil sections. The horizontal tail could be set at several incidence angles.

TESTS AND CORRECTIONS

The investigation was conducted in the Langley V/STOL tunnel; most of the tests were run at a dynamic pressure of 2394 N/m^2. The test Reynolds number at this dynamic pressure was 2.47×10^6 based on the wing mean aerodynamic chord of 0.579 meter. The test dynamic pressure had to be reduced to about one-half of the usual value in tests with the high spoiler deflections when the high-lift system was deflected in order to prevent rolling-moment overload on the strain-gage balance.

Longitudinal aerodynamic characteristics were obtained from tests conducted through an angle-of-attack range from approximately -4° to 20° in increments of 2°. Various stabilizer incidences were investigated to define the trimmed characteristics

over the test angle-of-attack range. Tests were also made with the horizontail tail removed to define the tail-off aerodynamic characteristics.

Lateral stability derivatives were obtained from tests conducted through the angle-of-attack range with the model sideslipped $\pm 5^{\circ}$. Lateral stability tests were conducted with various components removed – such as the horizontal tail, vertical tail, and dummy air inlet – to determine the contribution of these components.

The double-slotted flap and leading-edge slat were tested at various deflection angles and combinations of span (partial span, full span, differential deflection, and spanwise variation in deflection). The leading-edge slat was tested at deflection angles of 30°, 40°, 50°, and 60°, whereas the double-slotted flap was tested at deflection angles of 20°, 30°, 40°, 45°, 50°, and 60°. Some tests were made with a modified airfoil leading-edge slat, a slat that was shaped as though it had evolved from the upper surface of the nose of the basic wing. Several tests were made with the chord of the tip section of the leading-edge slat, both the original and the modified shape, increased to 20 percent of the wing chord.

The effectiveness of differentially deflected flaps as a roll-control device was determined for parts of both the partial-span flap $\left(0.32 \frac{y}{b/2} \text{ to } 0.80 \frac{y}{b/2}\right)$ and the full-span flap $\left(0.80 \frac{y}{b/2} \text{ to } 1.00 \frac{y}{b/2}\right)$ configuration for a range of flap deflections.

The effectiveness as a roll-control device of an upper surface spoiler on the right wing was determined through a range of deflection angles of 4°, 8°, 15°, 30°, 60°, and 75° with respect to the wing surface. Several tests were made with the spoiler gap ahead of the deflected high-lift system closed as well as opened to determine the effect of this gap.

Jet-boundary corrections, determined from reference 7, were applied to the measured data; tunnel blockage corrections, obtained from reference 8, were applied to the data. The drag data were corrected for balance-chamber pressure at the fuselage.

Pressure distributions were measured on the basic wing (high-lift system undeflected) and on each segment of the high-lift system at the wing mean aerodynamic chord station of the left wing panel. These pressure contours are presented herein without discussion.

PRESENTATION OF RESULTS

The static longitudinal and lateral aerodynamic characteristics obtained on the present model for the various test conditions and model configurations, along with the chordwise pressure distributions of the basic wing and flap deflected 40°, with and without the various leading-edge slat deflections, are shown in the following figures:

DISCUSSION

Longitudinal Aerodynamic Characteristics

Except for a few preliminary runs, transition strips were applied near the leading edges of the basic wing and the wing leading-edge slat.

Basic plain wing configuration.- Results obtained on the plain-wing configuration (high-lift system not deflected) are presented in figures 4 and 5. Figure 4 shows that the effect of Reynolds number variation ($R = 1.56 \times 10^6$ to 2.47×10^6), based on the wing mean aerodynamic chord of 0.579 meter, was small for the range investigated. The effect of leading-edge transition strips was also found to be negligible. (Compare figs. 4(a) and 4(b).)

A comparison of the results obtained with the various basic model components (fig. 5) shows the expected increase in lift coefficient and longitudinal stability when the horizontal tail was added.

The data showing the effect of addition of leading-edge slat on the basic complete model with the horizontal stabilizer at 0° are presented in figure 6. These data indicate that without the leading-edge slat, an abrupt pitch-up occurs between angles of attack of 12° and 13°. The same trend is observed with the horizontal tail removed; this trend indicates that a flow separation problem exists on the outboard part of the wing. Addition of a slat to the wing leading edge outboard of the wing glove alleviated this loss in stability to at least $\alpha = 18^\circ$, the maximum angle that could be tested with the present sting installation.

Basic partial-span-flap configuration.- The present investigation was undertaken primarily to investigate the aerodynamic characteristics of a partial-span high-lift system suitable for currently proposed high-speed aircraft. The high-lift system data presented, therefore, are predominantly for the partial-span flap (inboard and center portion) and the leading-edge slat (center and outboard portion) configuration. The longitudinal instability and stall effects observed for the basic plain wing were still evident when partial-span flaps were deflected through the flap deflection range. (See fig. 7.) Similar to the plain wing, addition of a leading-edge slat outboard of the glove considably improved the maximum lift and the longitudinal stability characteristics. These data indicate, therefore, that leading-edge slats delay separation on the flapped wing at any flap deflection angle tested and 50° was found to be the best of all the slat deflection angles tested. The slat delayed the flow separation and instability to higher angles of attack and also reduced the drag coefficient near stall. The maximum untrimmed lift coefficient obtained on the partial-span flap configuration was $C_{L,max} = 2.39$ with $\delta_f = 40^\circ$ and $\delta_s = 50^\circ$. (See fig. 7(d).)

Effects of flap span and of spanwise variation of flap and slat deflections.- Data obtained with near optimum leading-edge slat deflection ($\delta_s = 50^o$) through a range of flap deflections are presented in figure 8(b) for partial-span flap (inboard and center) and in figure 9(b) for full-span flap (inboard, center, and outboard). Comparison of these results show some increase in maximum lift coefficient with an increase in flap span. The best flap-slat combination, $\delta_f = 40^o$ and $\delta_s = 50^o$, showed an increase in untrimmed $C_{L,max}$ from 2.39 to 2.51 as a result of increasing the flap span. The added lift on the outboard part of the wing increased the nosedown pitching moment because it acts behind the moment center of the swept wing. However, the pitch-up tendency near $\alpha = 15^o$ was not appreciably changed with the increased flap span.

A variation of spanwise deflection of the full-span flap configuration was investigated to determine whether the spanwise lift might be improved. Figure 10 shows that the reduction of flap angle toward the wing tip slightly reduced the lift coefficient.

A variation of spanwise deflection of the leading-edge slat for the partial-span flap configuration was investigated in an attempt to improve the lift characteristics. These data, presented in figure 11, show that at all flap deflections, a uniform slat deflection of 50^o is helpful; however, an inboard deflection of less than 50^o or an outboard deflection of 60^o, in general, resulted in pitch-up.

Effect of leading-edge slat geometry.- Geometric changes to the leading-edge slat were investigated to assess the effects of increasing the slat chord and modifying the slat airfoil. The chord of the outboard section (tip) of the slat was increased from 0.15c to 0.20c for both the basic St. Cyr slat airfoil and the modified airfoil which had the upper surface contour of the wing near the leading edge. The modified slat airfoil represented a slat that formed the nose section of the wing airfoil when retracted. Basic data for the modified airfoil leading-edge slat with 0.15c for slat deflections of 40^o and 50^o through a range of partial-span flap deflections are presented in figure 12. Data for the extended chord tip slat (basic and modified) for several partial-span flap deflections are presented in figure 13 and summarized in figure 14.

Increasing the slat chord at the tip portion resulted in a slight decrease in lift throughout the angle-of-attack range for the basic slat for all flap deflections (compare figs. 14(a) and 14(b)), whereas there was very little effect of increased chord for the modified airfoil slat except at the higher angles of attack where there was a small increase in lift for the extended chord. The effect of modifying the airfoil shape of the 0.15c slat (fig. 14(a)) was a small lift loss throughout most of the angle-of-attack range with a sizable decrease in C_L from 0.10 to 0.20 near maximum lift, depending on the flap deflection. This trend was about the same, but with reduced lift loss, for the extended-chord configuration.

Longitudinal Stability and Control

Data showing the effectiveness of the horizontal tail for configurations having various combinations of partial-span flap and slat deflections are presented in figure 15. These results indicate that the horizontal tail was effective in trimming the configurations at any flap-slat deflection for the angle-of-attack range of the tests. These results also show that for some flap-slat deflections (for example, fig. 15(g), $\delta_f = 40^\circ$ and $\delta_s = 40^\circ$), the model became unstable at high-lift conditions (angles of attack above approximately 15°). The instability at high lift is basically a problem associated with flow separation on the wing as mentioned in the "Partial-Span Flap" section.

In an attempt to improve the stability at high-lift conditions, stabilizer tests were made with spanwise variation of the deflection of the leading-edge slat with the partial-span flap at $\delta_f = 40^\circ$. The data for the center slat deflected 40° and the outboard slat deflected 50° are presented in figure 16; and, when compared with the data of figure 15(g) (both parts of the slat deflected 40°), the data show a slight improvement in stability above $\alpha = 15^\circ$ for the configuration with the outboard slat at 50°.

Lateral Control

Differential flap deflections.- The effects of differential flap deflection on the left- and right-wing panels were investigated as a means for providing lateral control. The basic data for various δ_a (left minus right drooped aileron deflection angles) through a range of partial-span flap deflections (inboard and center segments) are presented in figures 17(a) to 17(f) and summarized in figure 17(g) for $\alpha = 0^\circ$ and $\alpha = 15^\circ$. These data show that the differential flap deflections were not very effective in producing lateral control. In fact, for the higher flap deflections, a decrease in the desired rolling moment was obtained, especially at the higher angles of attack where adverse roll was experienced. The adverse rolling moment was caused by stalling of the flap segment having the largest deflection angle (a loss in lift on this wing panel rather than the desired increase). These data also indicate that the small amount of lateral control ΔC_l obtained decreased with increased flap deflection as well as angle of attack for the range of δ_a of the tests. Limited data for the full-span flap configuration (fig. 18) indicated that differential deflection of the outboard flap segment also proved to be ineffective, again because the flap was apparently stalled.

Upper surface spoiler deflection.- The addition of an upper surface spoiler ($\delta_{spoiler} = 30^\circ$) on the right-wing panel (fig. 18(b)) produced an incremental rolling-moment coefficient of about $\Delta C_l = 0.085$ (for α up to $\approx 15^\circ$) with the flap deflected 50° with $\delta_a = 10^\circ$ for the outboard flap segment.

The upper surface wing spoiler was further investigated through a spoiler deflection range of 4°, 8°, 15°, 30°, 60°, and 75° for model configurations without differential flap

deflection and with and without the spoiler gap open. (See fig. 2(d).) The basic data presented in figures 19(a) and 19(b) show the effectiveness of the spoiler (gap open) for the partial-span flap configuration for two high-lift system deflections. These data are summarized in figure 19(c) and the results indicate that the spoiler was a very effective lateral control device throughout the spoiler-deflection range of the test up to a maximum value of $\Delta C_l = 0.116$ for δ_f and $\delta_s = 50^o$. The incremental value of ΔC_l increased with increasing $\delta_{spoiler}$ but seemed to level off near $\delta_{spoiler} = 75^o$. In contrast to the differential-flap deflection data of figure 17(g), the lateral control for the spoiler configuration (fig. 19(c)) did not drop off with increasing angle of attack, at least up to $\alpha = 15^o$. The data of figures 20(a) to 20(c) show the effectiveness of the spoiler for a clean-wing configuration (no spoiler gap with flap undeflected) and for a full-span flap configuration (spoiler gap open and closed for $\delta_f = 20^o$ and $\delta_s = 40^o$). The data are summarized in figure 20(d). Comparing the results of figures 19(a) (partial-span flap) and 20(b) (full-span flap) shows that there was not much difference in the spoiler effectiveness for these two configurations for the same high-lift system deflection, $\delta_f = 20^o$. The effect of the spoiler gap is shown in the summary figure 20(d) and indicates that there was a negligible effect on lateral control whether the spoiler gap was opened or closed at $\alpha = 15^o$, at least for the limited spoiler deflections tested with the spoiler gap closed. However, at the lower angles of attack, closing the spoiler gap greatly decreased the lateral-control effectiveness of the spoiler.

Because of the larger lift capable of being spoiled, the roll increment produced by the spoiler is greater for the deflected flap configuration than for the undeflected flap configuration (clean wing, fig. 20(a)).

Lateral Stability Derivatives

The static lateral stability derivatives of the model are presented in figures 21 to 24. The directional-stability derivative C_{n_β} shows that the body alone was directionally unstable and that the addition of the wing did not appreciably alter the body-alone values of C_{n_β}. (See fig. 21.) Addition of the vertical tail to the wing body made the complete model configuration directionally stable throughout the angle-of-attack range of the investigation. The data presented in figure 22 and summarized in figure 23 show that the directional stability at low and moderate angles of attack increased with increasing deflection of the high-lift system. A large loss in directional stability was indicated at angles of attack greater than about 16^o for all model configurations. The data trends suggest that directional instability would occur for angles of attack greater than 20^o. Comparison of the data obtained with and without the vertical tail (fig. 22) indicates that the loss of directional stability can be attributed to the wing-body characteristics rather than to a loss in the vertical-tail contribution.

The effect on the static-lateral stability derivatives of a change in flap span is presented in figure 24. These results indicate that there was little improvement in extending the partial-span flap to the full-span flap, except that the full-span flap configuration showed a very slight increase in effective dihedral $\left(-C_{l_\beta}\right)$.

Positive effective dihedral derivatives $\left(-C_{l_\beta}\right)$ for the complete clean-wing configuration (figs. 21 and 22(a)) show that the negative value of $-C_{l_\beta}$ increased with increasing angle of attack up to the point where flow separation occurs ($\alpha = 12^o$), and with further increase in angle of attack, C_{l_β} abruptly reduces to zero. The effective dihedral for the body alone (fig. 21) was essentially zero.

When the partial-span flap was deflected, a considerable increase in $-C_{l_\beta}$ was obtained (compare fig. 22(a) with figs. 22(b) to 22(g)) primarily because of the increased lift due to the flap and the effect of the asymmetrical wing sweep in sideslip. For angles of attack above approximately 12^o, the negative values of C_{l_β} (flap deflected) increased abruptly as compared with the abrupt reduction in C_{l_β} (as mentioned before) for the unflapped configuration. The negative values of C_{l_β} increased slightly up to moderately high-lift system deflections, $\delta_f = 45^o$ and $\delta_s = 50^o$, and then became smaller for the higher deflections because of separation effects on the flap and slat.

The contribution to the side-force derivative $\left(C_{Y_\beta}\right)$ was negative and fairly constant for the clean-wing configuration. (See fig. 21 or 22(a).) The same was true for all high-lift system configurations up to $\alpha \approx 15^o$ to 16^o where a decrease in C_{Y_β} occurred at the higher angles of attack, especially for the moderate high-lift system deflections, $\delta_f = 30^o$, $\delta_s = 30^o$ and $\delta_f = 40^o$, $\delta_s = 40^o$. (See figs. 22(a) to 22(g).)

SUMMARY OF RESULTS

A low-speed investigation was conducted in the Langley V/STOL tunnel to determine the effects of a double-slotted flap, high-lift system on the static longitudinal and lateral stability aerodynamic characteristics of a 42^o swept high-wing model having a supercritical airfoil. The wing had an aspect ratio of 6.78, and the high-lift system consisted of a leading-edge slat and a double-slotted trailling-edge flap. The results of this investigation may be summarized as follows:

1. A leading-edge slat delayed flow separation on both the plain and flapped wing at any flap deflection. The optimum slat deflection was about 50^o. The slat delayed pitch-up to higher angles of attack and reduced the drag coefficient near stall.

2. The maximum untrimmed lift coefficient obtained with the partial-span flap was $C_{L,max} = 2.39$. Increasing the flaps to full span increased the maximum untrimmed lift coefficient to 2.51 and increased the nose-down pitching-moment coefficient.

3. Change in airfoil shape of the leading-edge slat as well as extension of the chord of the outboard slat segment from 0.15 chord to 0.20 chord had no beneficial effect on maximum lift or stability characteristics.

4. With the horizontal tail on, the model (flaps off or deflected) was longitudinally stable up to angles of attack where flow separation occurred; however, for some conditions at angles of attack α of 12° to $\cdot\cdot^{\circ}$, the model had a tendency to pitch-up.

5. Differential flap deflection was not effective as a method of roll control, and in some cases, had an adverse effect. The addition of a partial-span spoiler on the right-wing upper surface was an effective lateral control device with a maximum value of incremental rolling moment ($\Delta C_l = 0.116$) for a spoiler deflection of 75° for the model with flap and slat deflections of 50°.

6. For the clean-wing configuration at small sideslip angles ($\beta = \pm 5^{\circ}$), static lateral stability parameters showed that the negative values of the effective dihedral parameter (C_{l_β}) increased with increasing angle of attack up to the point where flow separation occurs ($\alpha \approx 12^{\circ}$); and with further increase in angle of attack C_{l_β} abruptly reduces to zero. For the configurations with the high-lift system deflected, a considerable increase in the effective dihedral parameter was indicated, and it increased abruptly above an angle of attack of 12°.

7. The complete model configuration in the clean-wing condition was directionally stable throughout the angle-of-attack range. The static directional stability parameter C_{n_β} for all high-lift system deflections was positive, but a large loss in C_{n_β} occurred at high angles of attack (above $\alpha = 15^{\circ}$ to 16°) for all model configurations. The data trends indicate that directional instability would be expected for angles of attack somewhat above 20°.

Langley Research Center,
National Aeronautics and Space Administration,
Hampton, Va., April 3, 1974.

REFERENCES

1. Whitcomb, Richard T.; and Clark, Larry R.: An Airfoil Shape for Efficient Flight at Supercritical Mach Numbers. NASA TM X-1109, 1965.

2. Goodson, Kenneth W.: Low-Speed Aerodynamic Characteristics of a Rectangular, Aspect-Ratio-6, Slotted Supercritical Airfoil Wing Having Several High-Lift Flap Systems. NASA TM X-2317, 1971.

3. Harris, Charles D.: Wind-tunnel Investigation of Effects of Trailing-Edge Geometry on a NASA Supercritical Airfoil Section. NASA TM X-2336, 1971.

4. Fournier, Paul G.; and Sleeman, William C., Jr.: Low-Speed Aerodynamic Characteristics of a Model Having a 42° Swept Low Wing With a Supercritical Airfoil, Double-Slotted Flaps, and a T-Tail. NASA TM X-2582, 1972.

5. Fournier, Paul G.; and Sleeman, William C., Jr.: Effects of Wing Height on Low-Speed Aerodynamic Characteristics of a Model Having a 42° Swept Wing, a Supercritical Airfoil, Double-Slotted Flaps, and a Low Tail. NASA TM X-2794, 1973.

6. Mechtly, E. A.: The International System of Units – Physical Constants and Conversion Factors (Second Revision). NASA SP-7012, 1973.

7. Gillis, Clarence L.; Polhamus, Edward C.; and Gray, Joseph L., Jr.: Charts for Determining Jet-Boundary Corrections for Complete Models in 7- by 10-Foot Closed Rectangular Wind Tunnels. NACA WR L-123, 1945. (Formerly NACA ARR L5G31.)

8. Herriot, John G.: Blockage Corrections for Three-Dimensional-Flow Closed-Throat Wind Tunnels, With Consideration of the Effect of Compressibility. NACA Rep. 995, 1950. (Supersedes NACA RM A7B28.)

TABLE I - BASIC WING COORDINATES

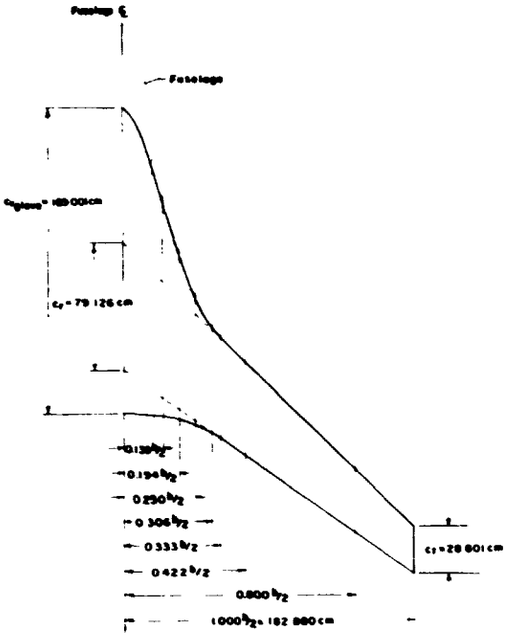

x/c	$\frac{z_u}{c}$	$\frac{z_l}{c}$	$\frac{z_u}{c}$	$\frac{z_l}{c}$	$\frac{z_u}{c}$	$\frac{z_l}{c}$	$\frac{z_u}{c}$	$\frac{z_l}{c}$	$\frac{z_u}{c}$	$\frac{z_l}{c}$	$\frac{z_u}{c}$	$\frac{z_l}{c}$	$\frac{z_u}{c}$	$\frac{z_l}{c}$	$\frac{z_u}{c}$	$\frac{z_l}{c}$
	$\frac{y}{b/2}$ = 0 139 c = 128.270 cm		$\frac{y}{b/2}$ = 0 194 c = 99 314 cm		$\frac{y}{b/2}$ = 0 250 c = 77 724 cm		$\frac{y}{b/2}$ = 0.306 c = 65.430 cm		$\frac{y}{b/2}$ = 0.333 c = 62.329 cm		$\frac{y}{b/2}$ = 0 422 c = 57 874 cm		$\frac{y}{b/2}$ = 0.800 c = 38.867 cm		$\frac{y}{b/2}$ = 1.000 c = 28 801 cm	
0	0.0317	0.0317	0.0281	0.0281	0.0327	0 0327	0.0291	0.0291	0.0294	0.0294	0.0225	0 0225	-0.0185	-0.0185	-0.0635	-0.0635
.0025	.0418	.0213	.0432	.0233	.0415	.0235	0388	.0190	.0367	.0204	0318	0132	-.0129	- 0260	-.0585	-.0717
.0050	.0450	.0182	.0471	.0197	.0464	.0186	.0437	.0155	0408	.0163	0351	.0103	-.0086	-.0294	- 0573	-.0732
.0100	.0497	.0137	.0531	.0148	.0523	.0144	.0474	0122	.0448	.0131	.0395	.0073	-.0065	- 0327	-.0539	-.0755
.0200	.0556	.0083	0596	.0086	.0598	.0092	.0536	.0086	.0490	.0082	.0437	.0033	-.0002	- 0384	-.0502	- 0802
.0300	.0602	.0044	.0639	.0059	.0654	.0057	.0582	.0031	.0530	.0054	.0472	.0000	.0019	- 0414	-.0471	-.0838
.0400	.0636	.0012	.0673	.0031	.069₀	0023	.0609	-.0006	.0557	.0036	.0494	-.0020	.0039	-.0435	- 0441	-.0850
0500	.0667	-.0012	.0701	.0008	.0719	-.0010	.0631	-.0023	.0579	.0015	.0516	-.0041	.0064	-.0439	-.0440	-.0855
.0750	.0735	-.0065	.0750	-.0041	.0771	-.0049	.0672	-.0066	.0623	-.0020	.0557	-.0075	.0088	-.0441	-.0379	-.0838
.1000	.0778	-.0101	.0788	-.0079	0794	-.0088	.0695	-.0089	0660	-.0051	0595	-.0102	.0146	-.0454	-.0340	-.0836
.1500	.0851	-.0152	.0836	-.0141	.0835	-.0123	.0749	-.0120	0718	-.0089	.0653	-.0143	.0212	- 0454	-.0264	-.0794
.2000	.0901	- 0190	.0867	-.0179	.0858	-.0141	.0776	-.0144	.0758	-.0108	.0691	-.0154	.0262	-.0438	-.0195	- 0764
.2500	.0923	-.0208	.0885	-.0199	0876	- 0147	.0804	-.0151	.0775	-.0116	.0724	-.0157	0325	- 0425	-.0133	-.0713
.3000	.0931	-.0218	.0893	-.0205	0879	-.0144	.0815	- 0146	.0795	-.0117	.0746	- 0149	0359	- 0393	-.0066	-.0672
.3500	.0929	-.0220	.0887	-.0192	.0882	-.0137	.0829	- 0136	.0807	- 0105	.0755	-.0140	.0393	-.0370	-.0008	-.0617
.4000	.0917	-.0218	.0872	-.0169	.0873	-.0118	.0823	-.0116	0811	-.0082	0762	-.0118	.0432	- 0337	0052	- 0556
.4500	.0899	-.0200	.0854	-.0143	.0863	-.0092	.0815	-.0083	.0810	-.0061	.0759	-.0096	.0457	- 0306	.0113	- 0508
.5000	.0877	-.0160	0831	-.0110	.0853	-.0057	.0811	-.0062	.0803	-.0038	.0757	-.0060	.0479	-.0256	0172	-.0442
.5500	.0842	-.0105	0806	-.0070	.0833	- 0013	.0800	- 0023	.0795	.0000	.0757	-.0017	0505	- 0199	.0228	-.0386
.6000	.0807	-.0059	.0780	-.0028	0807	.0033	.0788	.0027	.0784	0057	.0755	0028	.0523	-.0133	.0284	-.0317
.6500	.0758	.0008	.0749	.0026	.0783	0088	0776	.0089	.0774	.0133	.0746	.0110	.0545	-.0055	.0340	-.0220
.7000	.0716	.0071	.0739	.0090	.0748	.0144	.0747	.0163	.0761	.0217	.0737	.0204	.0564	.0060	.0381	-.0086
.7500	.0670	.0137	.0668	.0161	.0714	.0219	.0718	.0248	.0741	0319	.0717	.0300	.0581	.0174	.0425	.0044
.8000	.0626	.0192	.0624	.0226	.0667	.0286	.0681	.0326	.0711	.0408	.0691	.0389	.0575	.0263	.0441	.0150
.8500	.0560	.0253	.0568	.0279	.0614	.0343	.0637	.0388	.0672	.0473	.0658	.0455	.0586	.0344	.0441	.0237
.9000	.0497	.0275	.0504	.0294	.0556	.0373	.0586	.0427	.0622	.0503	.0612	.0483	.0523	.0388	.0439	.0294
.9500	.0418	.0267	.0427	.0281	.0487	.0350	.0524	.0404	.0557	.0412	.0541	.0441	.0458	.0356	.0382	.0289
.9700	.0384	.0255	.0394	.0269	.0458	.0340	.0493	.0384	.0530	.0409	.0509	.0408	.0422	.0326	.0344	.0244
.9800	.0364	.0246	.0381	.0258	.0444	.0327	.0479	0373	.0511	.0404	.0491	.0384	.0406	.0314	.0301	.0212
.9900	.0347	.0236	.0361	.0253	.0425	.0320	.0462	.0357	.0489	.0376	0467	.0364	.0388	.0278	.0282	.0184
.9950	.0335	.0232	.0353	.0251	.0422	.0317	.0458	.0349	.0475	.0367	.0455	.0351	.0376	.0262	.0258	.0159
1.0000	.0332	.0226	.0345	.0243	.0415	.0310	.0450	.0344	.0463	.0360	.0444	.0342	.0359	.0250	.0247	.0143
r_{le}/c	0.0196		0.0210		0.0212		0.0186		0.0155		0.0149		0 0091		0.0031	

TABLE II.- PRESSURE ORIFICE LOCATIONS ON BASIC WING

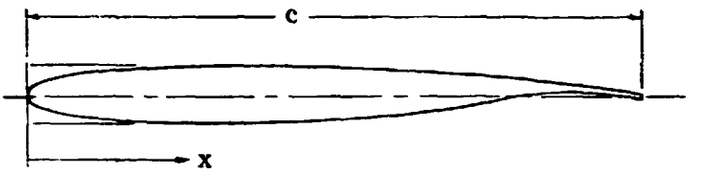

x/c
Upper and lower
Basic wing; $\frac{y}{b/2}$ = 0.422; and c = 57.861 cm
0
.0051
.0100
.0200
.0500
.1000
.1500
.2000
.3000
.4000
.5000
.6000
.7000
.7500
.8000
.9000
.9900

TABLE III.- PRESSURE ORIFICE LOCATIONS ON VARIOUS FLAP COMPONENTS

$\left[\frac{y}{b/2} = 0.422\right]$

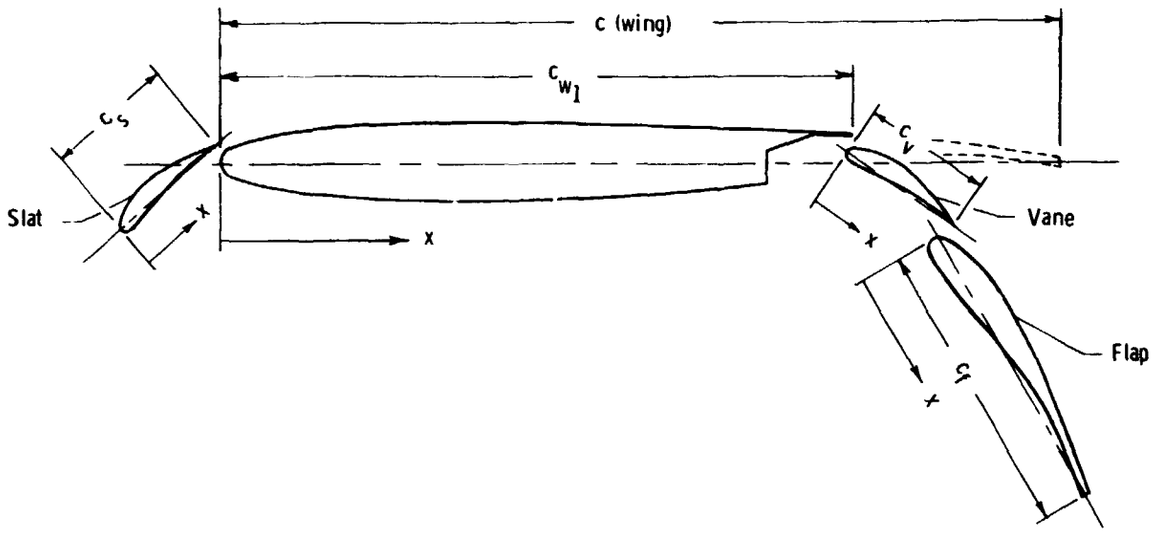

x/c_s		x/c_{w_1}	x/c_v		x/c_f	
Upper	Lower	Upper and lower	Upper	Lower	Upper	Lower
c_s = 7.219 cm slat		c_{w_1} = 43.396 cm forward section	c_v = 8.395 cm vane		c_f = 17.475 cm flap	
0	0	0	0	0	0	0
.0007	.0007	.0066	.0033	.0036	.0094	.0020
.0035	.0211	.0133	.0217	.0166	.0196	.0066
.0077	.0418	.0266	.0386	.0293	.0325	.0146
.0299	.0682	.0666	.0718	.0448	.0723	.0406
.0636	.1161	.1333	.1289	.0933	.1213	.0917
.1045	.1653	.2000	.1805	.1436	.2114	.1491
.1871	.2160	.2667	.2617	.1984	.2575	.2073
.2874	.3187	.4001	.3372	.2896	.3521	.3280
.4099	.4004	.5334	.4459	.4103	.4509	.4008
.4743	.4908	.6668	.5434	.5151	.5547	.5149
.5422	.5907	.8001	.6400	.6130	.6536	.6049
.6182	.6984	.9335	.7246	.7066	.7462	.6850
.6973	.7519	.9990 (Upper only)	.7684	.7539	.7916	.7297
.7346	.8040		.8140	.8018	.8228	.7793
.8444	.8972		.8952	.8987	.9077	.8795
.9729	.9792		.9637	.9850	.9781	.9856

TABLE IV.- LEADING-EDGE SLAT COORDINATES

(a) 0.15 slat

x/c_s	z_u/c_s	z_l/c_s	z_u/c_s	z_l/c_s
	$\frac{y}{b/2}$ = 0.320; c_s = 9.455 cm		$\frac{y}{b/2}$ = 1.000; c_s = 4.321 cm	
0	-0.0122	-0.0122	-0.0837	-0.0837
.0125	.0217	-.0351	-.0564	-.1000
.0250	.0366	-.0429	-.0444	-.1041
.0500	.0574	-.0505	-.0270	-.1064
.0750	.0740	-.0538	-.0134	-.1073
.1000	.0887	-.0542	-.0012	-.1061
.1500	.1109	-.0495	.0176	-.0998
.2000	.1277	-.0417	.0326	-.0897
.3000	.1467	-.0238	.0514	-.0682
.4000	.1506	-.0062	.0607	-.0485
.5000	.1461	.0110	.0647	-.0300
.6000	.1320	.0237	.0620	-.0129
.7000	.1076	.0281	.0531	-.0015
.8000	.0776	.0261	.0400	.0031
.9000	.0436	.0170	.0234	.0035
.9500	.0254	.0094	.0138	.0021
1.0000	.0062	0	.0043	0

TABLE IV.- LEADING-EDGE SLAT COORDINATES – Concluded

(b) 0.20c slat

x/c_s	z_u/c_s	z_l/c_s	z_u/c_s	z_l/c_s
	$\frac{y}{b/2} = 0.320$; $c_s = 12.606$ cm		$\frac{y}{b/2} = 1.000$; $c_s = 5.760$ cm	
0	-0.0092	-0.0092	-0.0628	-0.0628
.0125	.0163	-.0263	-.0423	-.0750
.0250	.0275	-.0322	-.0333	-.0781
.0500	.0431	-.0379	-.0203	-.0798
.0750	.0555	-.0404	-.0101	-.0805
.1000	.0665	-.0407	-.0009	-.0796
.1500	.0832	-.0371	.0132	-.0749
.2000	.0958	-.0313	.0245	-.0673
.3000	.1100	-.0179	.0386	-.0512
.4000	.1130	-.0047	.0455	-.0364
.5000	.1096	.0083	.0485	-.0225
.6000	.0990	.0178	.0465	-.0094
.7000	.0807	.0211	.0398	-.0011
.8000	.0582	.0196	.0300	.0023
.9000	.0327	.0128	.0176	.0026
.9500	.0191	.0071	.0104	.0016
1.0000	.0047	0	.0032	0

TABLE V.- FLAP-VANE COORDINATES

x/c_v	z_u/c_v	z_l/c_v	z_u/c_v	z_l/c_v	z_u/c_v	z_l/c_v
	c_v = 10.795 cm; $\frac{y}{b/2}$ = 0.0139		c_v = 9.455; $\frac{y}{b/2}$ = 0.320		c_v = 4.321 cm; $\frac{y}{b/2}$ = 1.000	
0	-0.0049	-0.0049	-0.0122	-0.0122	-0.0837	-0.0837
.0125	.0300	-.0280	.0217	-.0351	-.0564	-.1000
.0250	.0450	-.0366	.0366	-.0429	-.0444	-.1041
.0500	.0663	-.0446	.0574	-.0505	-.0270	-.1064
.0750	.0832	-.0480	.0740	-.0538	-.0134	-.1073
.1000	.0982	-.0487	.0887	-.0542	-.0012	-.1061
.1500	.1210	-.0442	.1109	-.0495	.0176	-.0998
.2000	.1379	-.0366	.1277	-.0417	.0326	-.0897
.3000	.1547	-.0190	.1467	-.0238	.0514	-.0682
.4000	.1600	-.0016	.1506	-.0062	.0607	-.0485
.5000	.1546	.0150	.1461	.0110	.0647	-.0300
.6000	.1394	.0275	.1320	.0237	.0620	-.0129
.7000	.1135	.0312	.1076	.0281	.0531	-.0015
.8000	.0815	.0295	.0776	.0261	.0400	.0031
.9000	.0457	.0187	.0436	.0170	.0234	.0035
.9500	.0267	.0102	.0254	.0094	.0138	.0021
1.0000	.0065	0	.0062	0	.0043	0

[redacted]

TABLE VI.- FLAP COORDINATES

x/c_f	z_u/c_f	z_l/c_f	z_u/c_f	z_l/c_f	z_u/c_f	z_l/c_f
	c_f = 34.392 cm; $\frac{y}{b/2}$ = 0.139		c_f = 22.060 cm; $\frac{y}{b/2}$ = 0.320		c_f = 10.081 cm; $\frac{y}{b/2}$ = 1.000	
0	0.0754	0.0754	0.0903	0.0903	-0.0252	-0.0252
.0100	.1012	.0572	.1184	.0708	-.0016	-.0393
.0200	.1130	.0535	.1296	.0651	.0072	-.0423
.0400	.1307	.0499	.1456	.0596	.0211	-.0452
.0600	.1433	.0499	.1570	.0576	.0317	-.0450
.1000	.1647	.0554	.1741	.0594	.0496	-.0380
.1500	.1824	.0613	.1900	.0669	.0675	-.0244
.2000	.1950	.0679	.1984	.0751	.0821	-.0115
.2500	.2016	.0727	.2030	.0843	.0950	.0006
.3000	.2053	.0790	.2048	.0938	.1046	.0124
.3517	.2072	.0857	.2054	.1035	.1115	.0233
.4189	.2049	.0931	.2030	.1155	.1179	.0373
.4851	.2001	.0982	.1991	.1255	.1228	.0495
.5458	.1950	.1016	.1947	.1336	.1260	.0605
.6160	.1869	.1033	.1890	.1395	.1264	.0706
.6811	.1758	.1033	.1820	.1424	.1256	.0787
.7451	.1669	.1016	.1745	.1414	.1229	.0830
.8089	.1569	.0997	.1668	.1365	.1160	.0816
.8717	.1455	.0975	.1572	.1279	.1061	.0763
.9337	.1352	.0923	.1459	.1166	.0906	.0631
1.0000	.1237	.0842	.1312	.1028	.0691	.0403

[redacted]

TABLE VII.- MODIFIED LEADING-EDGE SLAT COORDINATES

(a) 0.15c slat

x/c_s	z_u/c_s	z_l/c_s	x/c_s	z_u/c_s	z_l/c_s
	$\frac{y}{b/2} = 0.320$; $c_s = 9.455$ cm			$\frac{y}{b/2} = 1.000$; $c_s = 4.321$ cm	
0	0	0	0	0	0
.0125	.0459	-.0537	.0125	.0260	-.0356
.0250	.0629	-.0754	.0250	.0352	-.0391
.0500	.0834	-.0903	.0500	.0469	-.0380
.0750	.0982	-.0901	.0750	.0541	-.0329
.1000	.1092	-.0846	.1000	.0585	-.0237
.1500	.1206	-.0643	.1500	.0643	.0006
.2000	.1233	-.0379	.2000	.0659	.0062
.2500	.1220	-.0059	.2500	.0647	.0103
.3000	.1183	.0056	.3000	.0633	.0146
.4000	.1066	.0175	.4000	.0588	.0194
.5000	.0936	.0232	.5000	.0529	.0209
.6000	.0791	.0261	.6000	.0453	.0197
.7000	.0627	.0242	.7000	.0353	.0155
.8000	.0445	.0179	.8000	.0238	.0092
.9000	.0235	.0069	.9000	.0121	.0024
1.0000	0	-.0081	1.0000	0	-.0059
L.E. radius	0.0916		0.0333		
Lower radius	0.0458		0.0167		
Lower radius location . . .	0.0603	-0.0455	0.0194		-0.0200

TABLE VII.- MODIFIED LEADING-EDGE SLAT COORDINATES – Concluded

(b) 0.20c slat

x/c_s	z_u/c_s	z_l/c_s	x/c_s	z_u/c_s	z_l/c_s
	$\frac{y}{b/2}$ = 0.320; c_s = 12.606 cm			$\frac{y}{b/2}$ = 1.000; c_s = 5.760 cm	
0	0	0	0	0	0
.0125	.0345	-.0403	.0125	.0195	-.0267
.0250	.0472	-.0566	.0250	.0264	-.0293
.0500	.0626	-.0677	.0500	.0352	-.0285
.0750	.0737	-.0676	.0750	.0406	-.0247
.1000	.0819	-.0635	.1000	.0439	-.0178
.1500	.0904	-.0483	.1500	.0482	.0004
.2000	.0925	-.0284	.2000	.0494	.0046
.2500	.0915	-.0044	.2500	.0485	.007.
.3000	.0888	.0042	.3000	.0475	.0109
.4000	.0799	.0131	.4000	.0441	.0146
.5000	.0702	.0174	.5000	.0397	.0157
.6000	.0593	.0196	.6000	.0340	.0148
.7000	.0471	.0182	.7000	.0265	.0116
.8000	.0334	.0134	.8000	.0179	.0069
.9000	.0176	.0052	.9000	.0090	.0018
1.0000	0	-.0061	1.0000	0	-.0044
L.E. radius	0.0688		0.0250		
Lower radius	0.0344		0.0125		
Lower radius location . . .	0.0452	-0.0341	0.0146		-0.0150

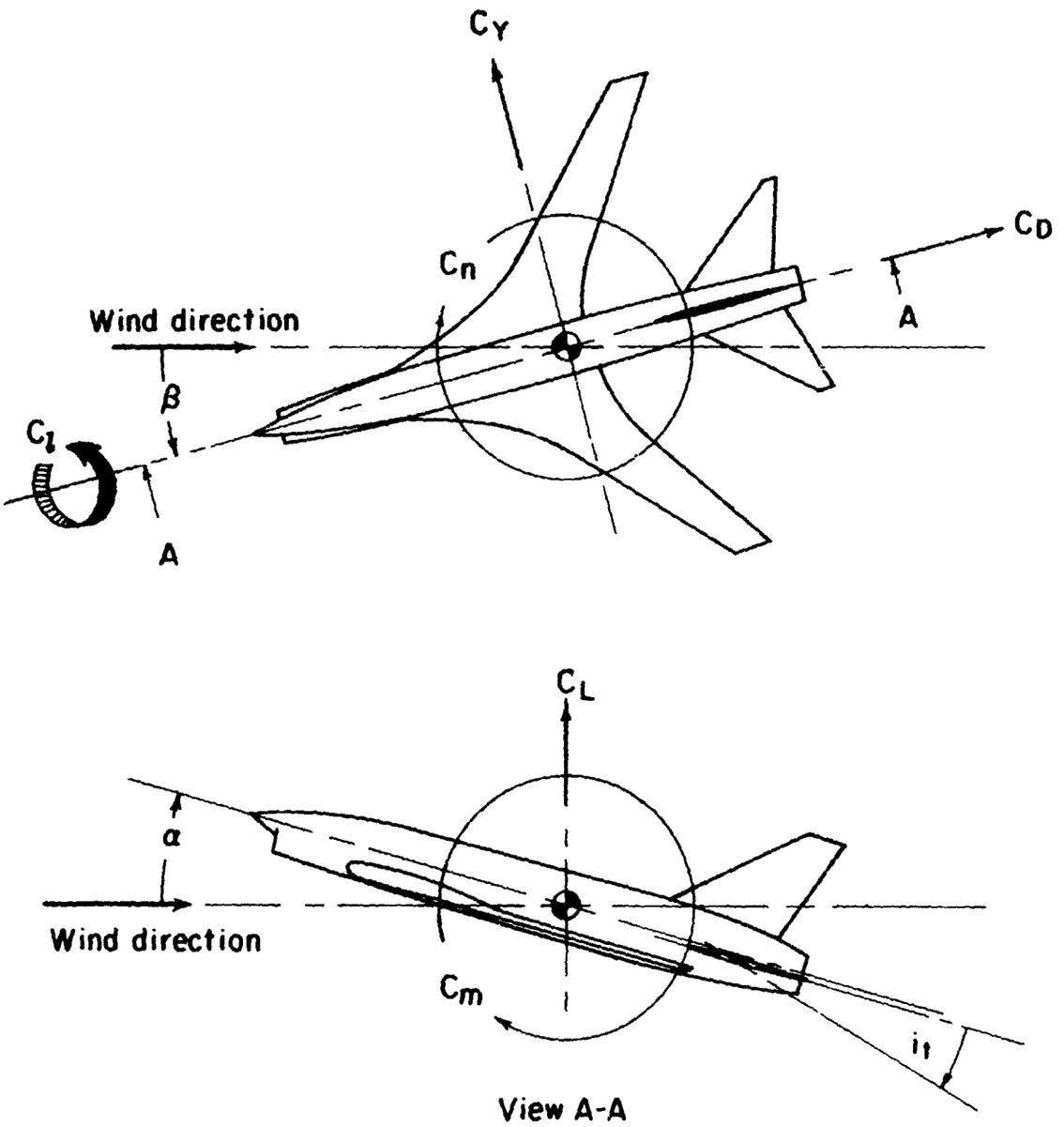

Figure 1.- System of axes. Positive directions of forces, moments, and angles are indicated by arrows.

Wing	
Area, m^2	197
Mean aerodynamic chord, cm	5787
Span, cm	365 76
Aspect ratio	6 78
Horizontal tail	
Area, m^2	076
Mean aerodynamic chord, cm	5486
Span, cm	16398
Aspect ratio	355
Vertical tail	
Area, m^2	050
Mean aerodynamic chord, cm	6680
Span, cm	8128

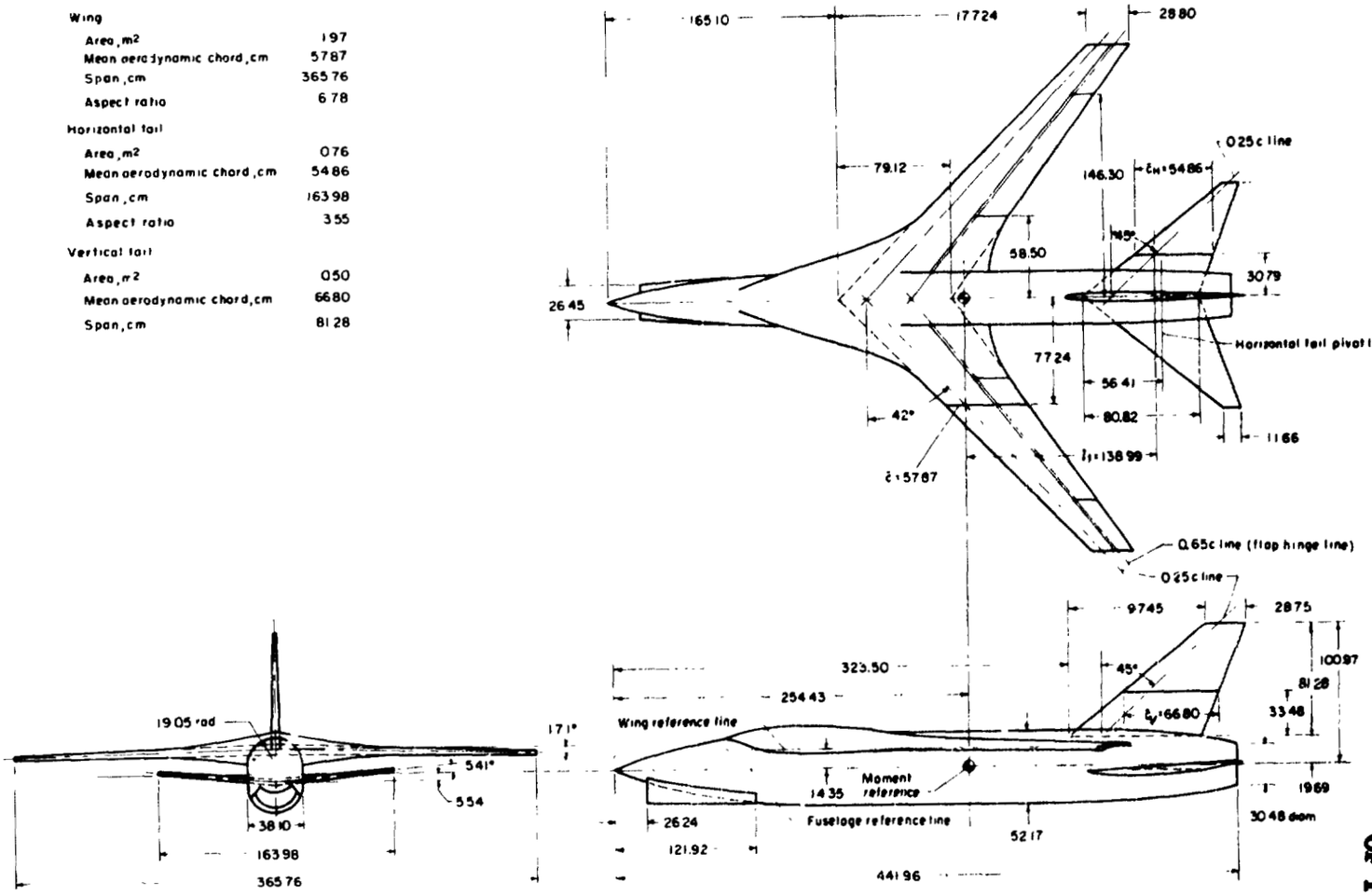

(a) Complete model geometric characteristics.

Figure 2.- Details of high-lift model. Dimensions in centimeters.

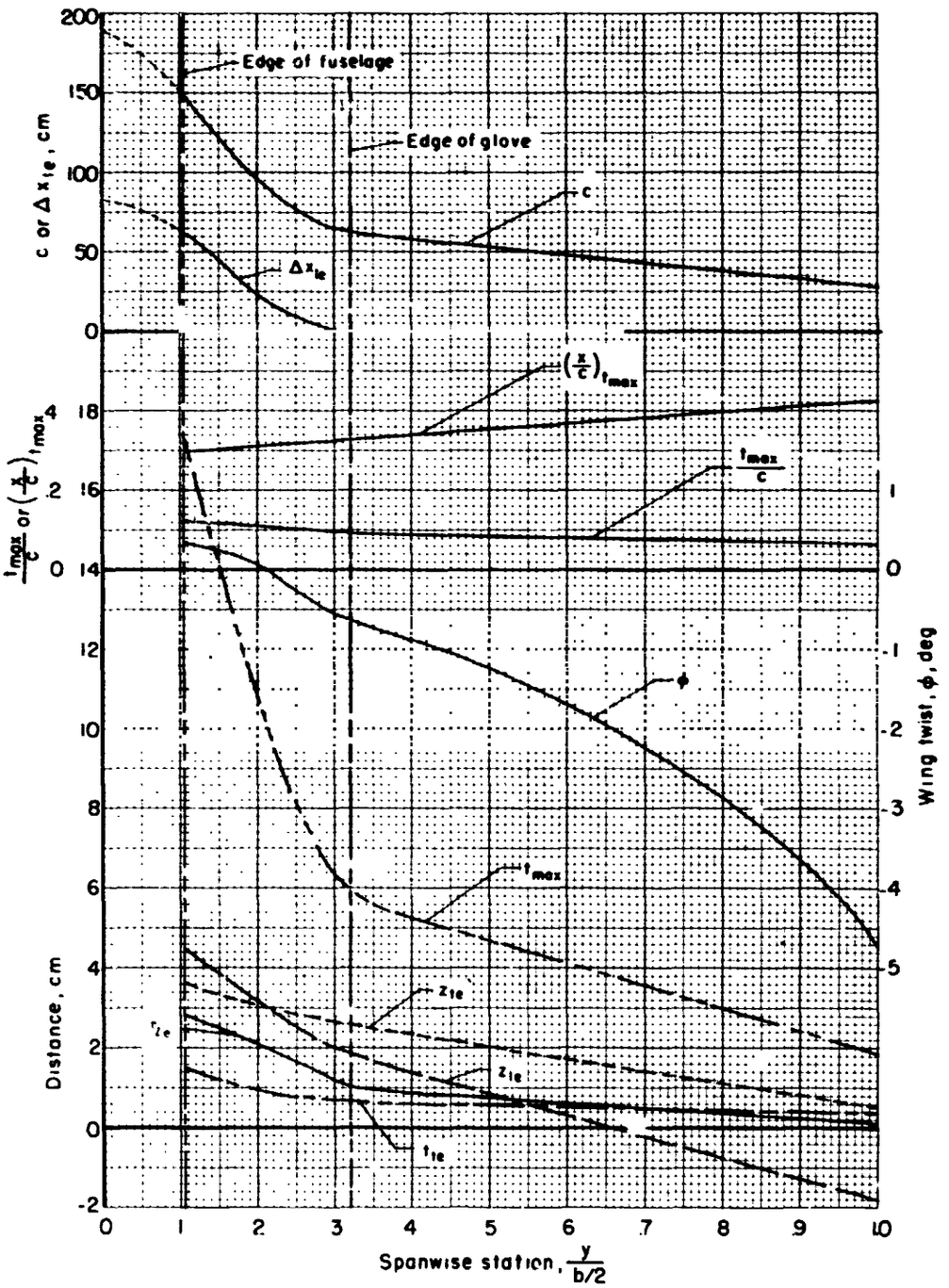

(b) Wing spanwise details.

Figure 2.- Continued.

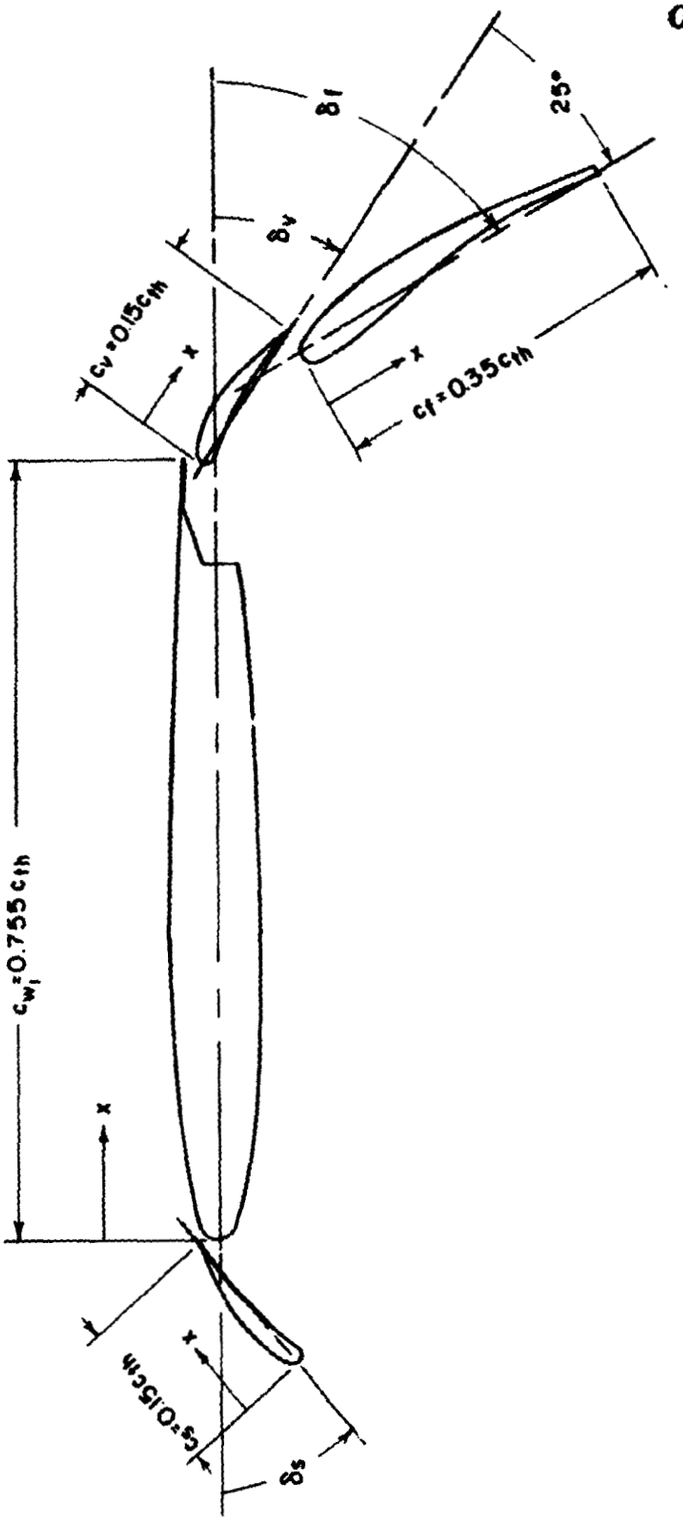

(c) Details of basic flap and slat system.

Figure 2.- Continued.

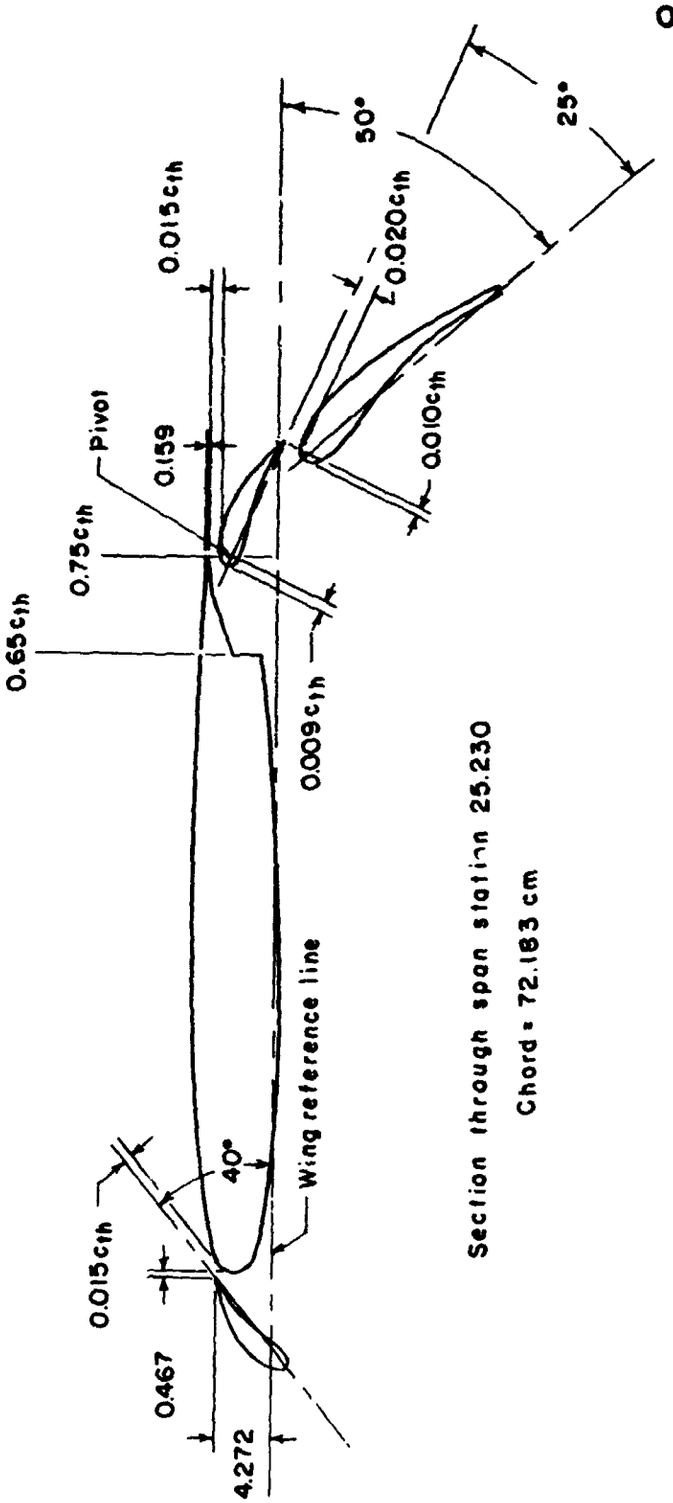

(c) Concluded.

Figure 2.- Continued.

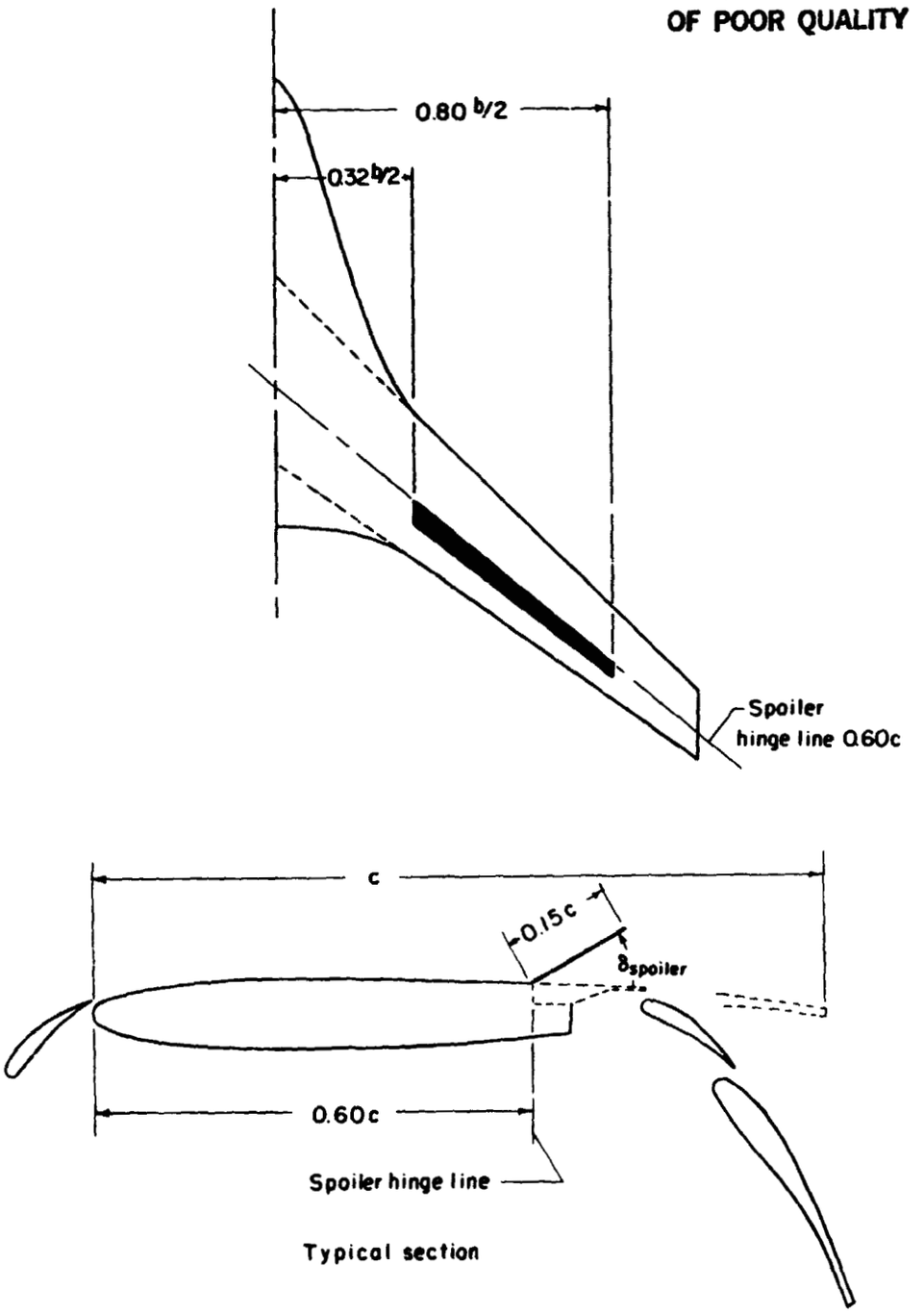

(d) Spoiler description and location (right wing panel).

Figure 2.- Concluded.

L-70-8545

(a) Clean-wing configuration.

Figure 3.- Photographs of model in Langley V/STOL tunnel.

L-70-8828

(b) Three-quarter front view with flap deflected.

Figure 3.- Continued.

L-70-8829

(c) Three-quarter front view, closeup of flap system.

Figure 3.- Continued.

L-70-8830

(d) Three-quarter rear view, flaps deflected.

Figure 3.- Concluded.

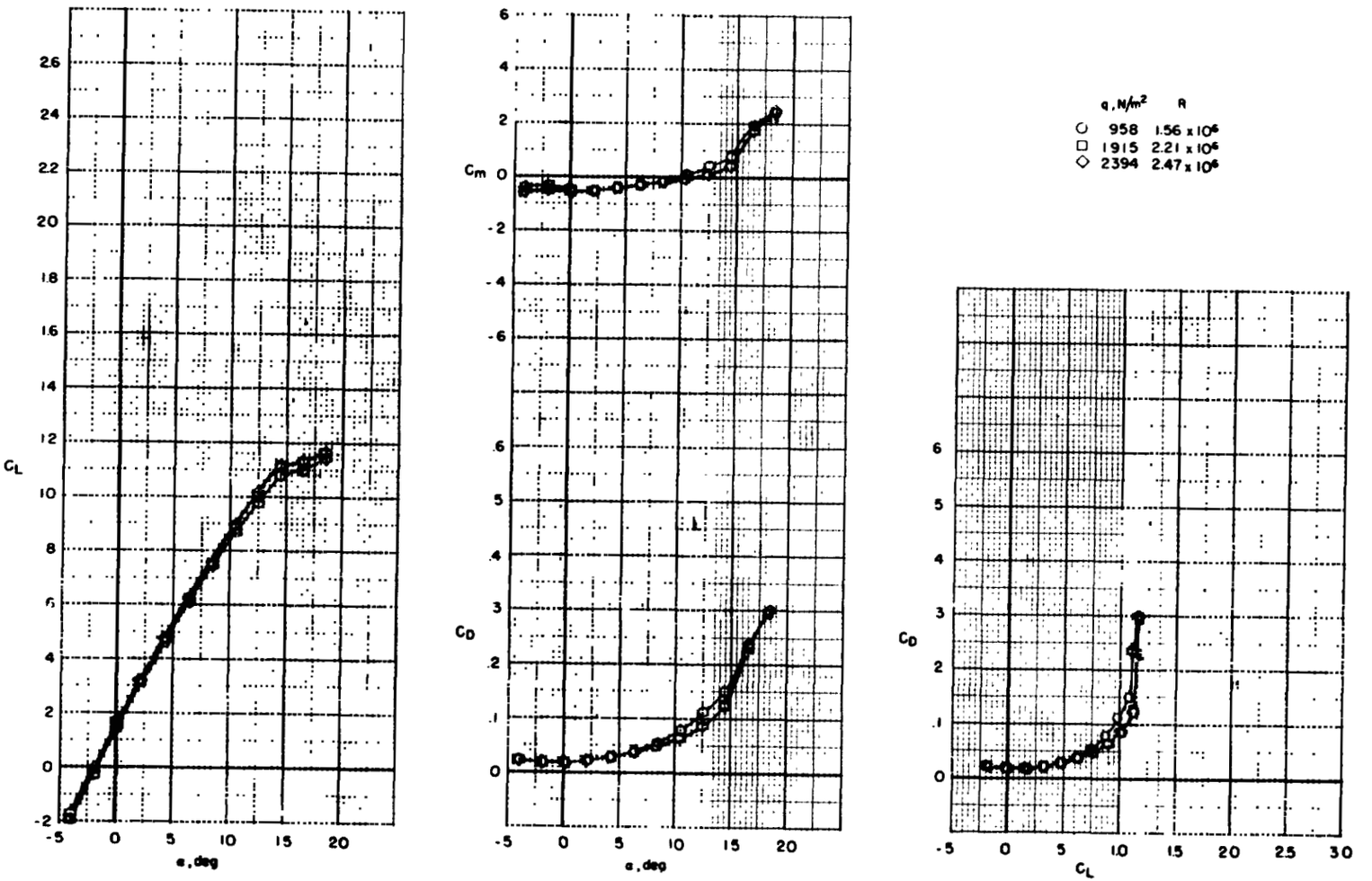

(a) Transition off.

Figure 4.- Effect of Reynolds number on the basic wing-body configuration. i_t = Off; vertical tail on; $\delta_f = 0^o$; δ_s = Off.

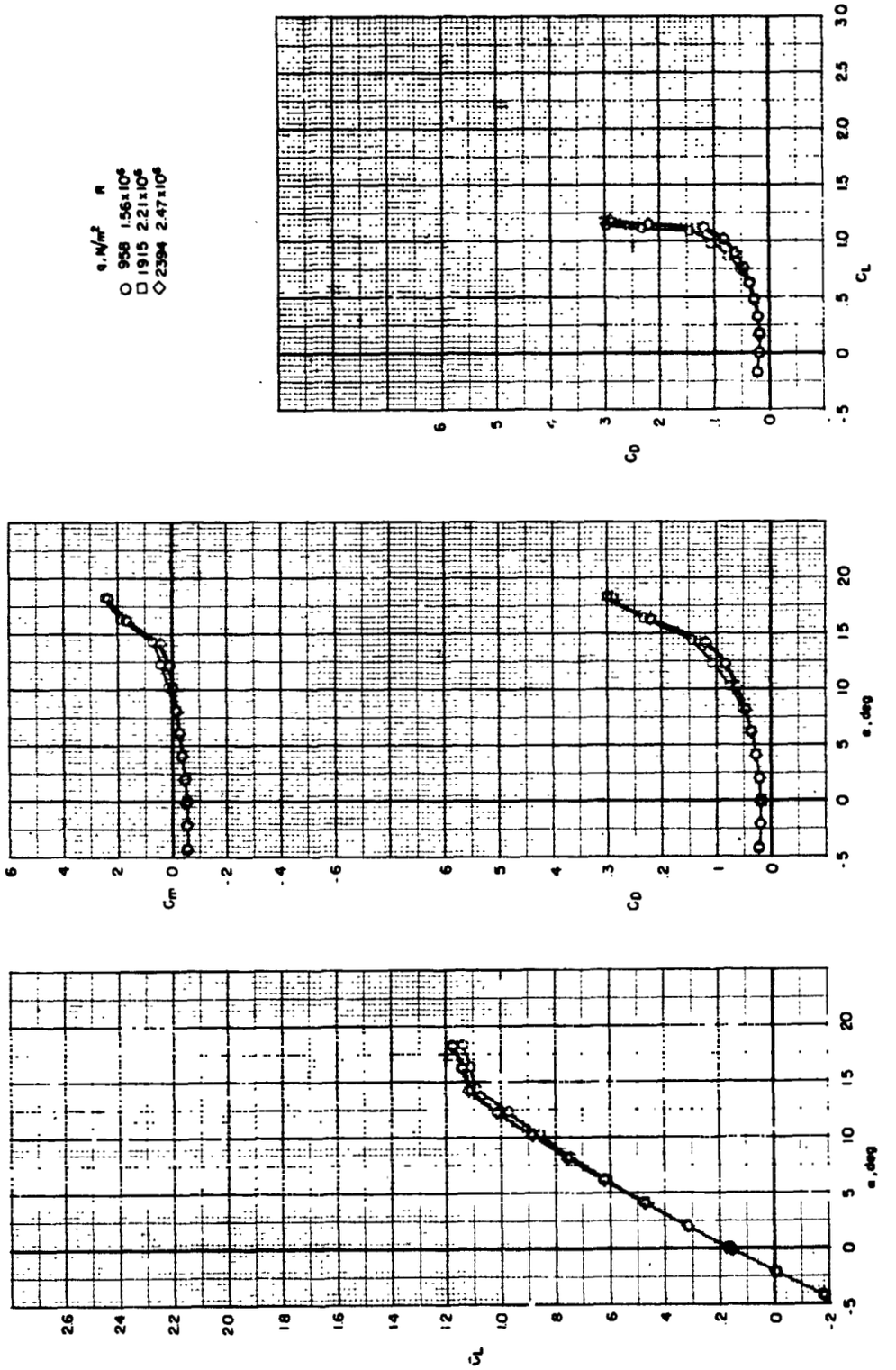

(b) Transition on.

Figure 4.- Concluded.

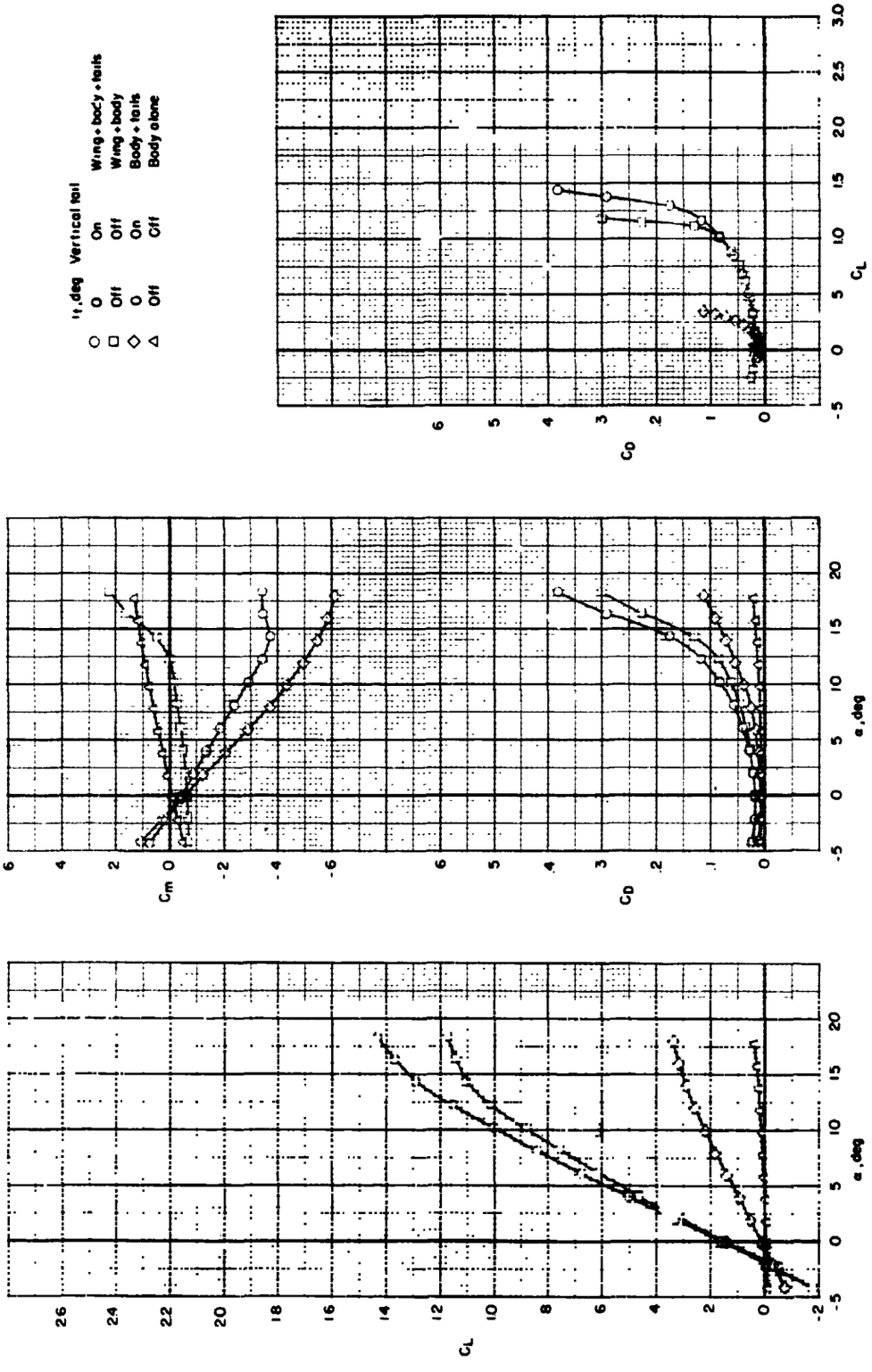

Figure 5.- Aerodynamic characteristics of the basic complete model and its components.

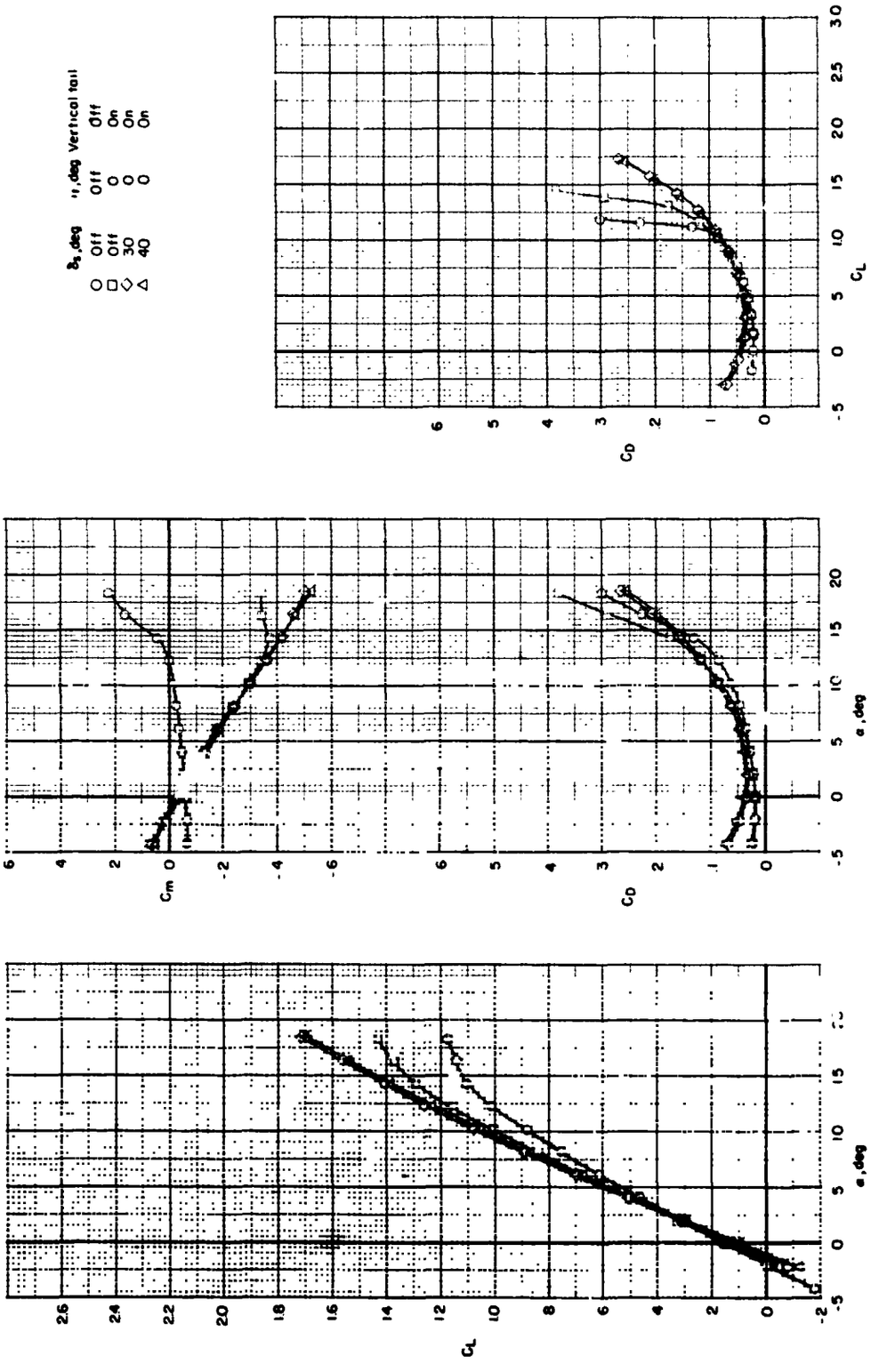

Figure 6.- Effect of leading-edge slat on the longitudinal aerodynamic characteristics of the basic model.

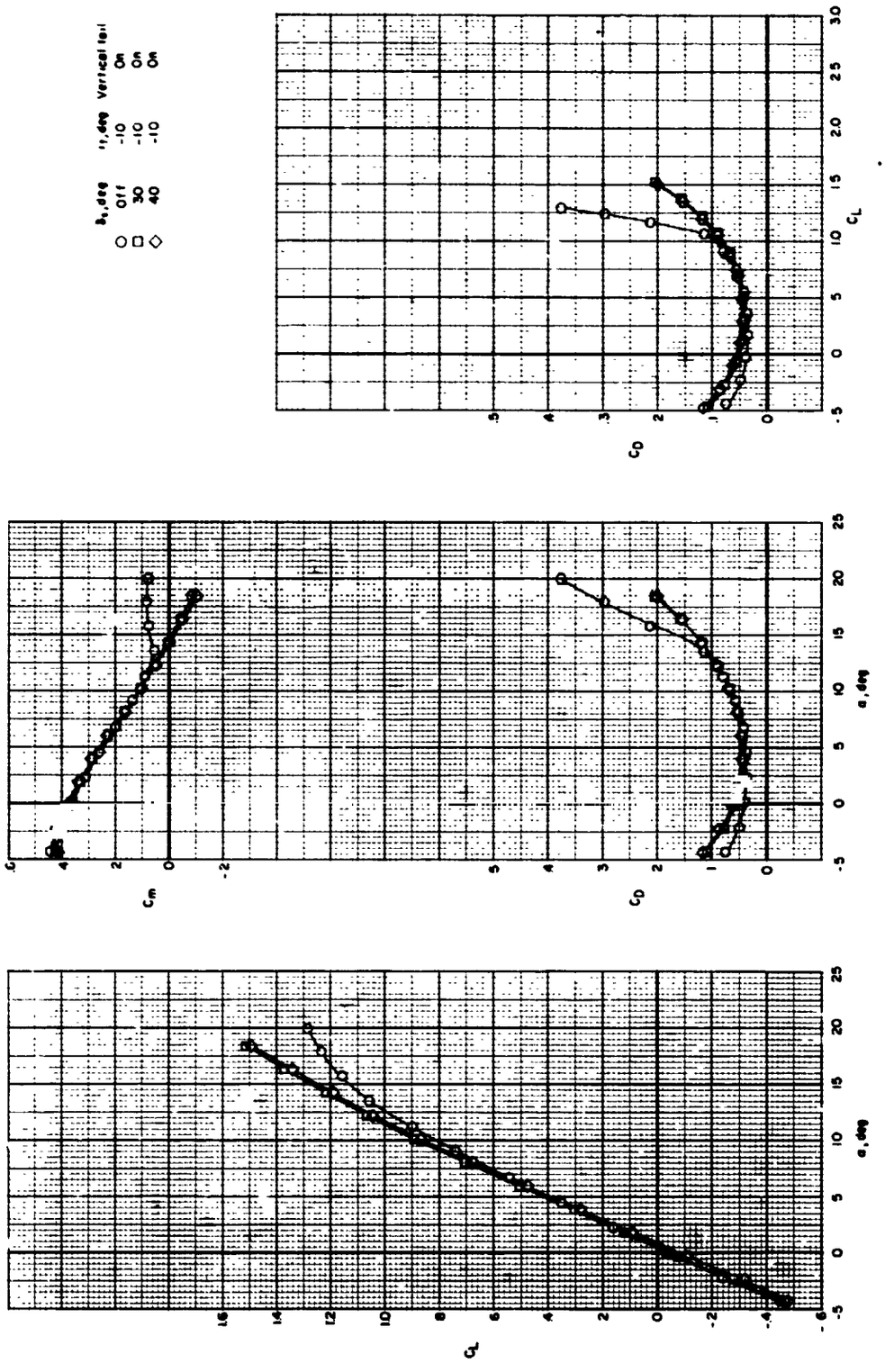

(a) $\delta_f = 0^o$.

Figure 7.- Effect of leading-edge slat deflection on longitudinal aerodynamic characteristics of complete model for several partial-span flap deflection angles (inboard and center). $i_t = -10^o$.

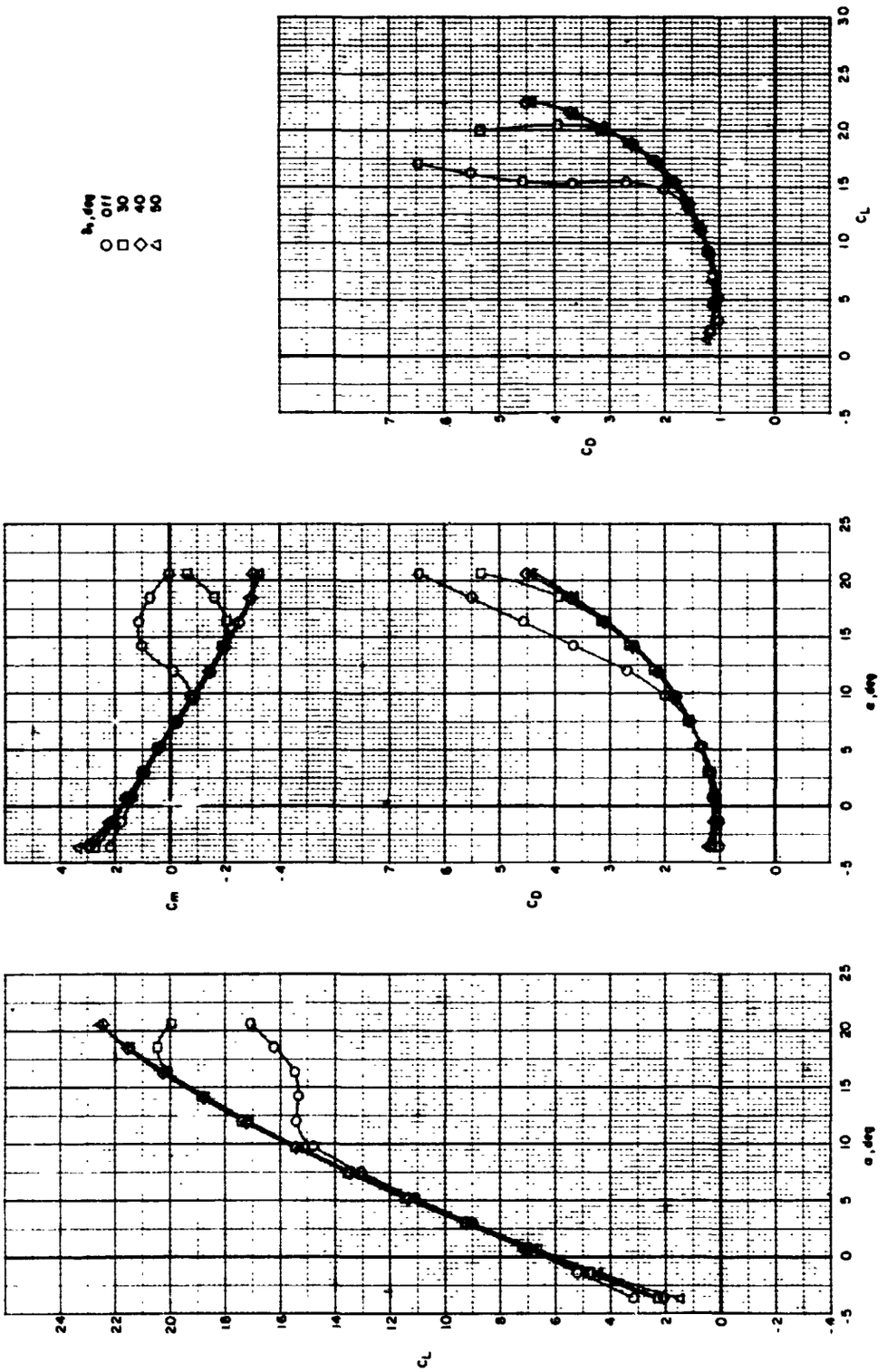

(b) $\delta_f = 20^o$.

Figure 7.- Continued.

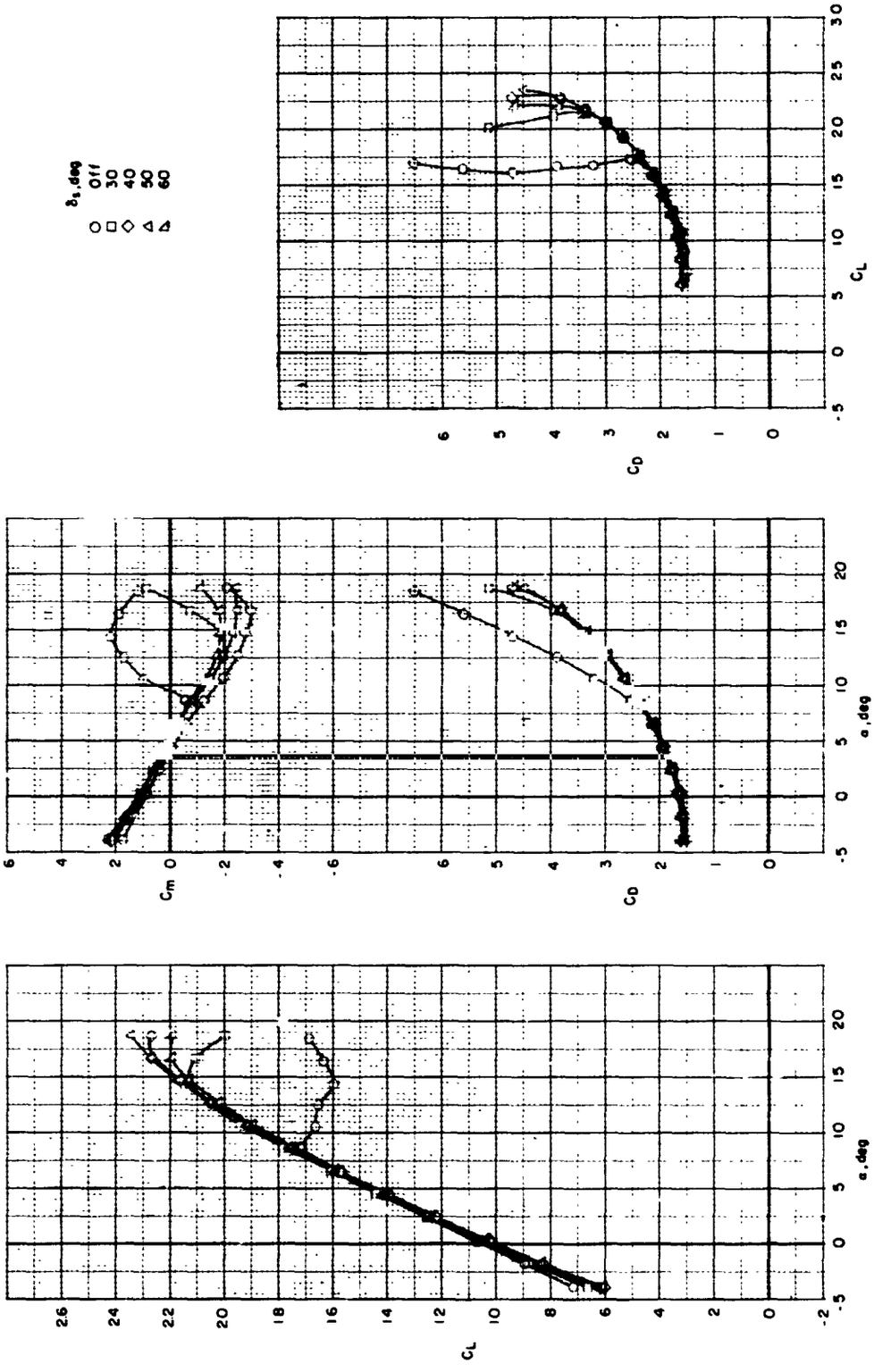

(c) $\delta_f = 30^o$.

Figure 7.- Continued.

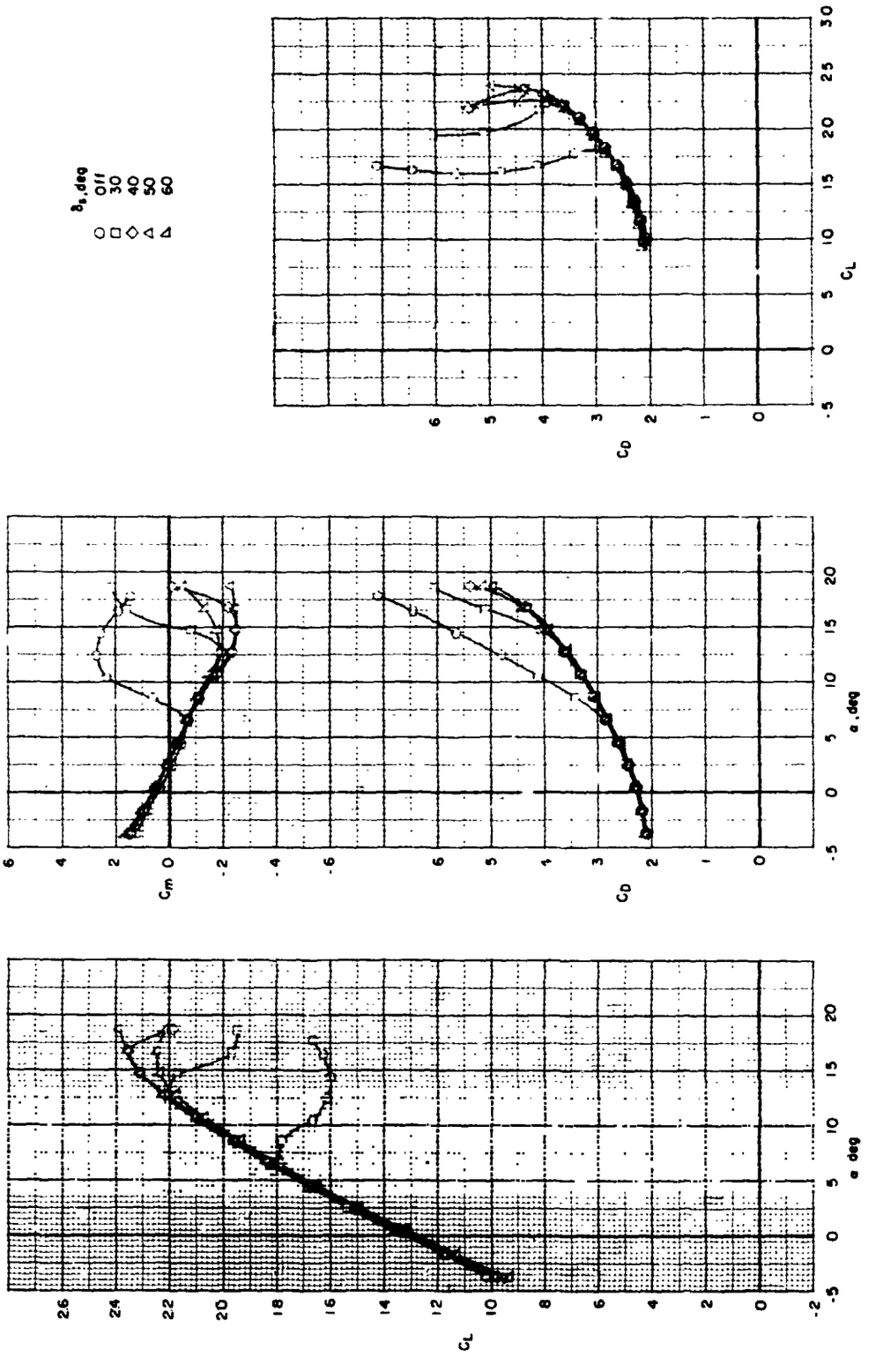

(d) $\delta_f = 40^o$.

Figure 7.- Continued.

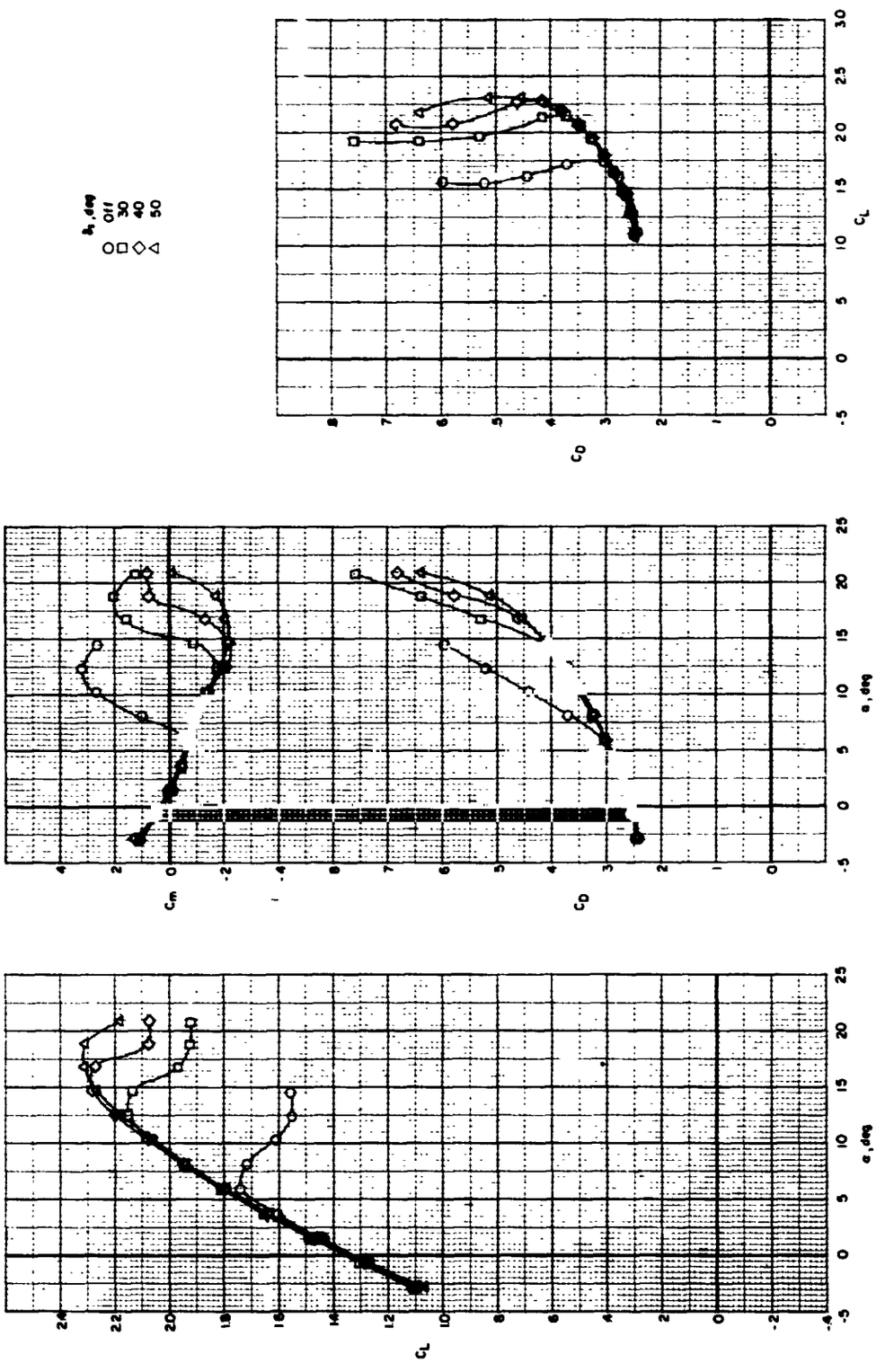

(e) $\delta_f = 45°$.

Figure 7.- Continued.

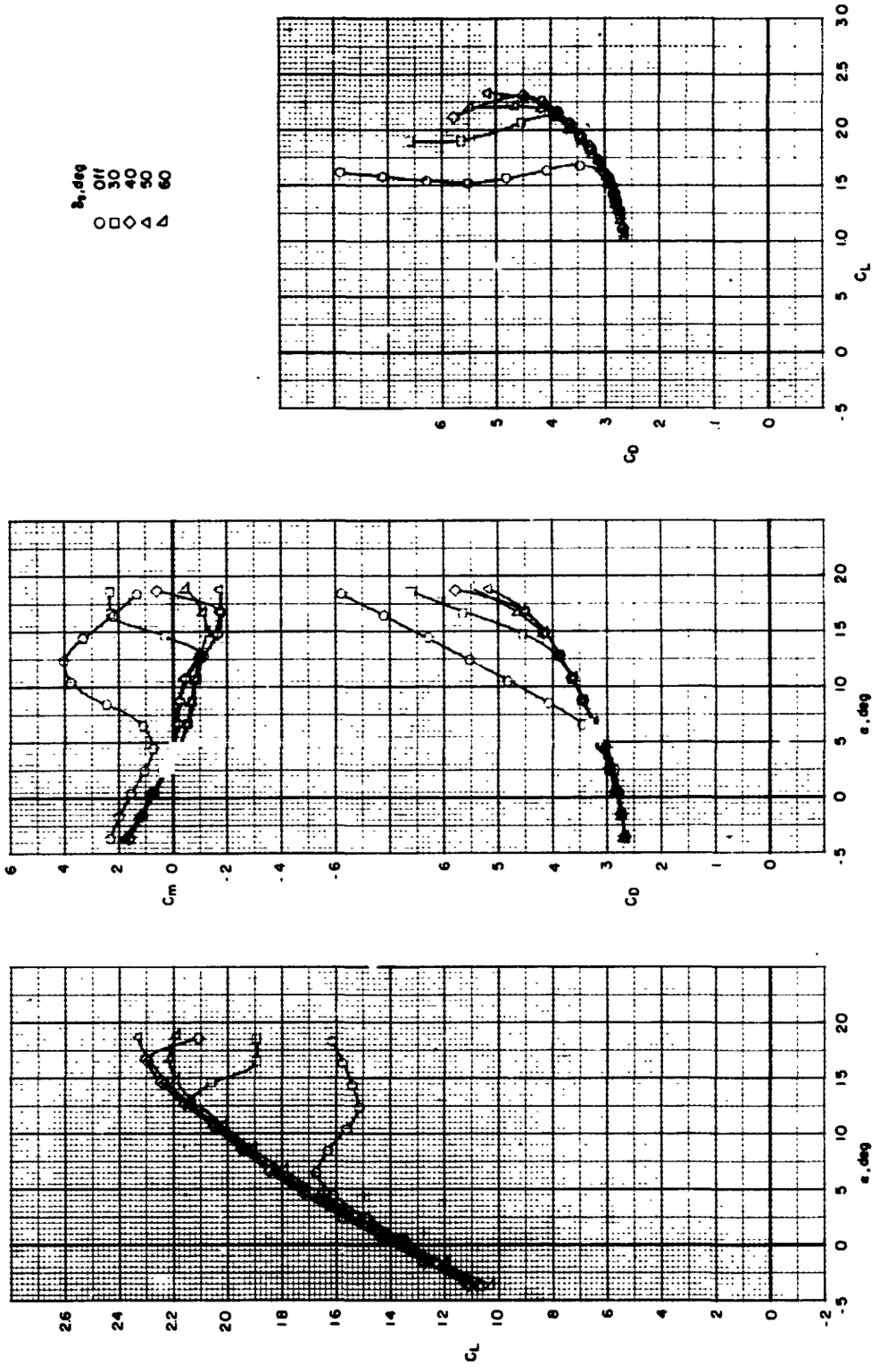

(f) $\delta_f = 50^o$.

Figure 7.- Continued.

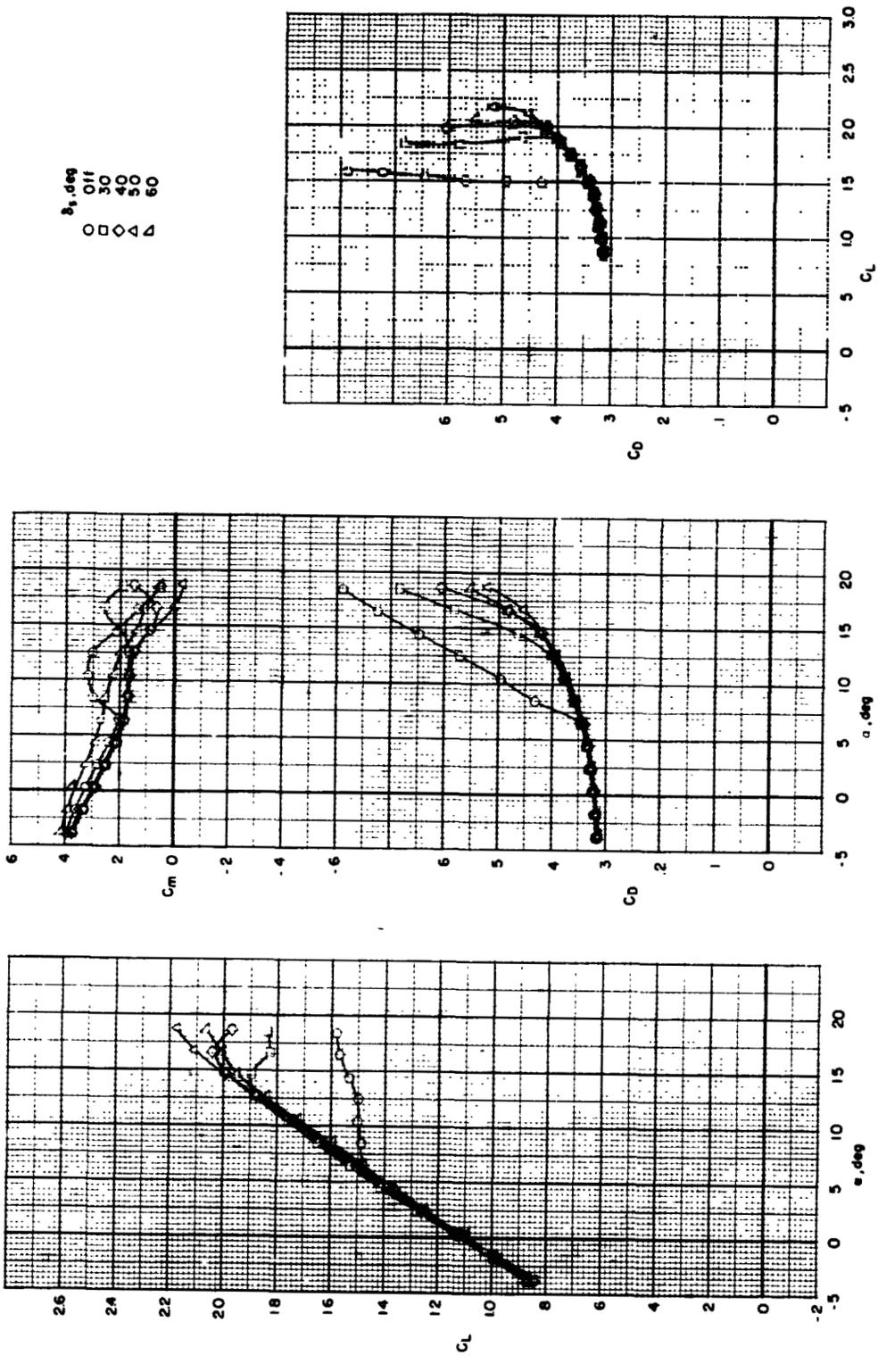

(g) $\delta_f = 60°$.

Figure 7.- Concluded.

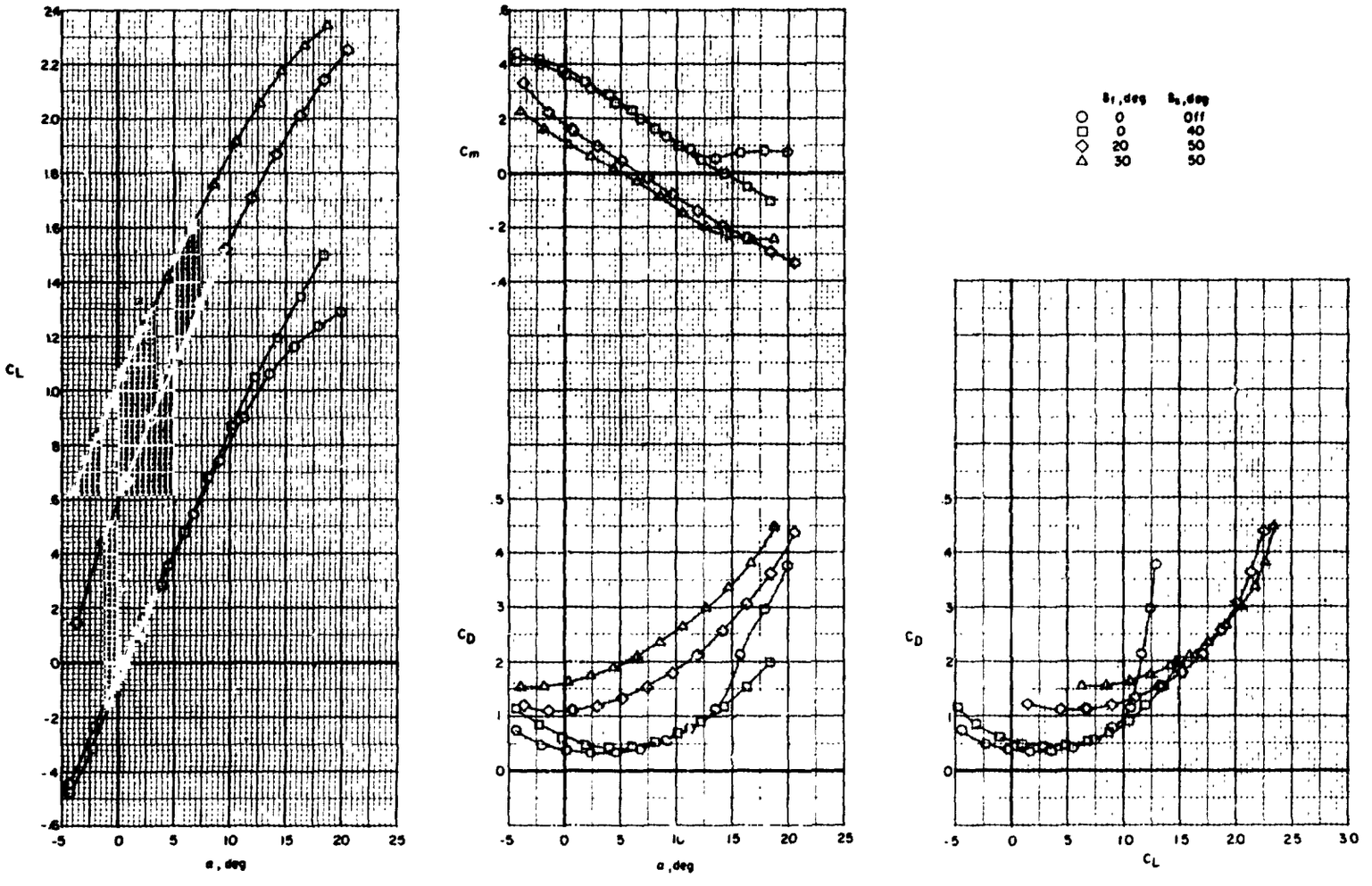

(a) Various δ_s.

Figure 8.- Effect of partial-span flap deflection (inboard and center) on longitudinal aerodynamic characteristics for several leading-edge slat deflections. $i_t = -10^o$; vertical tail on.

(b) $\delta_s = 50^o$.

Figure 8.- Concluded.

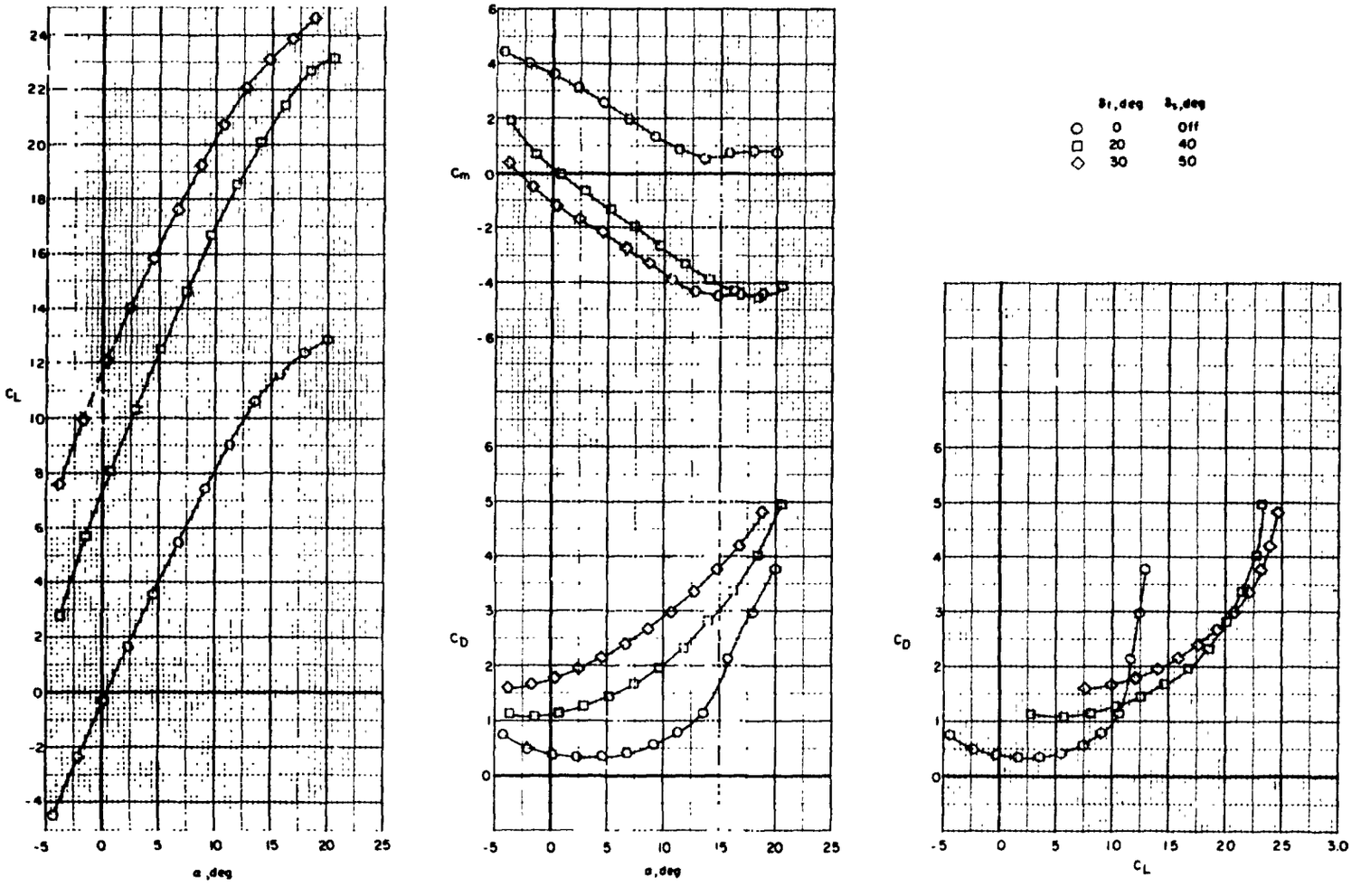

(a) Various δ_s.

Figure 9.- Effect of full-span flap deflection on longitudinal aerodynamic characteristics for several leading-edge slat deflections. $i_t = -10^o$; vertical tail on.

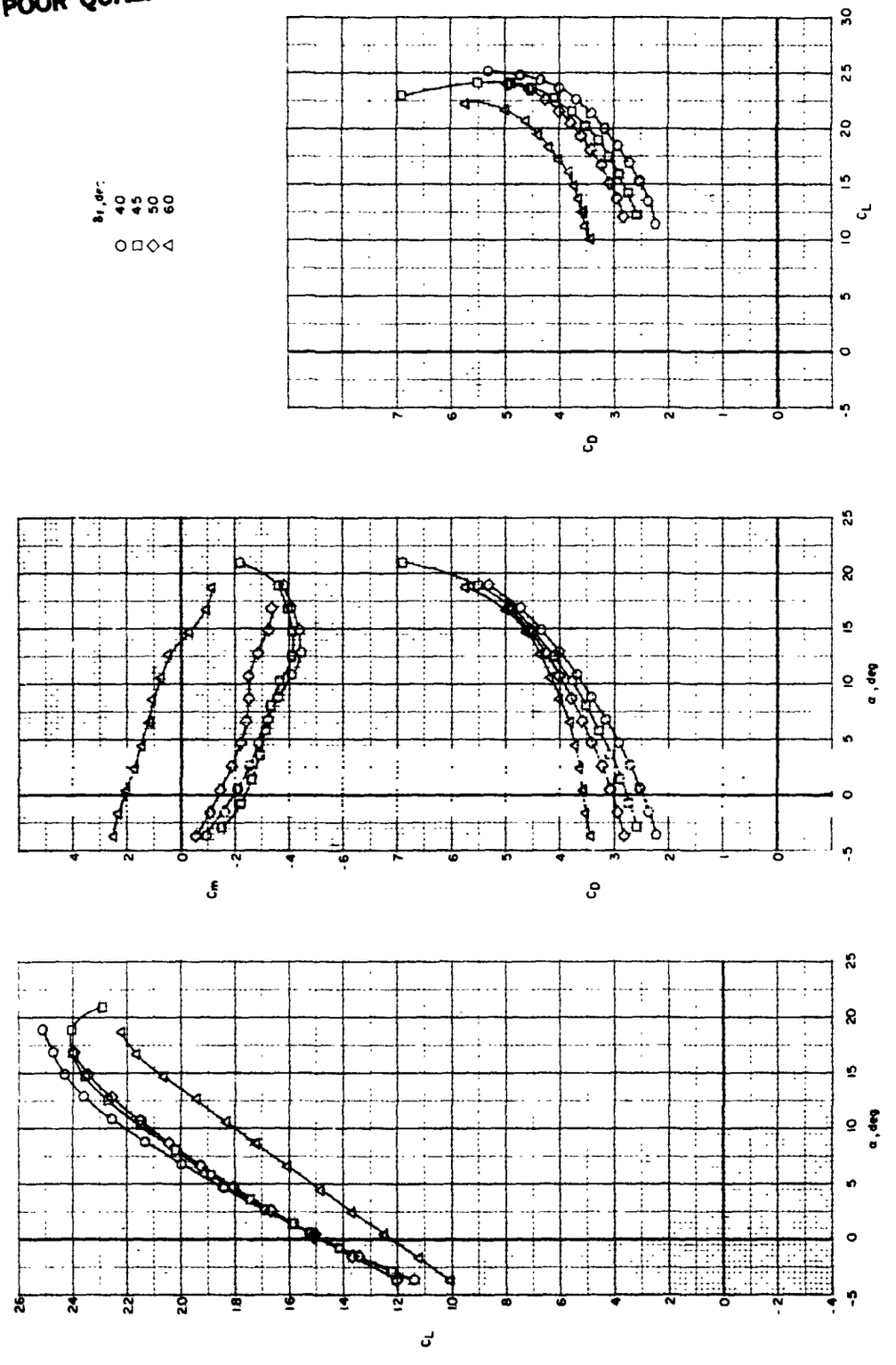

(b) $\delta_s = 50^o$.

Figure 9.- Concluded.

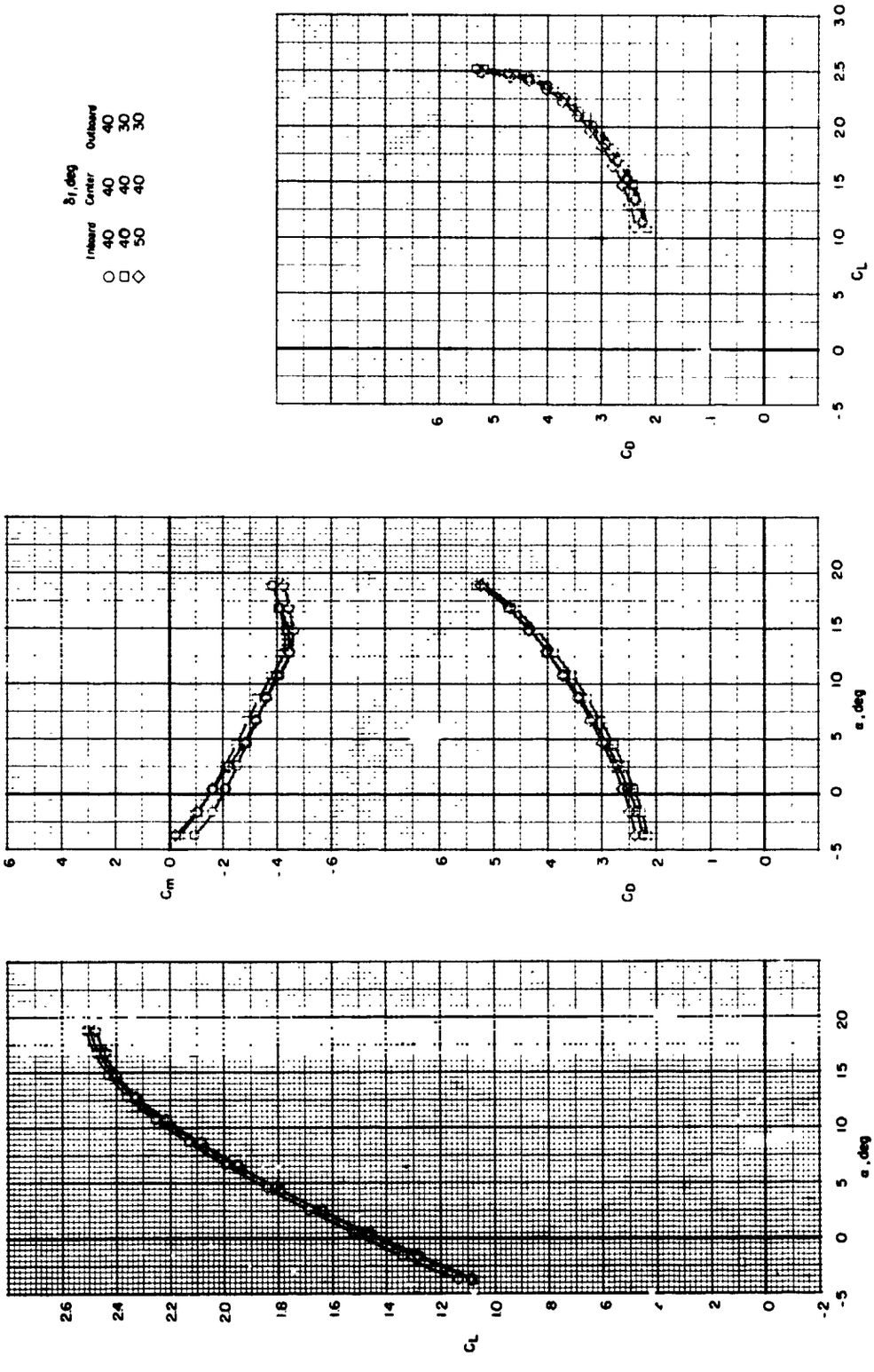

Figure 10.- Effect of spanwise variation in flap deflection on longitudinal aerodynamic characteristics of complete model for full-span flap with leading-edge slat deflected 50°. $i_t = -10°$.

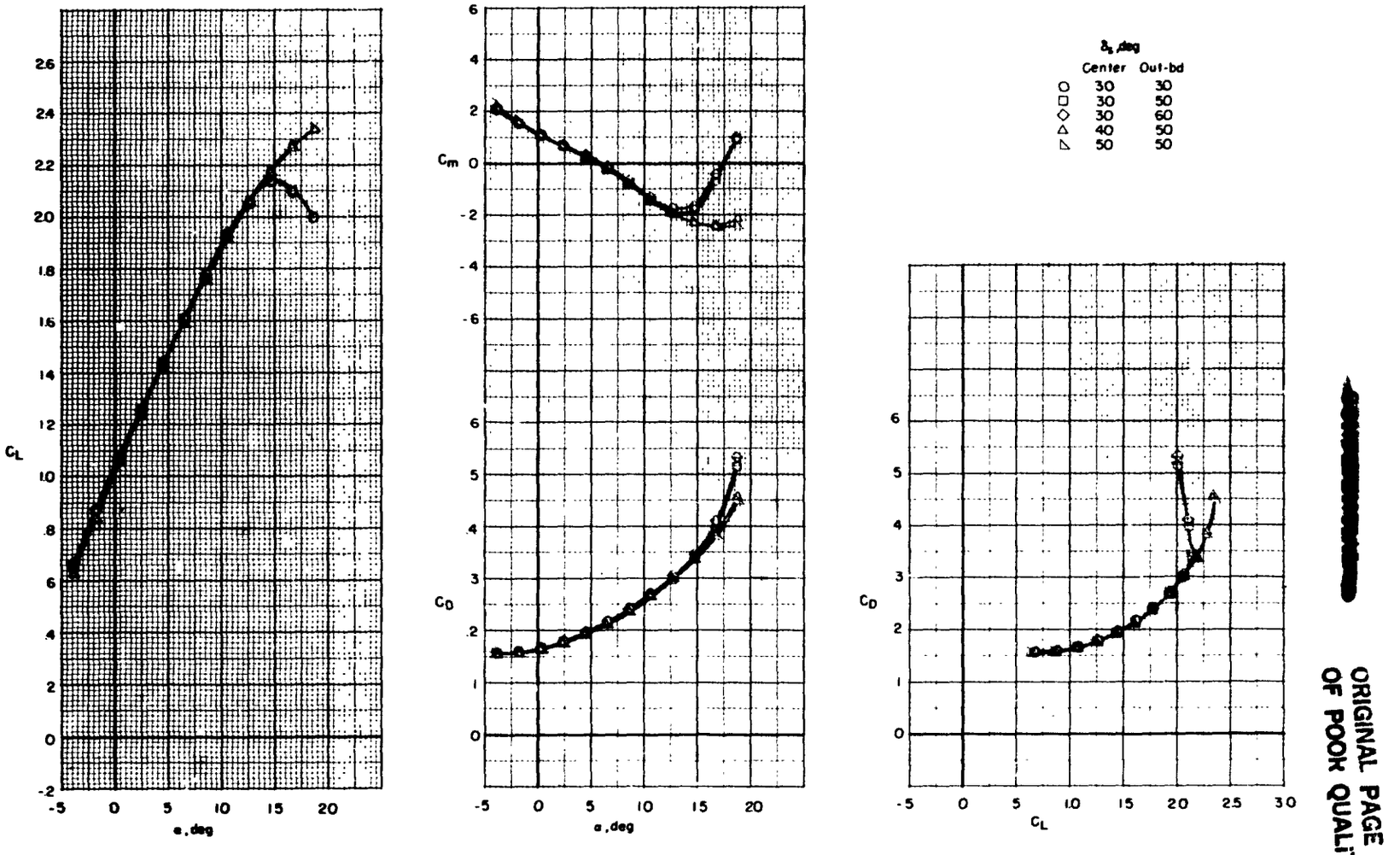

(a) $\delta_f = 30^o$.

Figure 11.- Effect of spanwise variation in leading-edge slat deflection on longitudinal aerodynamic characteristics of complete model for several partial-span flap deflections (inboard and center). $i_t = -10^o$.

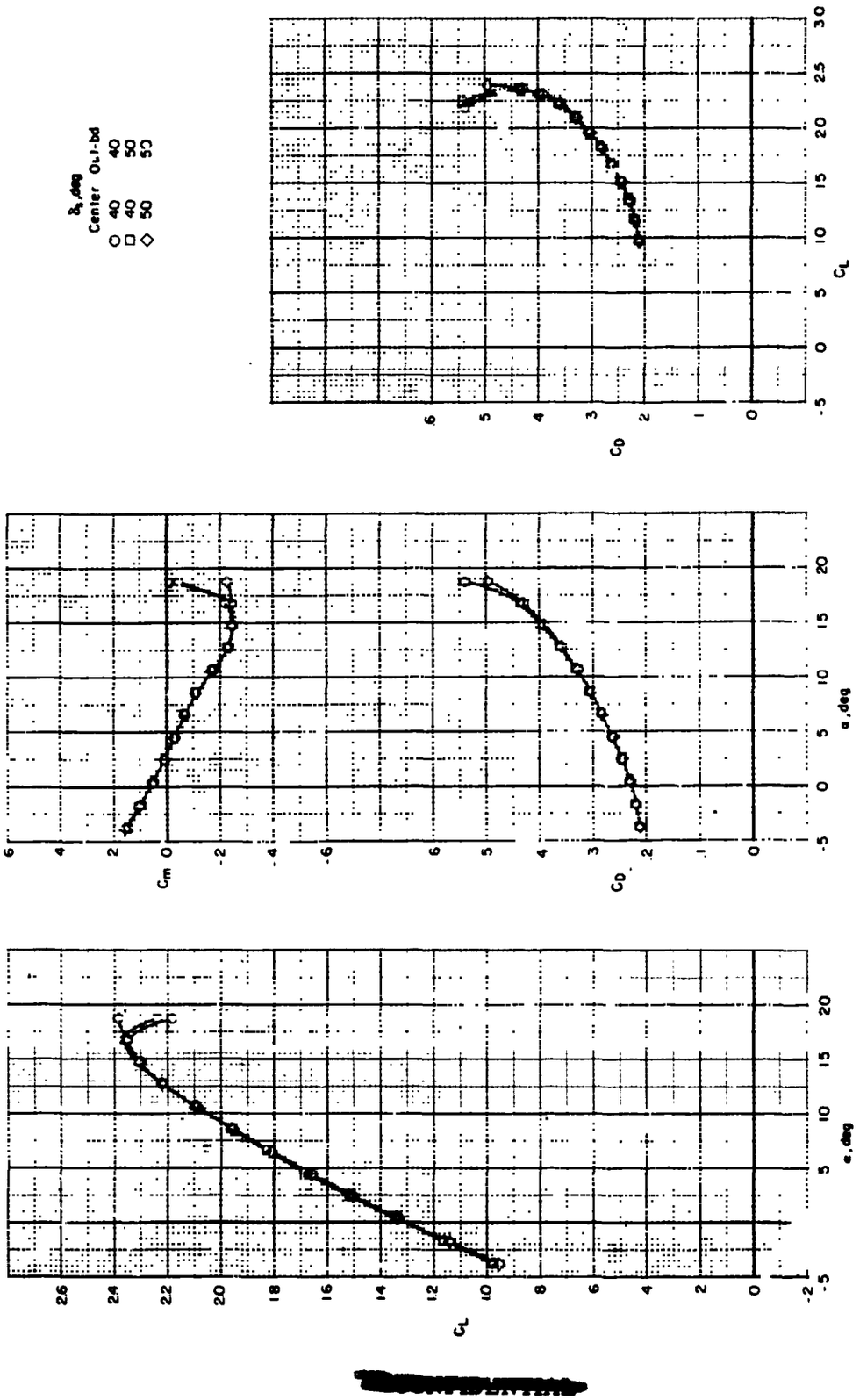

(b) $\delta_f = 40^o$.

Figure 11.- Continued.

ORIGINAL PAGE IS
OF POOR QUALITY

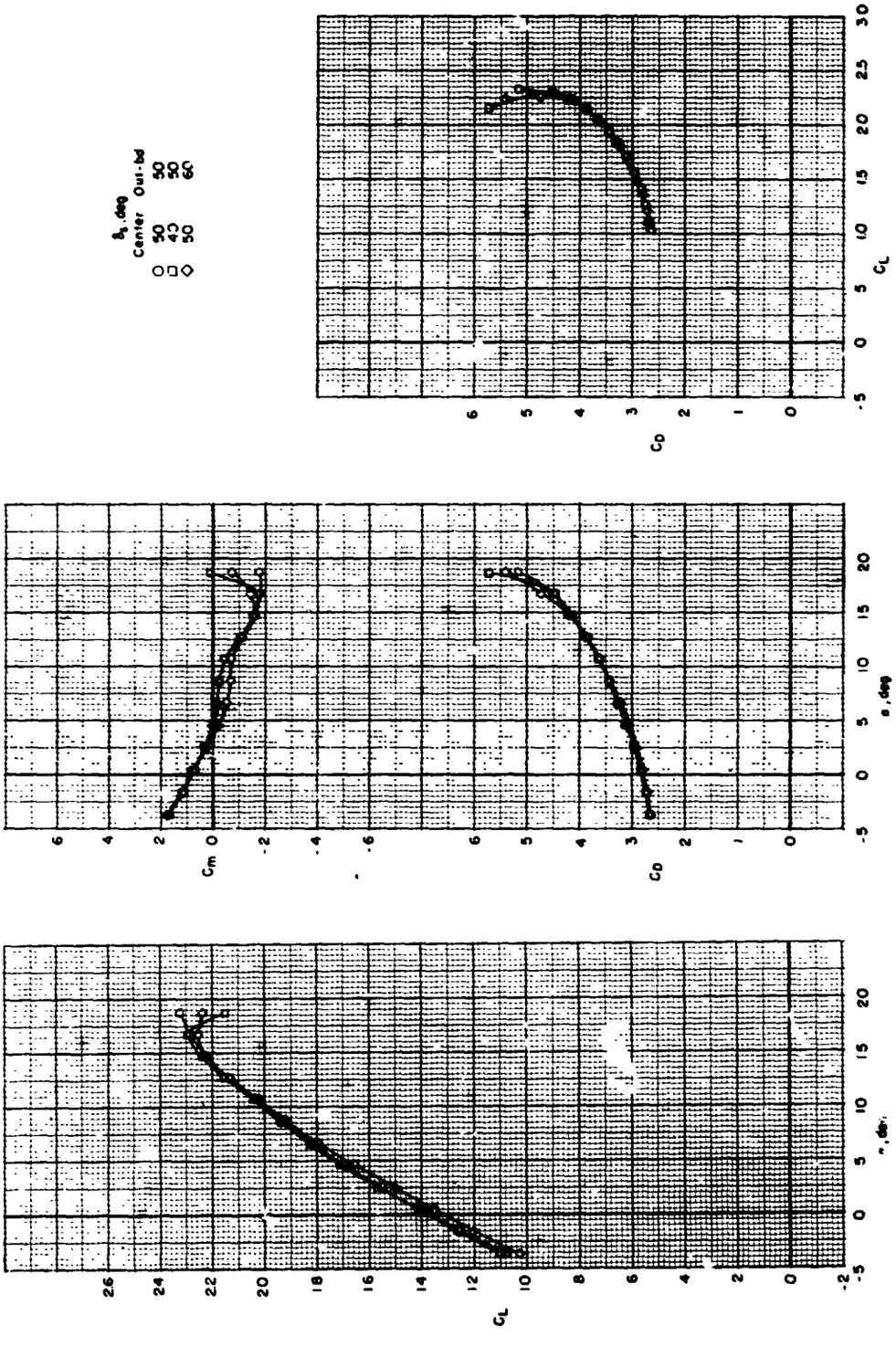

(c) $\delta_f = 50^o$.

Figure 11.- Concluded.

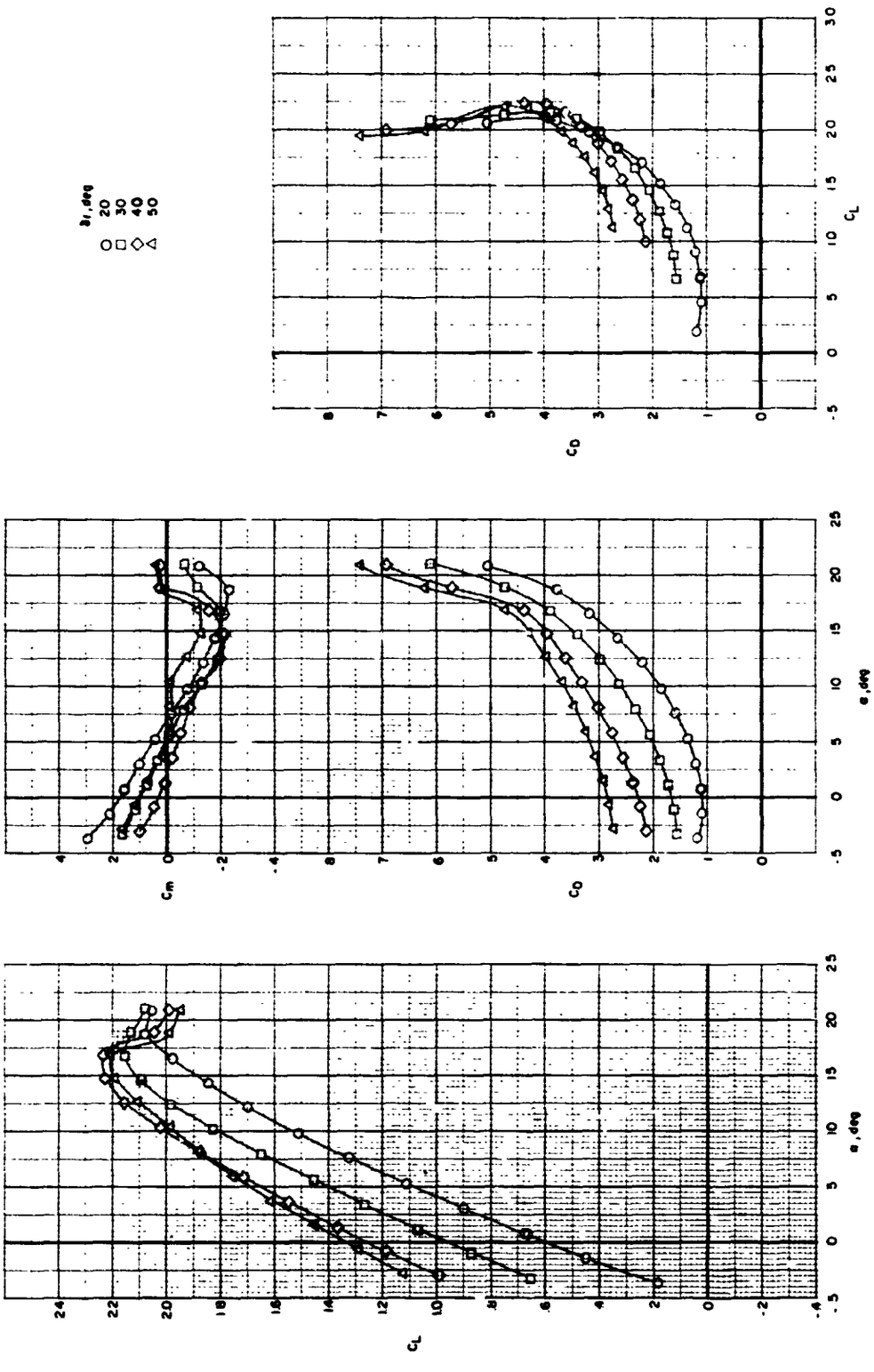

(a) $\delta_s = 40^o$.

Figure 12.- Effect of partial-span flap deflection (inboard and center) on longitudinal aerodynamic characteristics of complete model for several leading-edge slat deflections of the modified airfoil slat. $i_t = -10^o$.

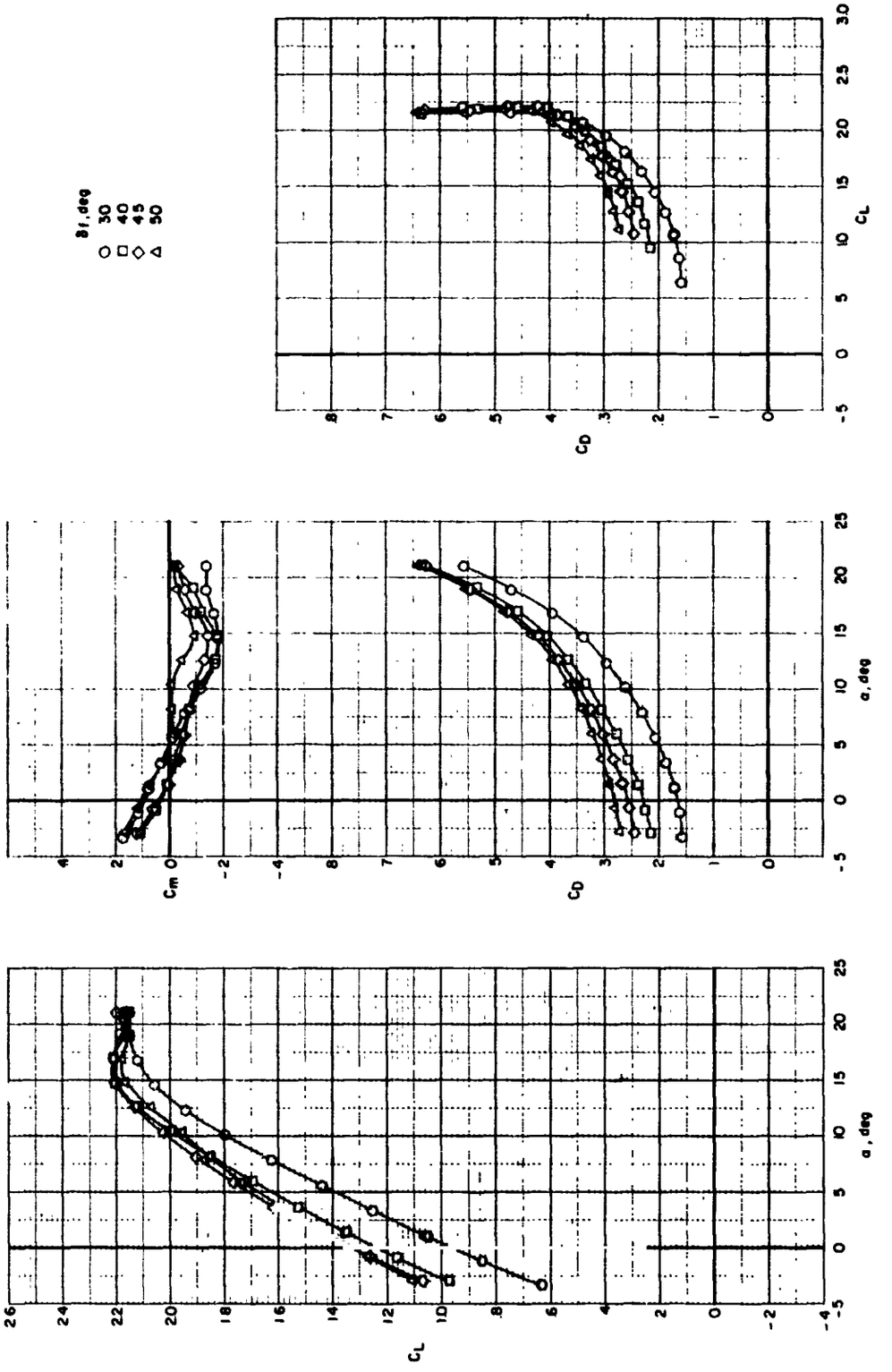

(b) $\delta_s = 50^o$.

Figure 12.- Concluded.

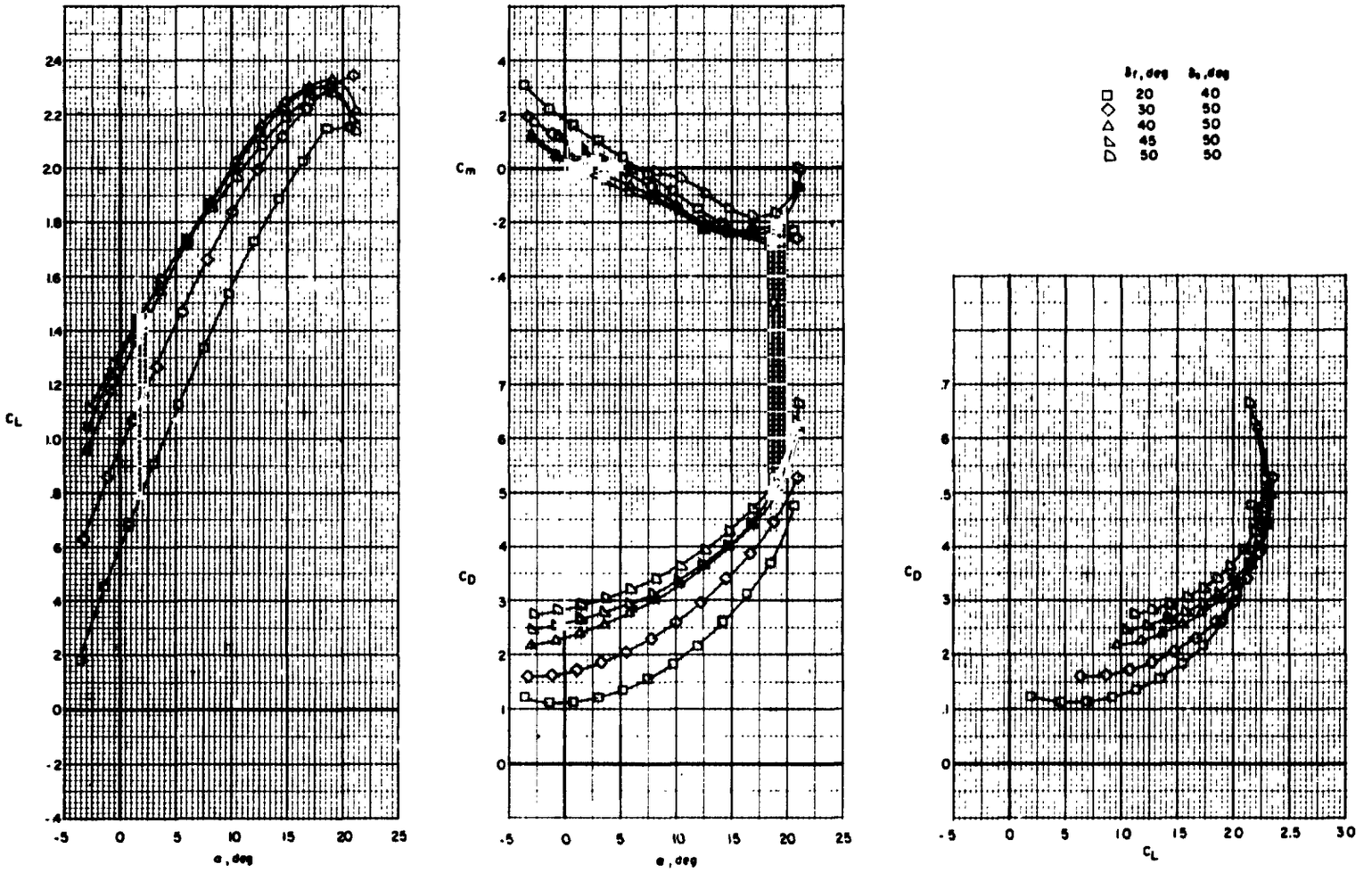

(a) Basic St. Cyr slat.

Figure 13.- Effect of partial-span flap deflection (inboard and center) on longitudinal aerodynamic characteristics of complete model with the outboard slat extended from 0.15c to 0.20c for two slat configurations. $i_t = -10^o$.

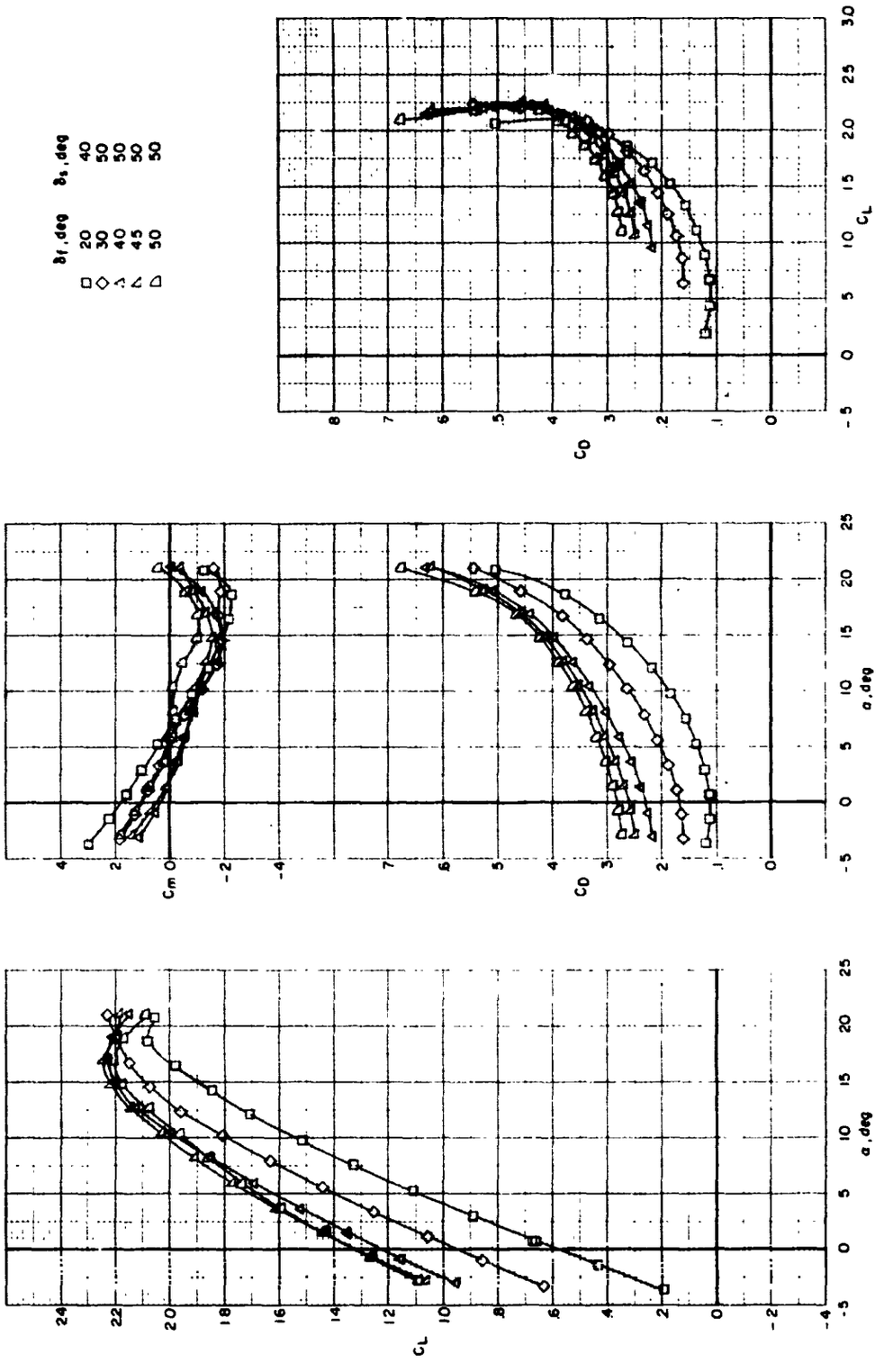

(b) Modified airfoil slat.

Figure 13.- Concluded.

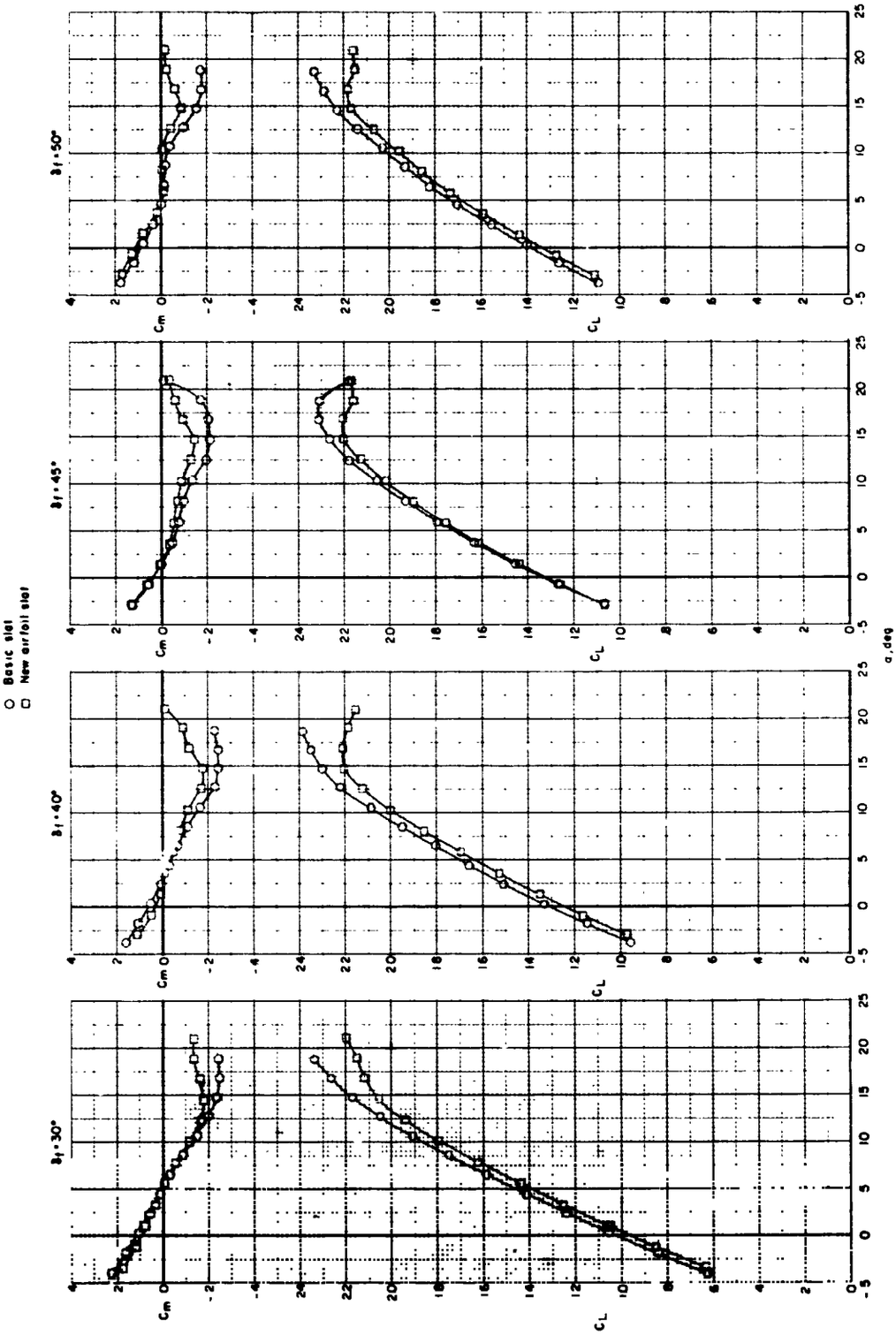

(a) 0.15c slat.

Figure 14.- Comparison of longitudinal aerodynamic characteristics of complete model with basic St. Cyr and modified airfoil slat with and without slat tip chord extension for several partial-span flap deflections and $\delta_s = 50^\circ$. $i_t = -10^\circ$.

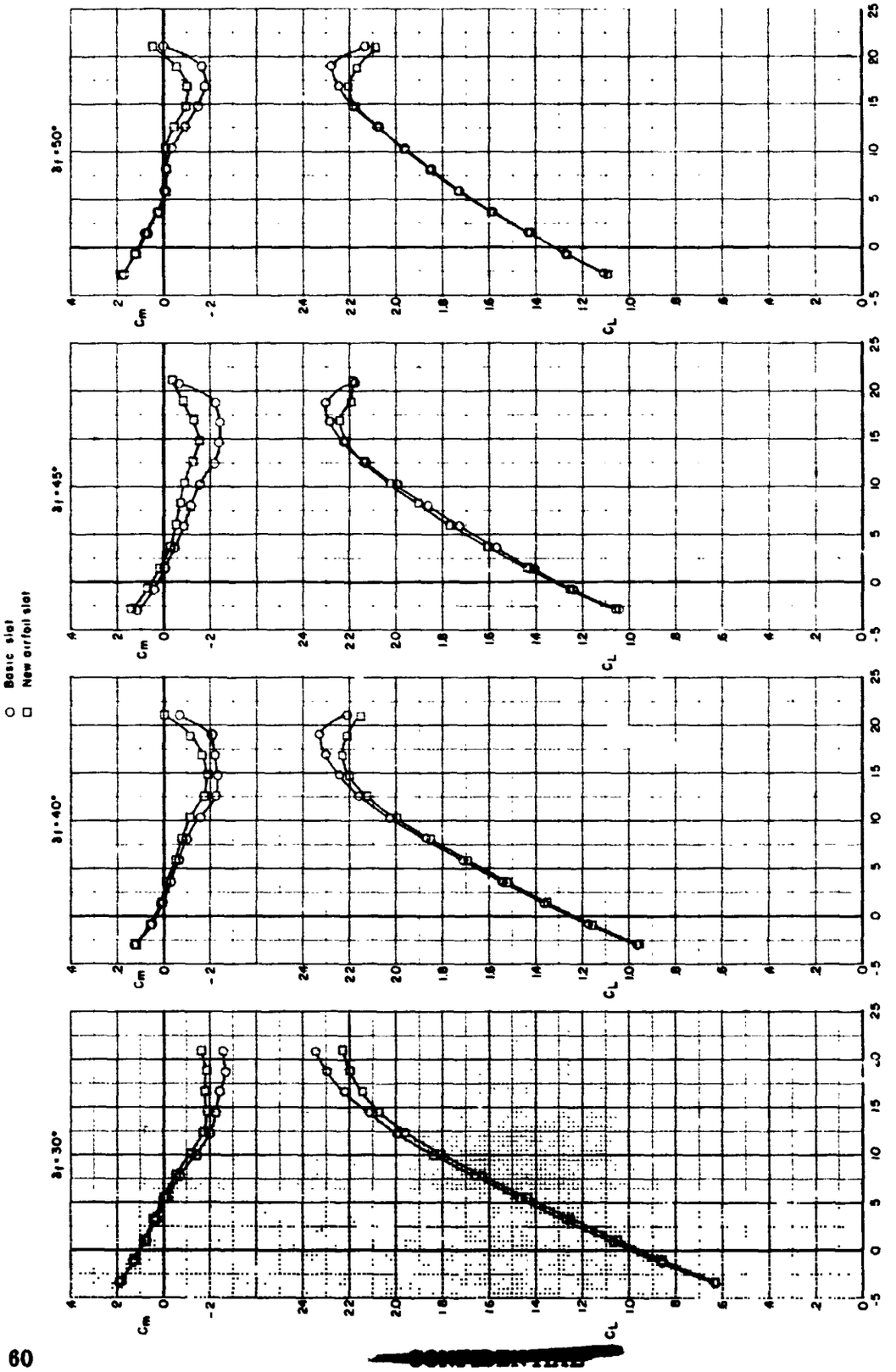

(b) 0.15c slat with 0.20c tip slat.

Figure 14.- Concluded.

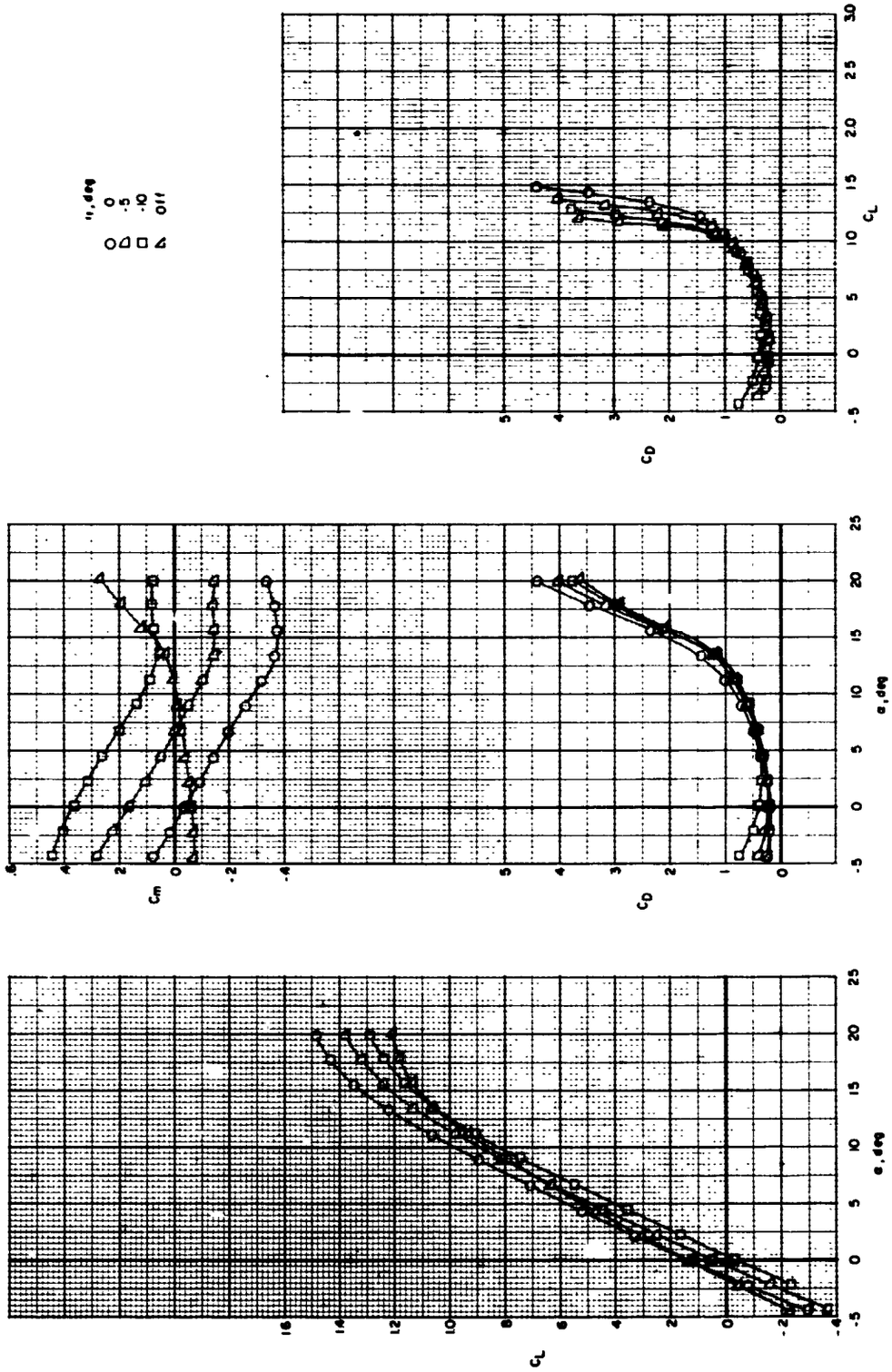

(a) $\delta_f = 0^o$; δ_s = Off.

Figure 15.- Longitudinal stability and control characteristics of complete model for several partial-span flap deflections (inboard and center) and leading-edge slat deflections.

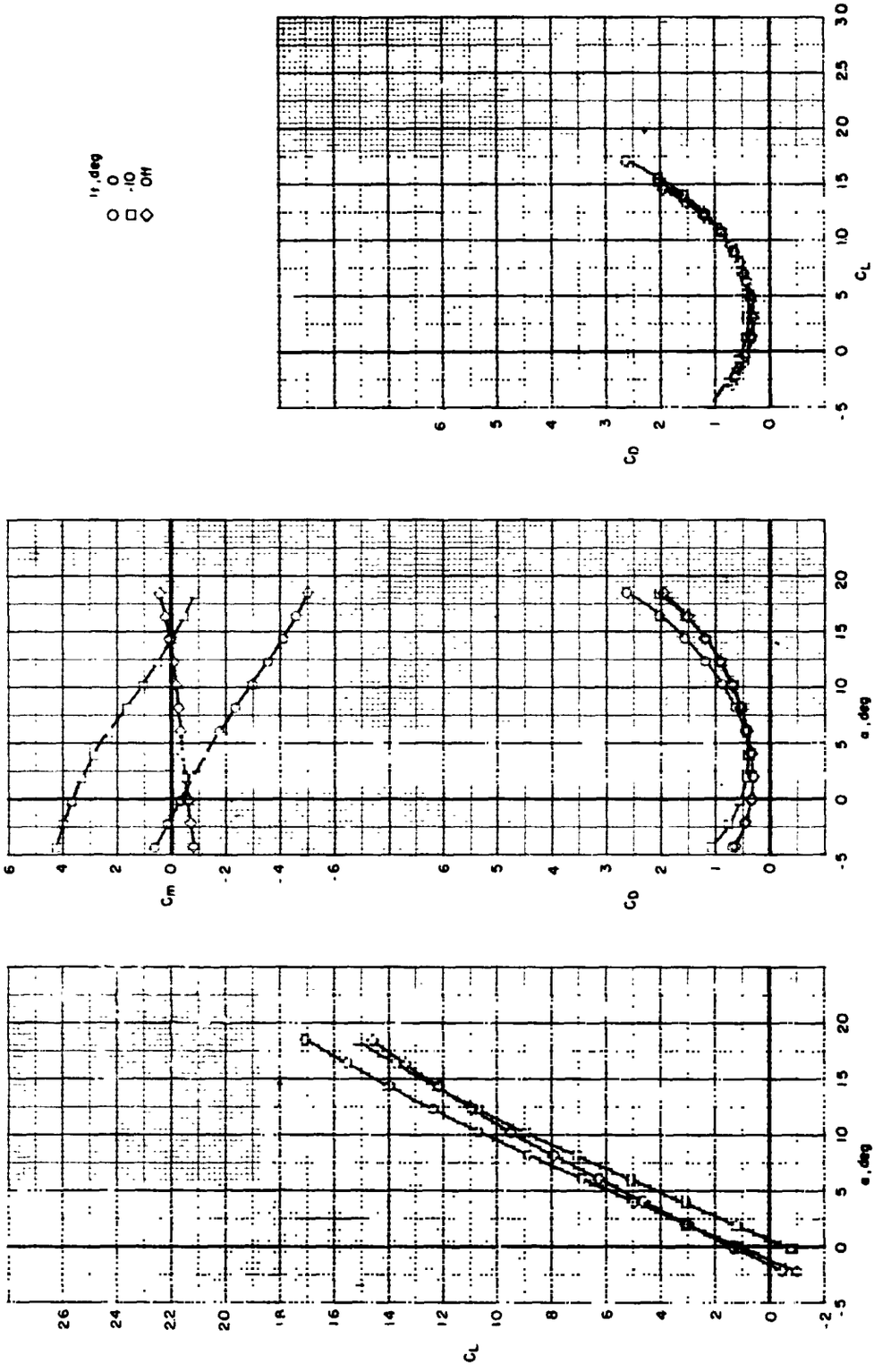

(b) $\delta_f = 0^o$; $\delta_s = 30^o$.

Figure 15.- Continued.

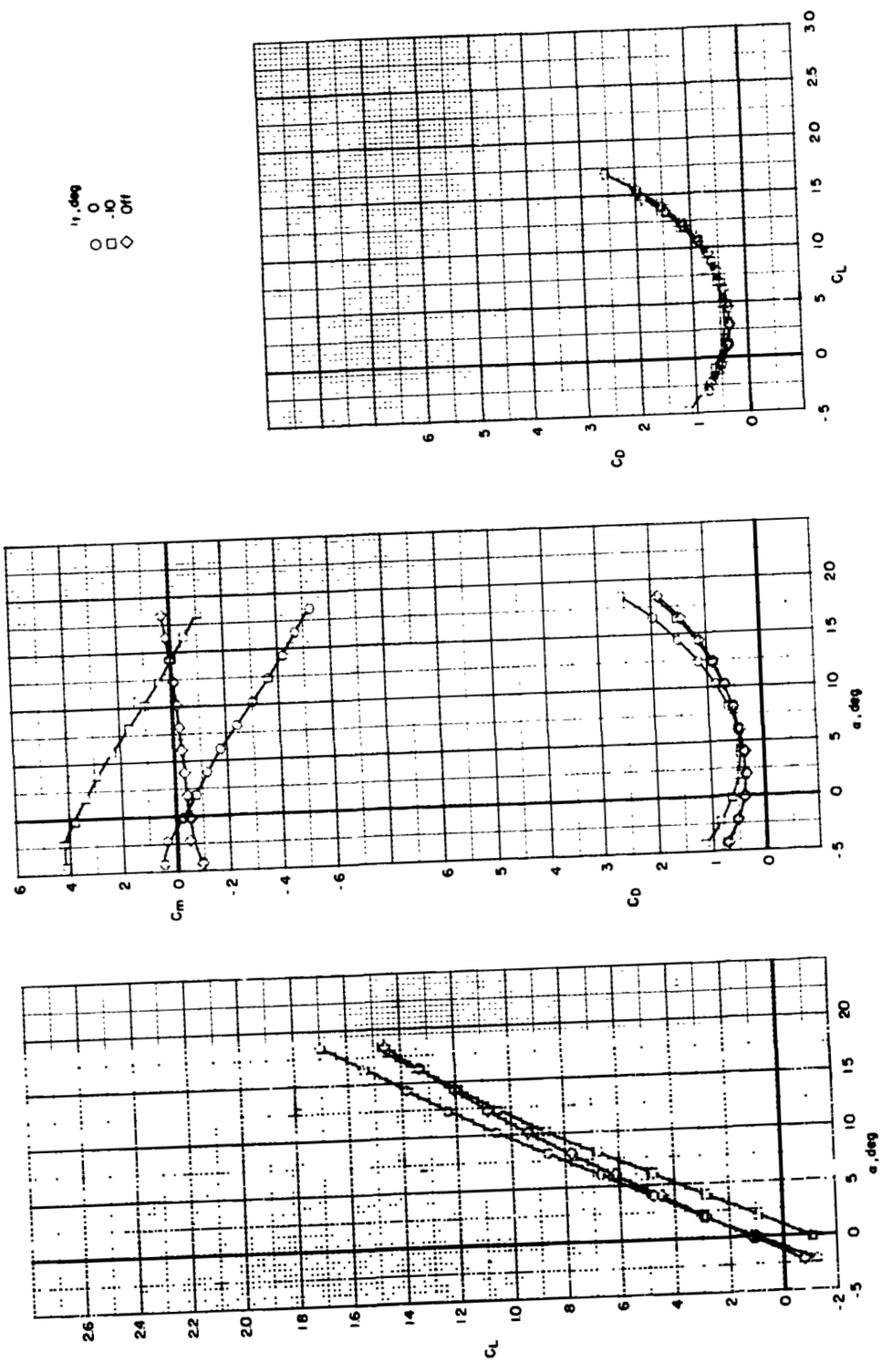

(c) $\delta_f = 0^o$; $\delta_s = 40^o$.

Figure 15.- Continued.

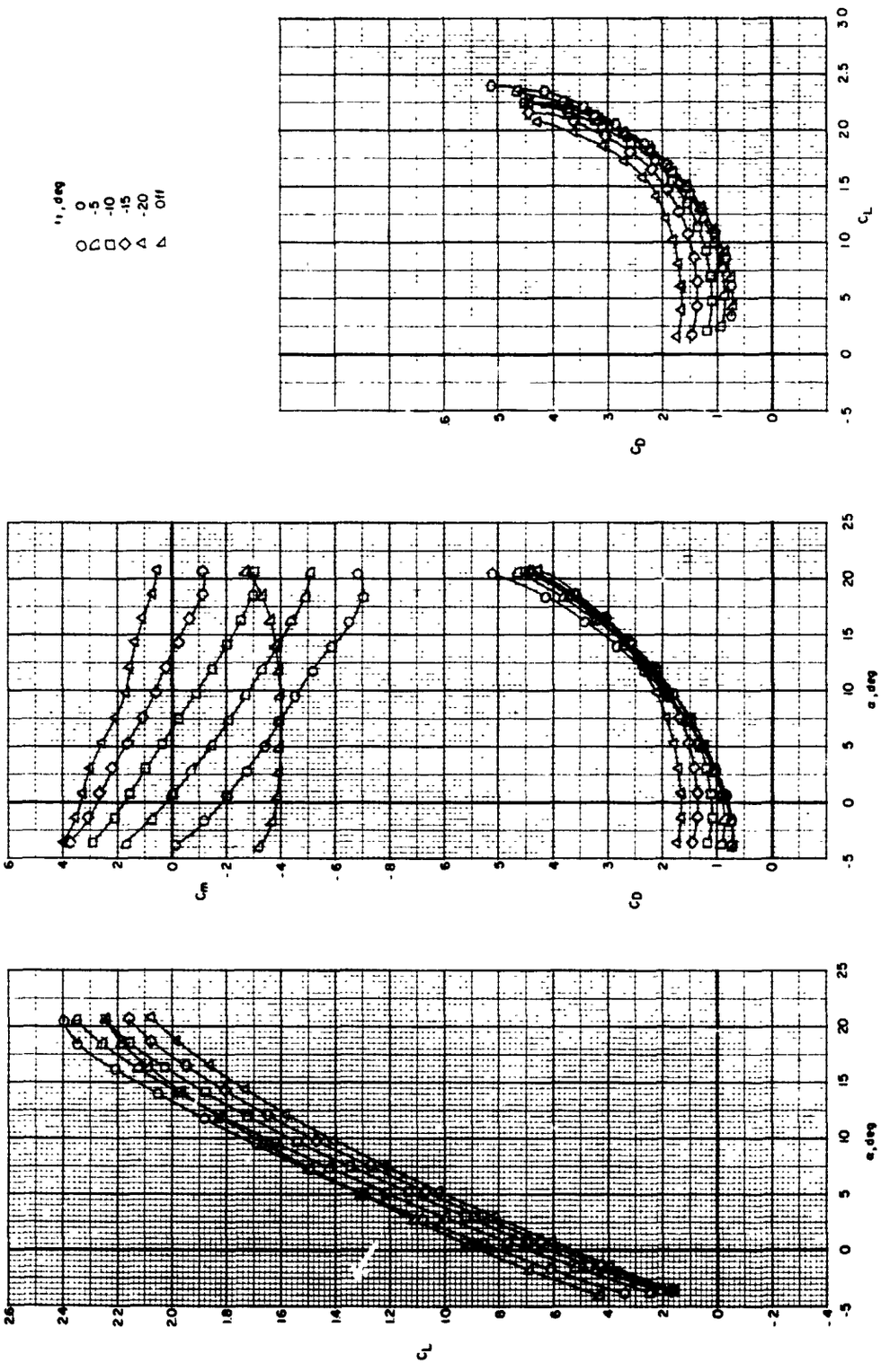

(d) $\delta_f = 20^o$; $\delta_s = 40^o$.

Figure 15.- Continued.

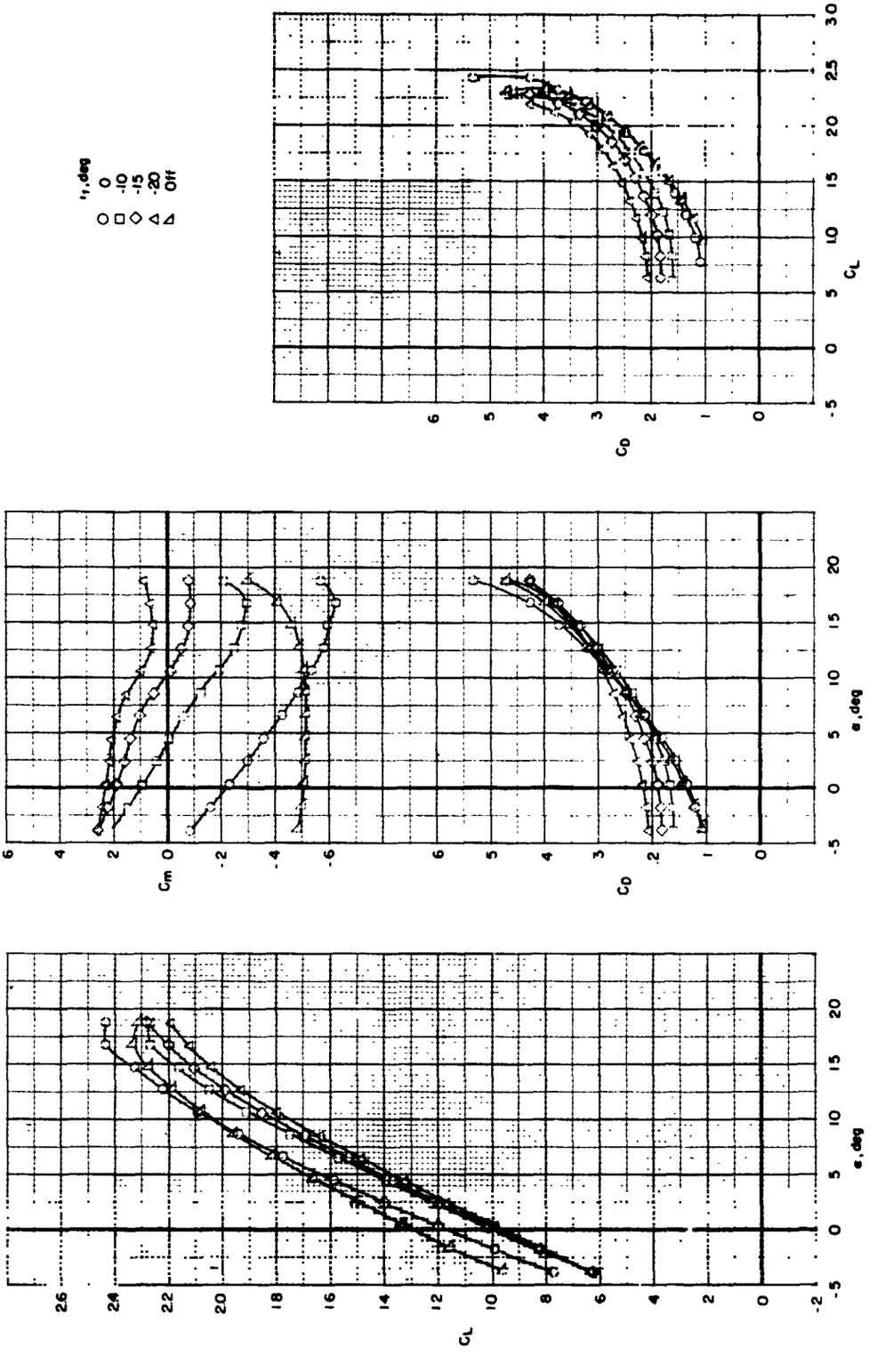

(e) $\delta_f = 30°$; $\delta_s = 40°$.

Figure 15.- Continued.

(f) $\delta_f = 30^o$; $\delta_s = 50^o$.

Figure 15.- Continued.

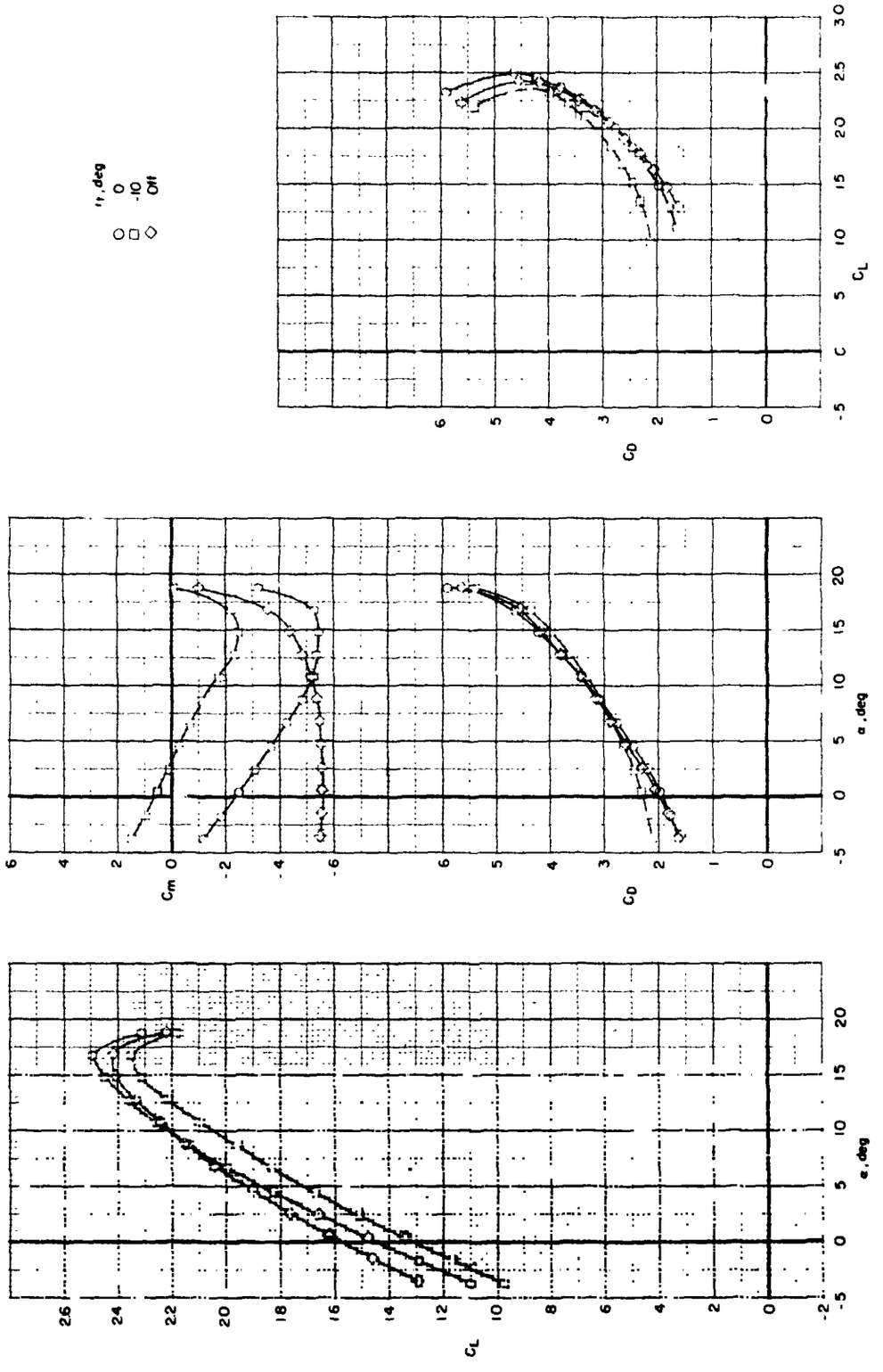

(g) $\delta_f = 40^o$; $\delta_s = 40^o$.

Figure 15.- Continued.

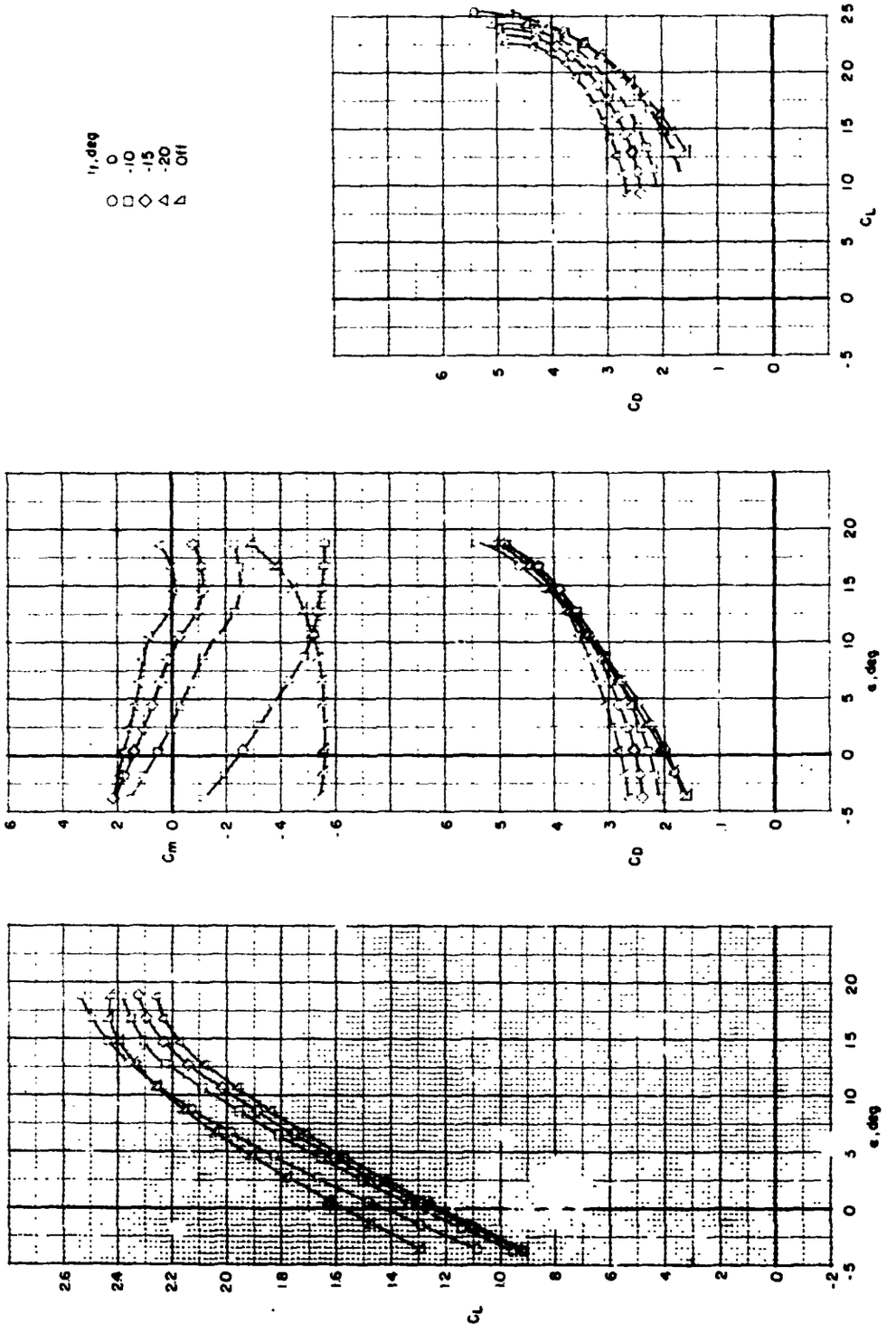

(h) $\delta_f = 40^o$; $\delta_s = 50^o$.

Figure 15.- Continued.

(l) $\delta_f = 45^o$; $\delta_s = 50^o$.

Figure 15.- Continued.

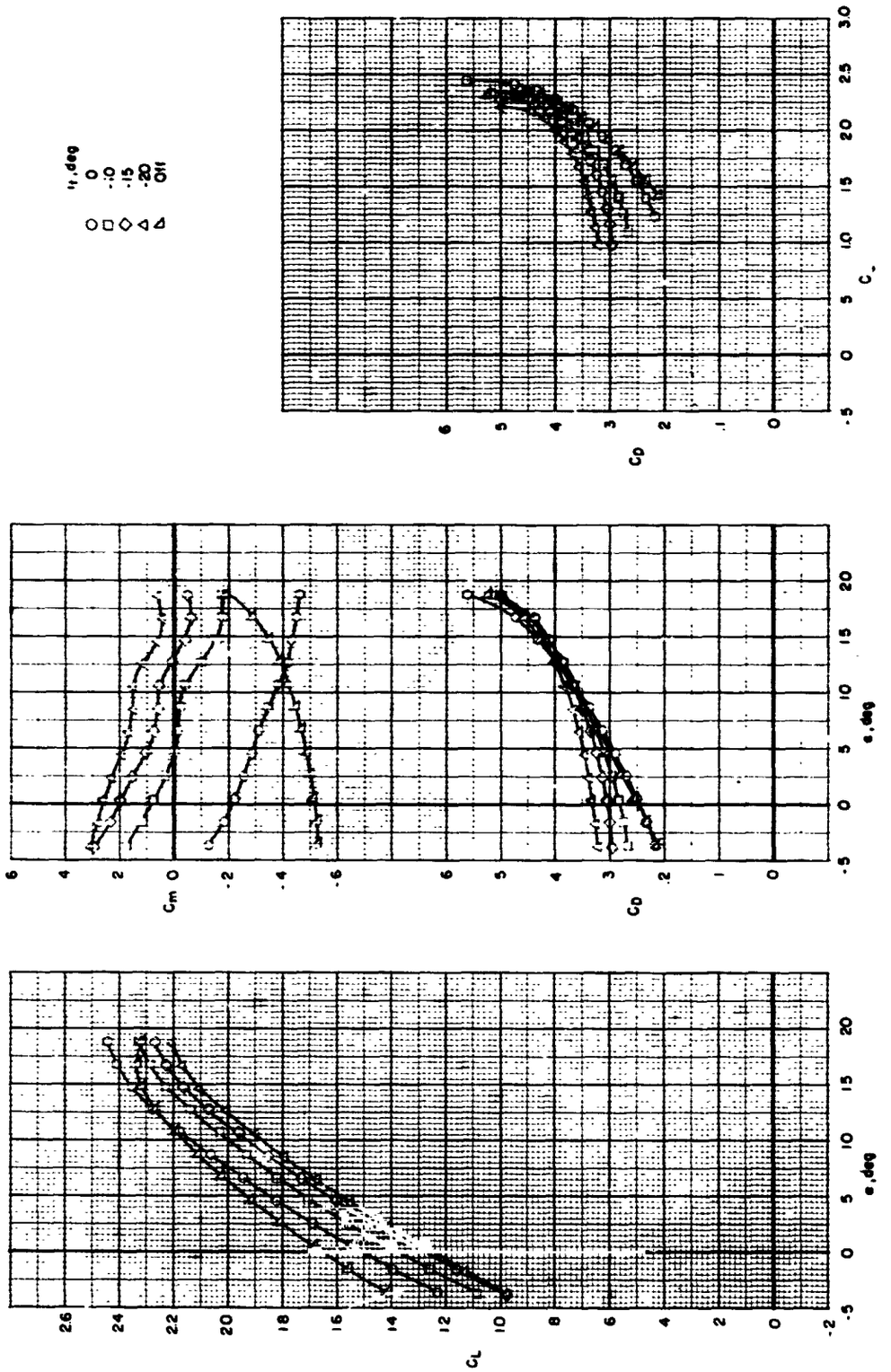

(j) $\delta_f = 50^o$; $\delta_s = 50^o$.

Figure 15.- Continued.

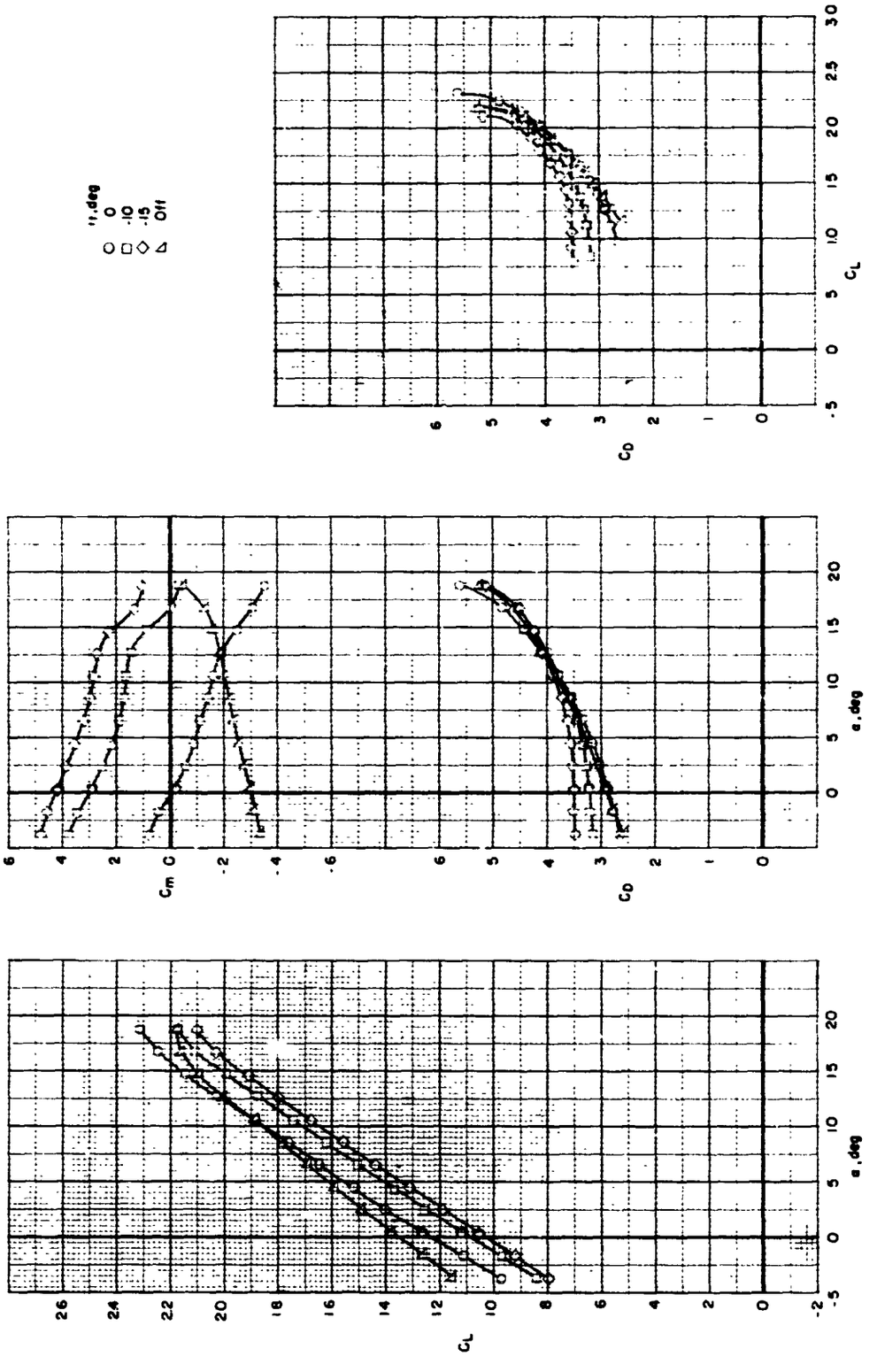

(k) $\delta_f = 60^o$; $\delta_s = 50^o$.

Figure 15.- Concluded.

Figure 16.- Longitudinal stability and control characteristics of complete model for partial-span flap deflected 40° and spanwise variation of leading-edge slat deflections. ($\delta_{s,center}$ = 40°; $\delta_{s,outboard}$ = 50°.)

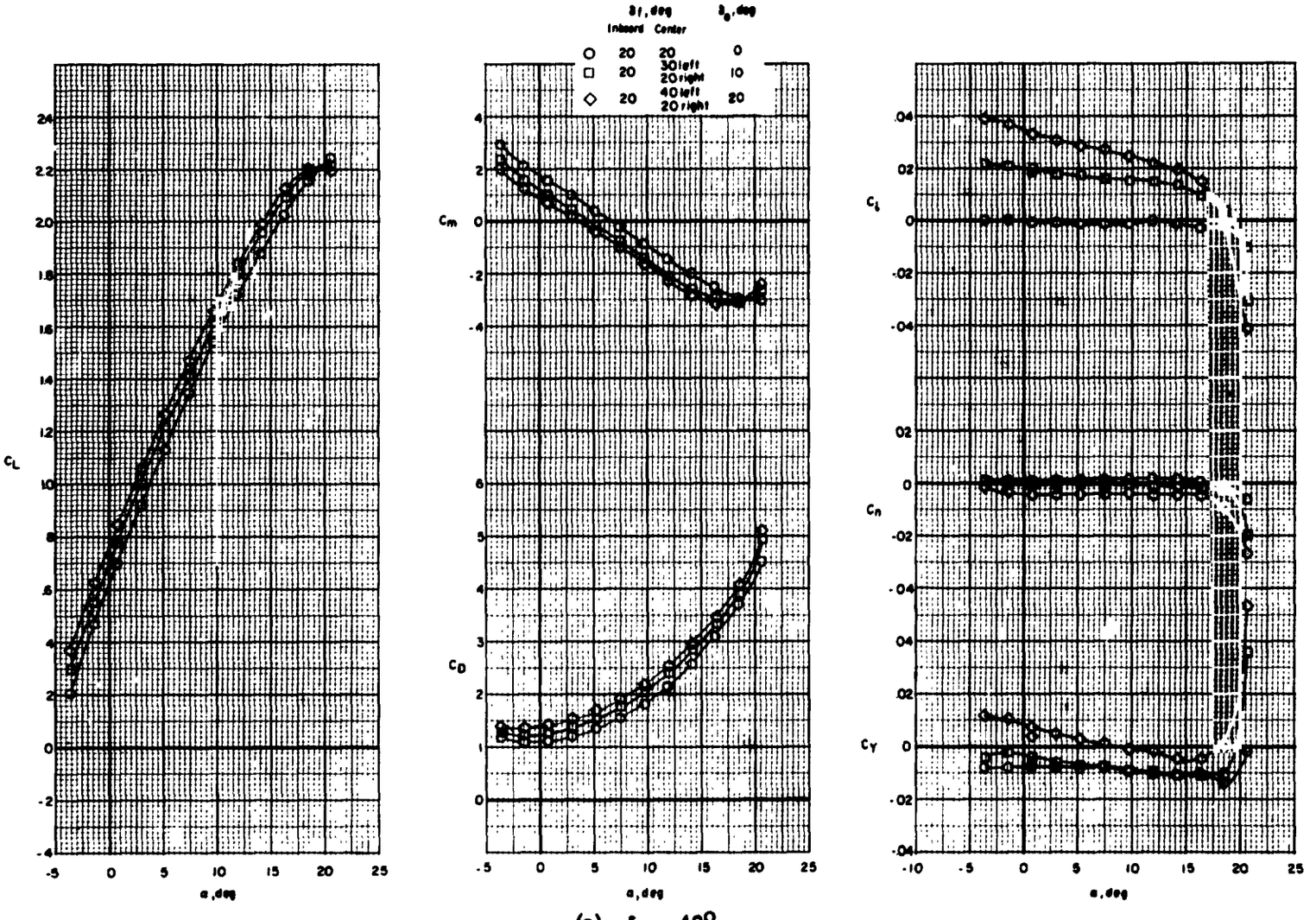

(a) $\delta_s = 40^\circ$.

Figure 17.- Effectiveness of differential flap deflected (center) used as drooped aileron for lateral control for several leading-edge slat deflections for complete model with partial-span flap (inboard and center). $i_t = -10^\circ$.

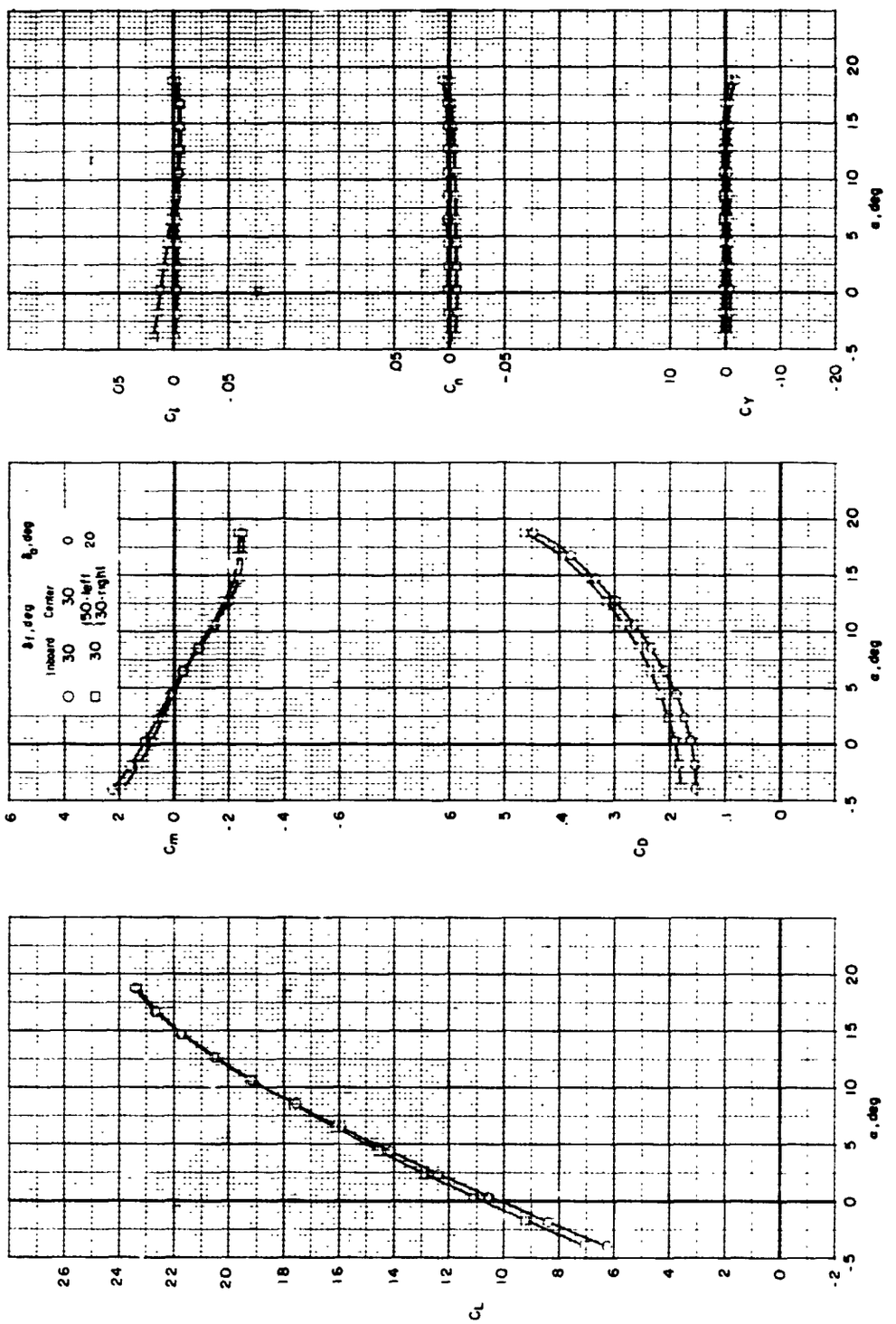

(b) $\delta_s = 50^0$.

Figure 17.- Continued.

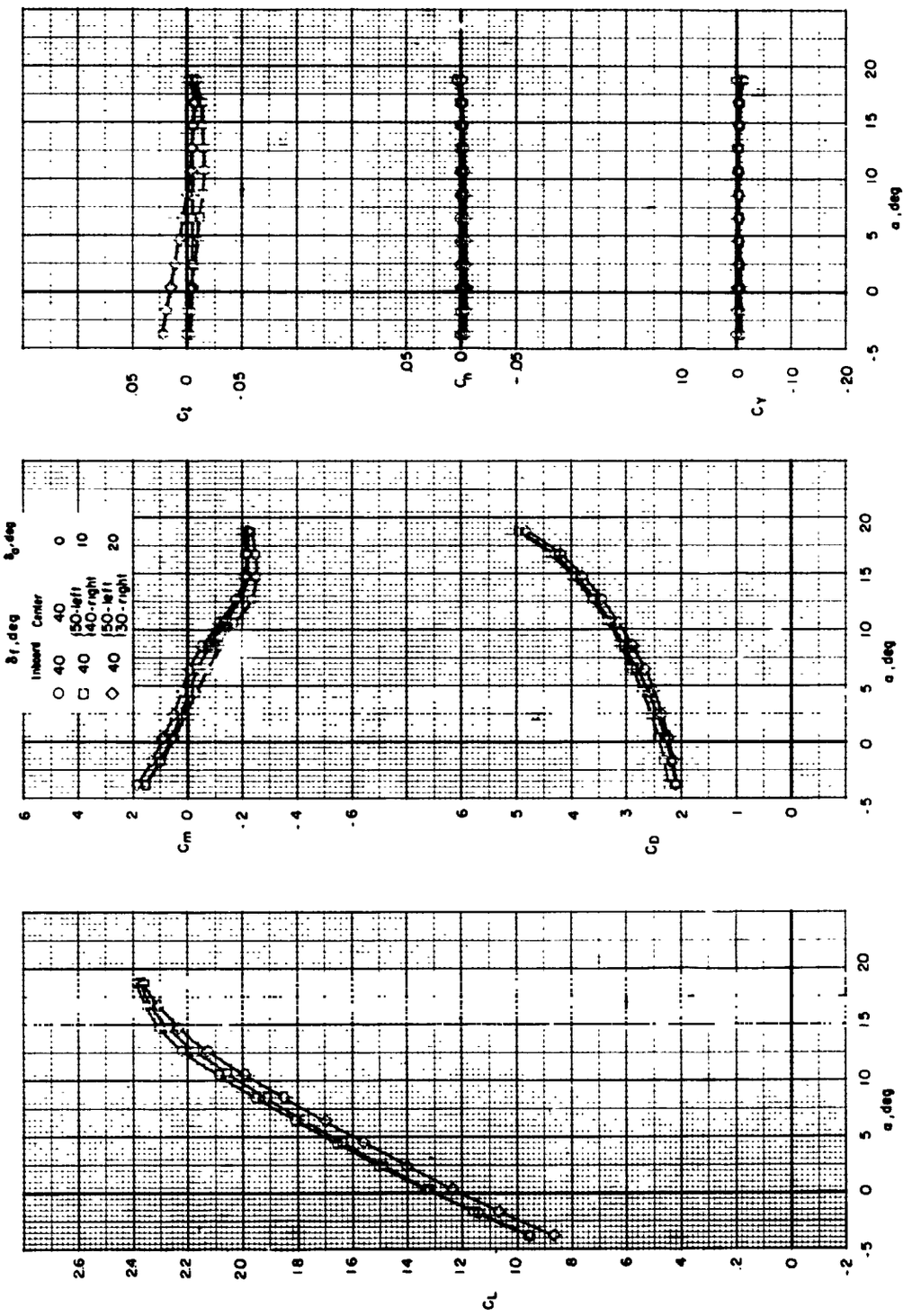

(c) $\delta_s = 50^o$.

Figure 17.- Continued.

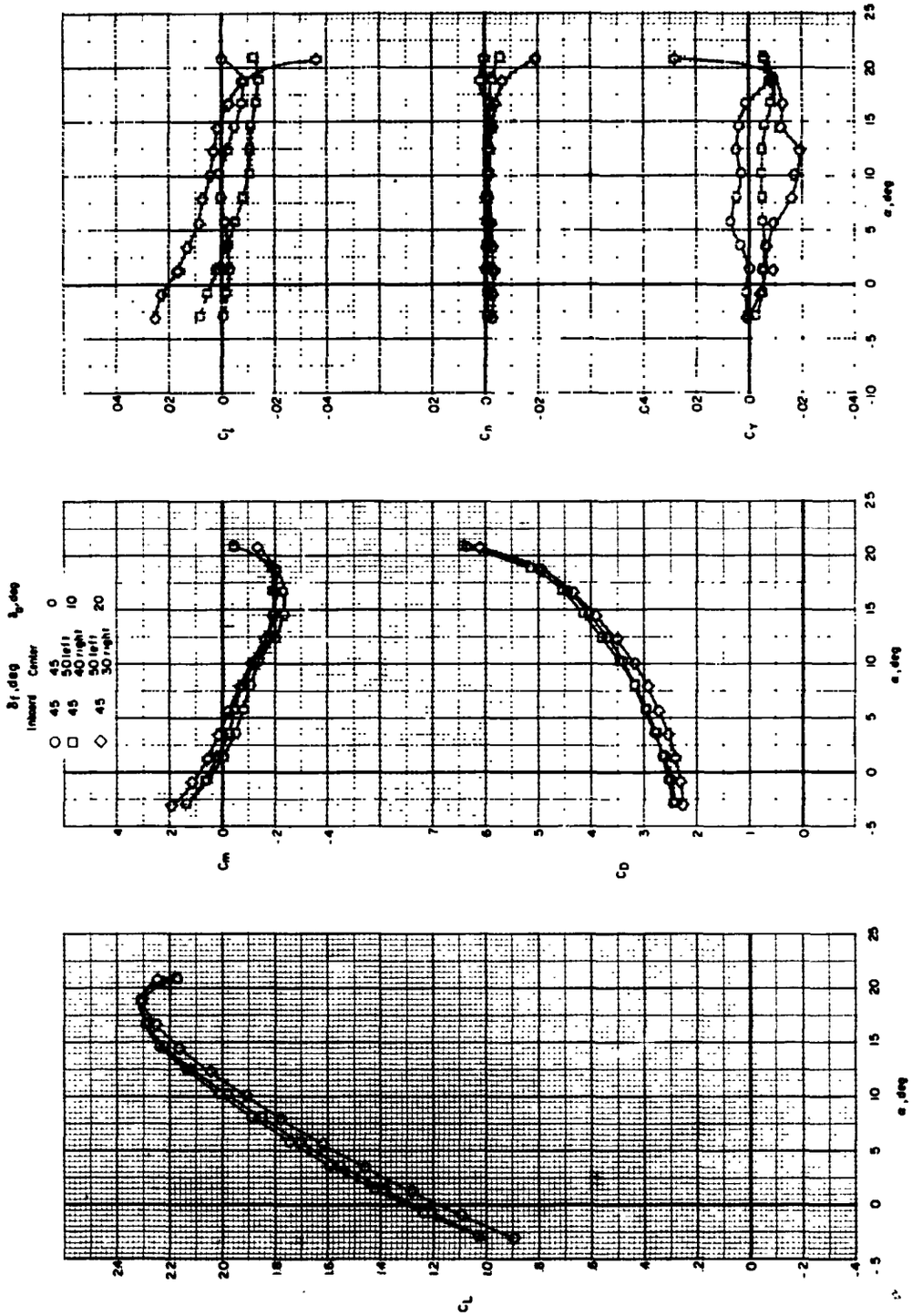

(d) $\delta_s = 50^o$.

Figure 17.- Continued.

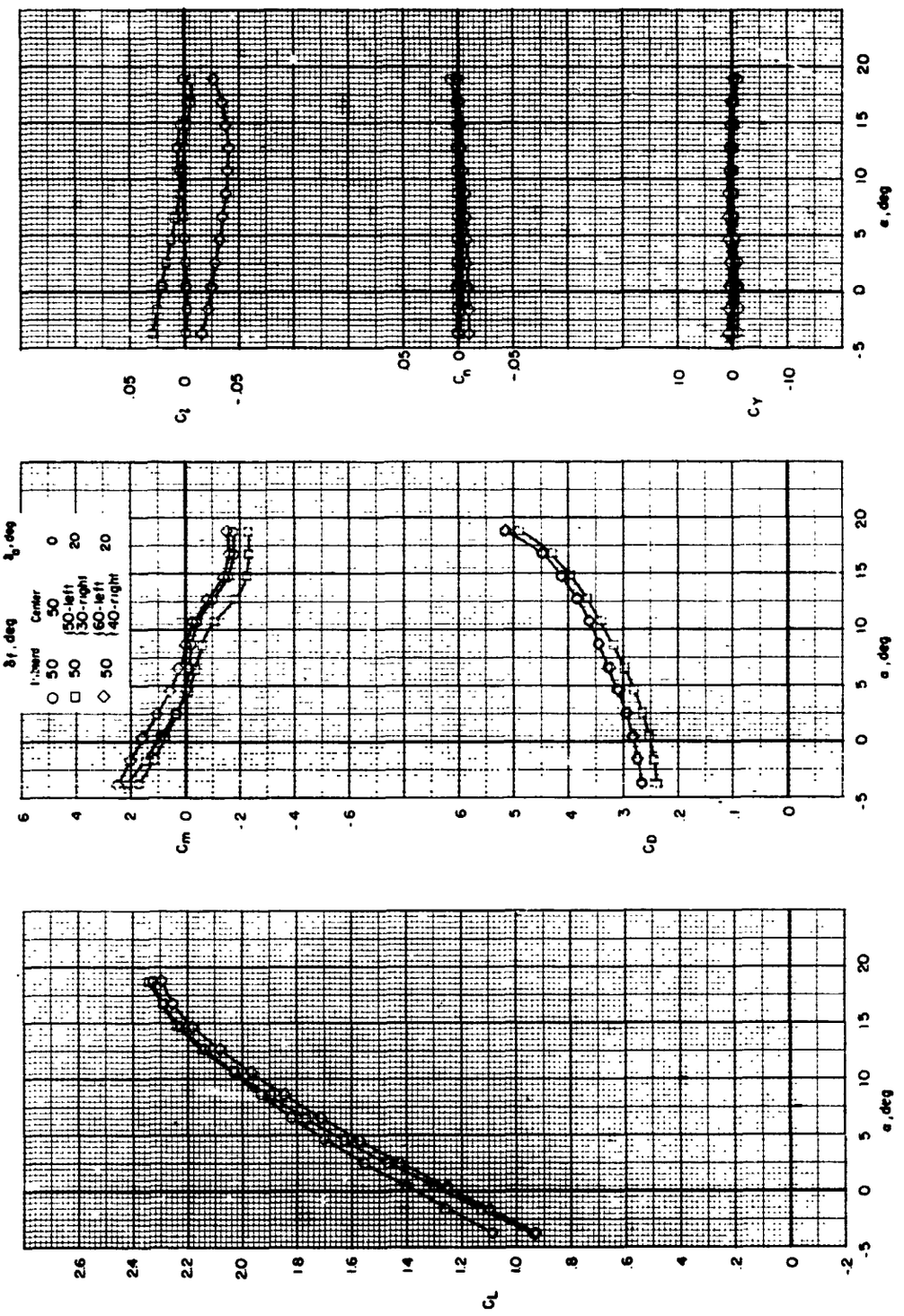

(e) $\delta_s = 50°$.

Figure 17.- Continued.

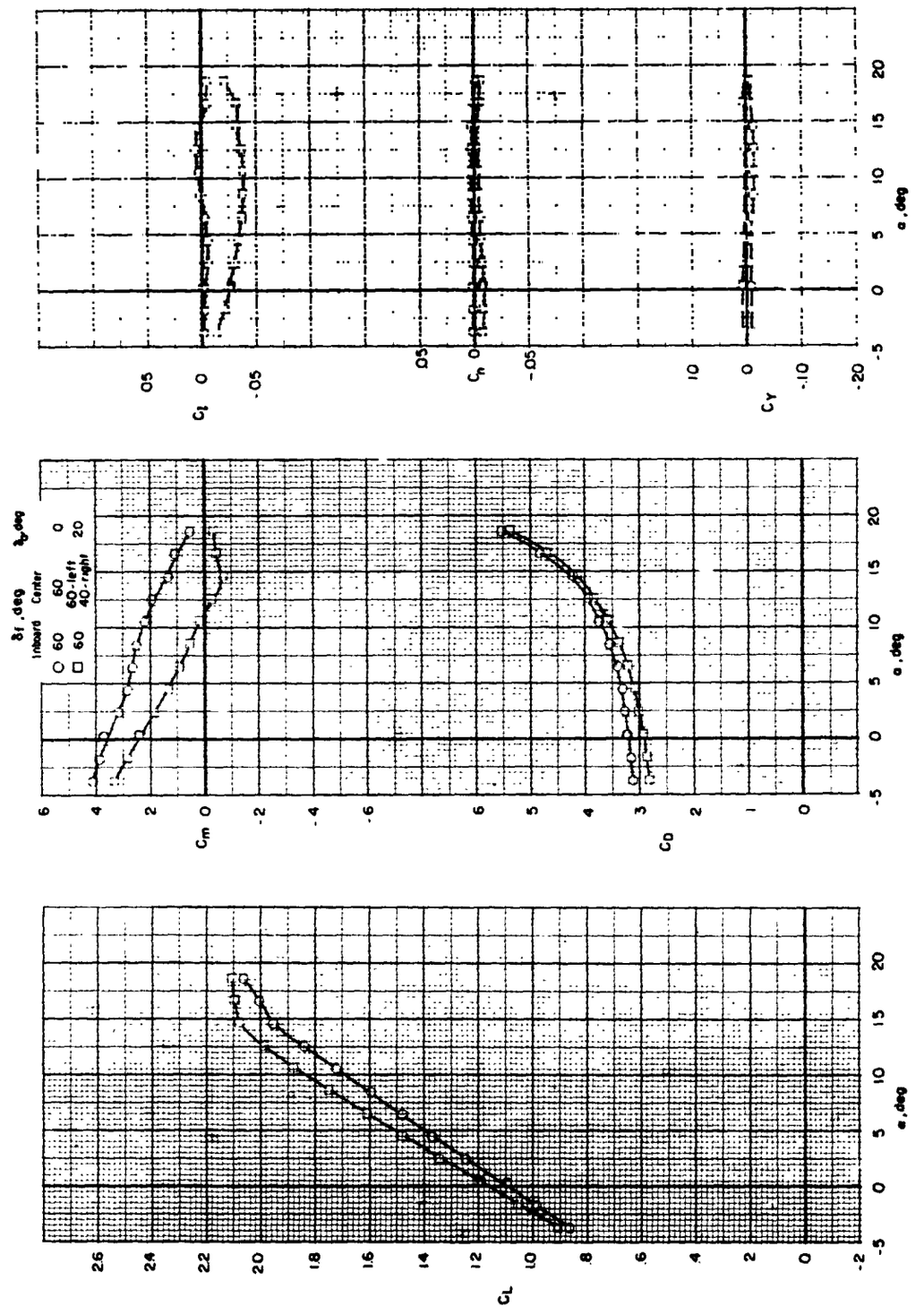

(f) $\delta_s = 50^o$.

Figure 17.- Continued.

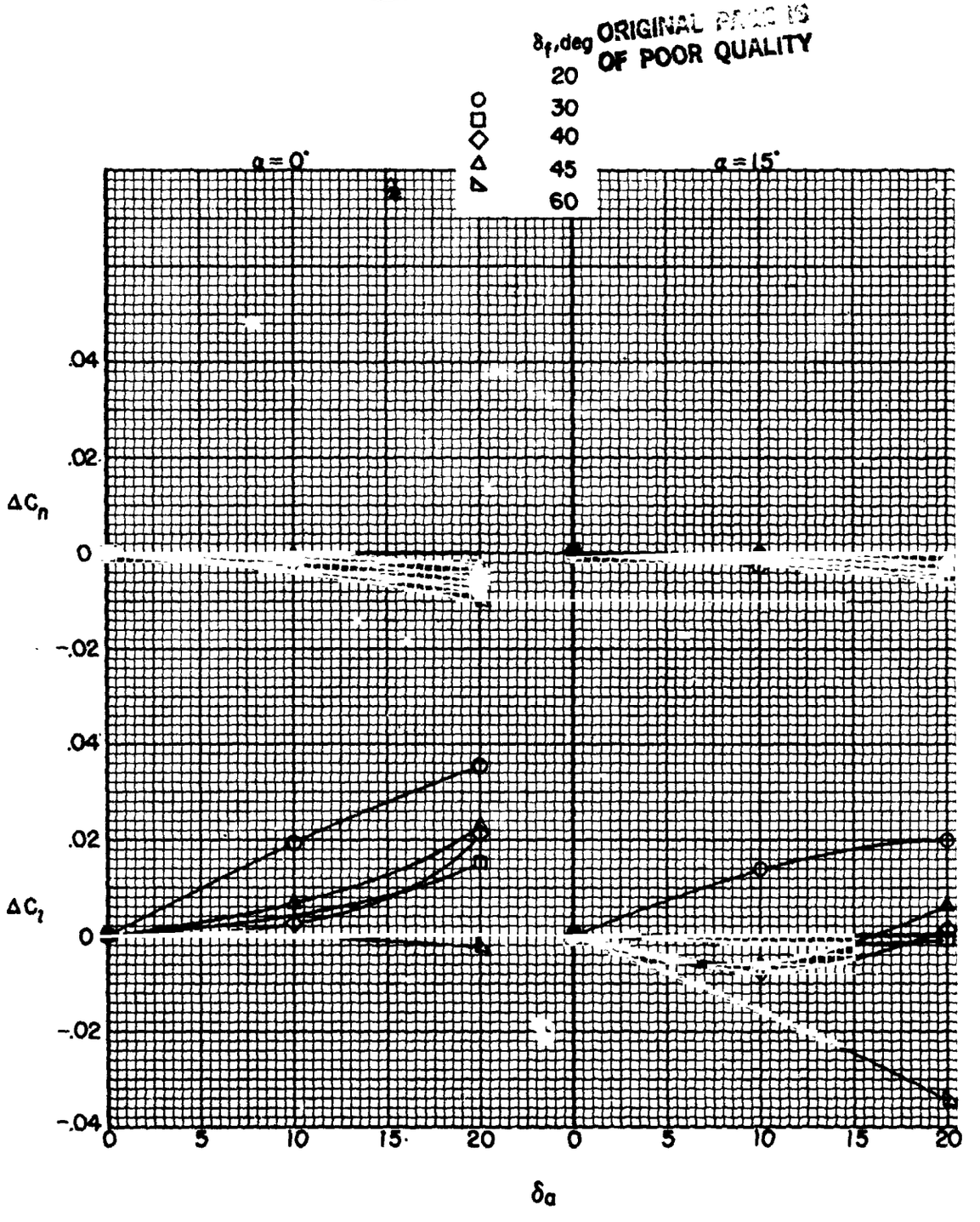

(g) δ_a.

Figure 17.- Concluded.

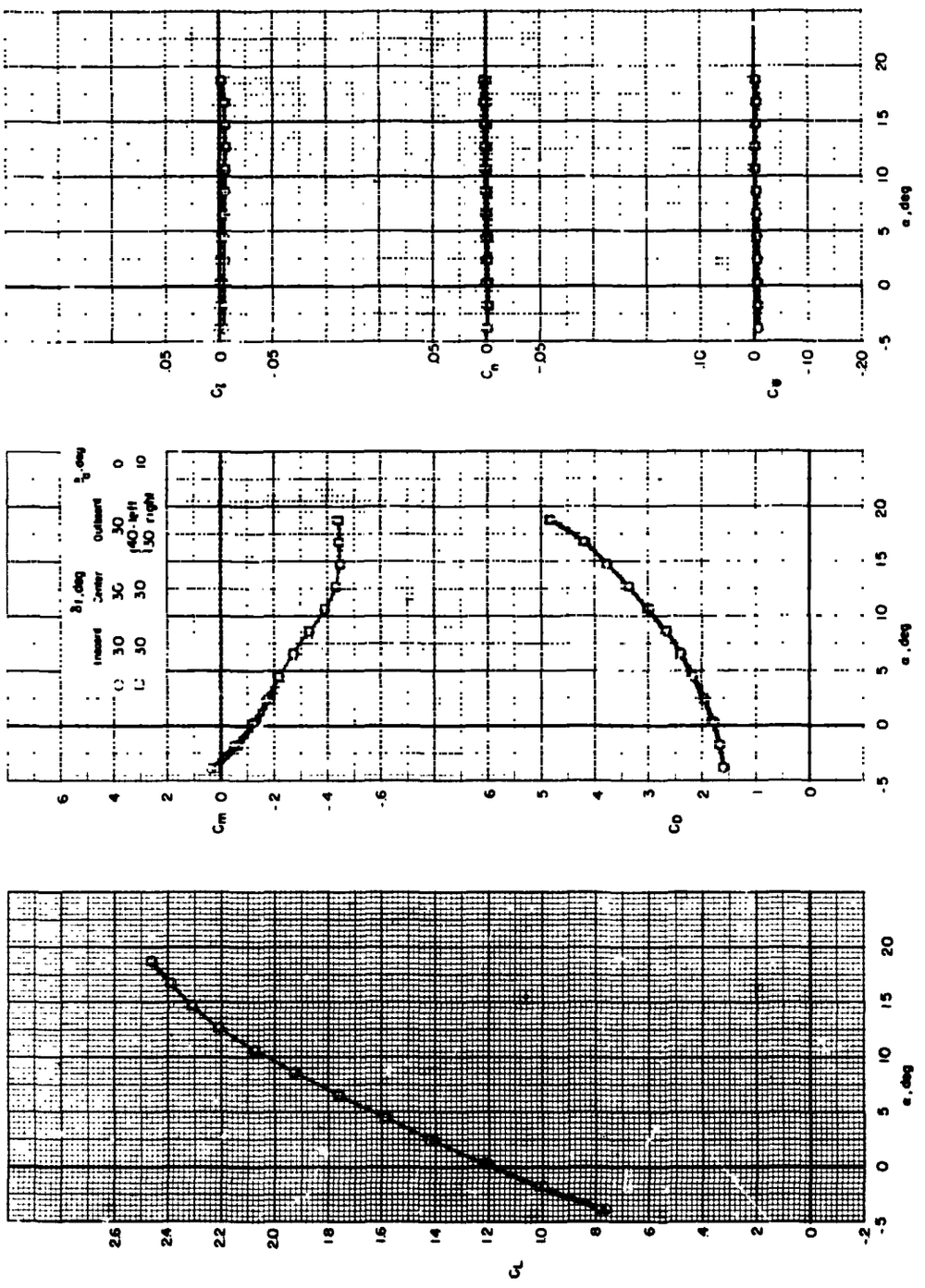

(a) $\delta_f = 30^0$.

Figure 18.- Effectiveness of differential flap deflection (outboard portion) as drooped aileron for lateral control with $\delta_g = 50^0$ for complete model with full-span flaps. $i_t = -10^0$.

ORIGINAL PAGE IS
OF POOR QUALITY

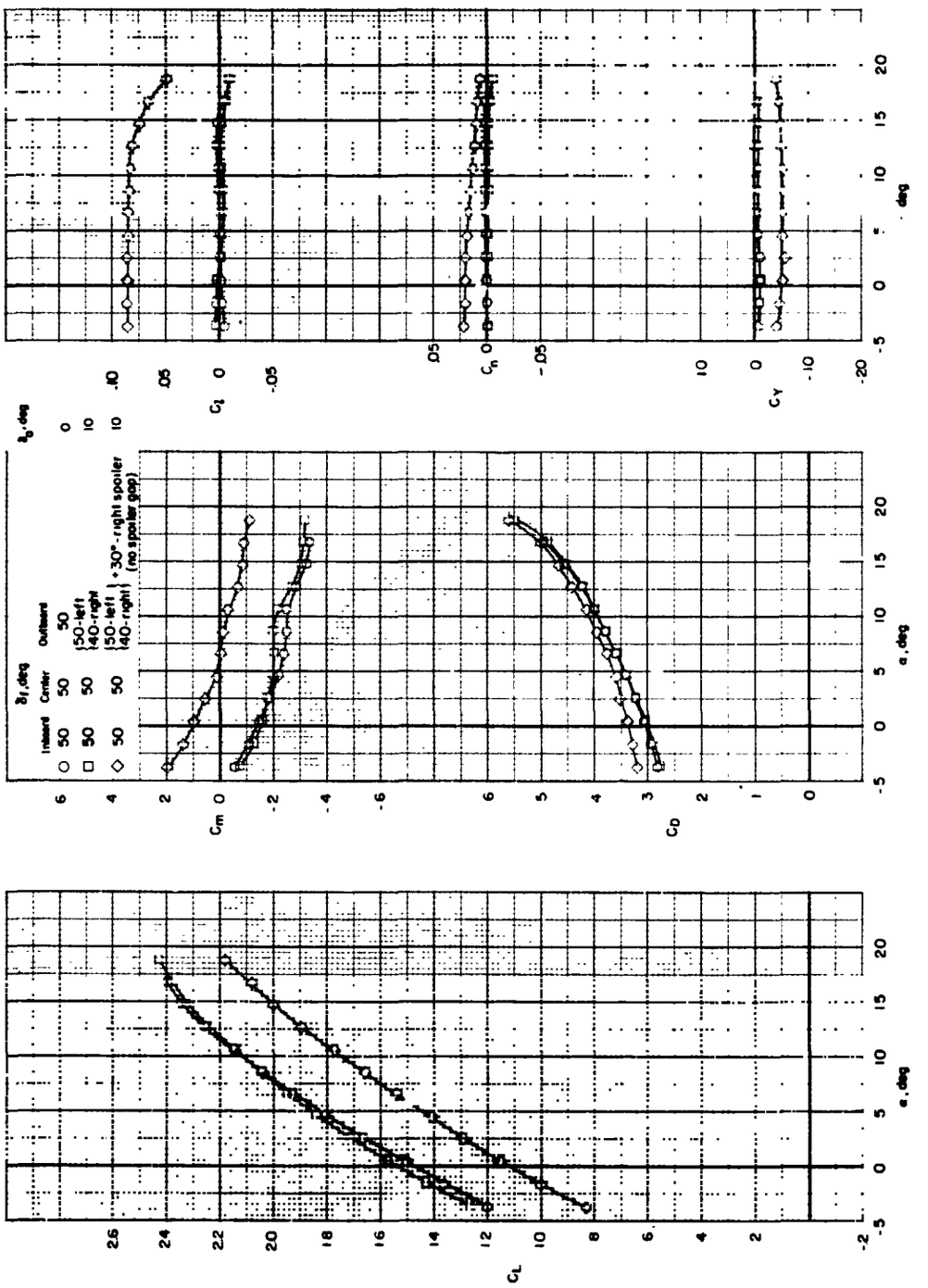

(b) $\delta_f = 50°$.

Figure 18.- Concluded.

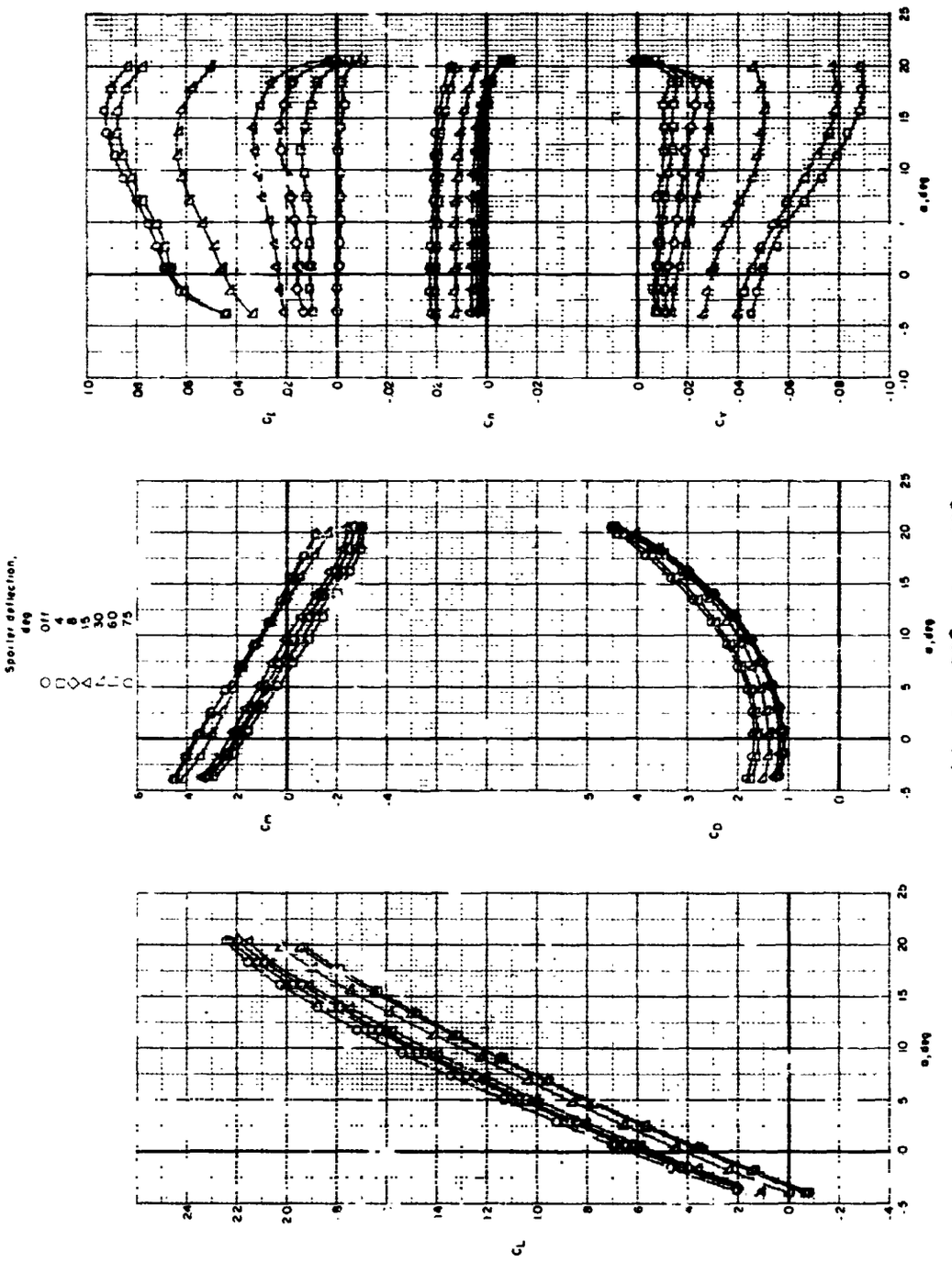

(a) $\delta_f = 20^0$; $\zeta_s = 40^0$.

Figure 19.- Effectiveness of right wing upper surface spoiler as lateral control for several leading-edge slat and partial-span flap deflections (inboard and center) for complete model configuration with $i_t = 10^0$. Spoiler gap open.

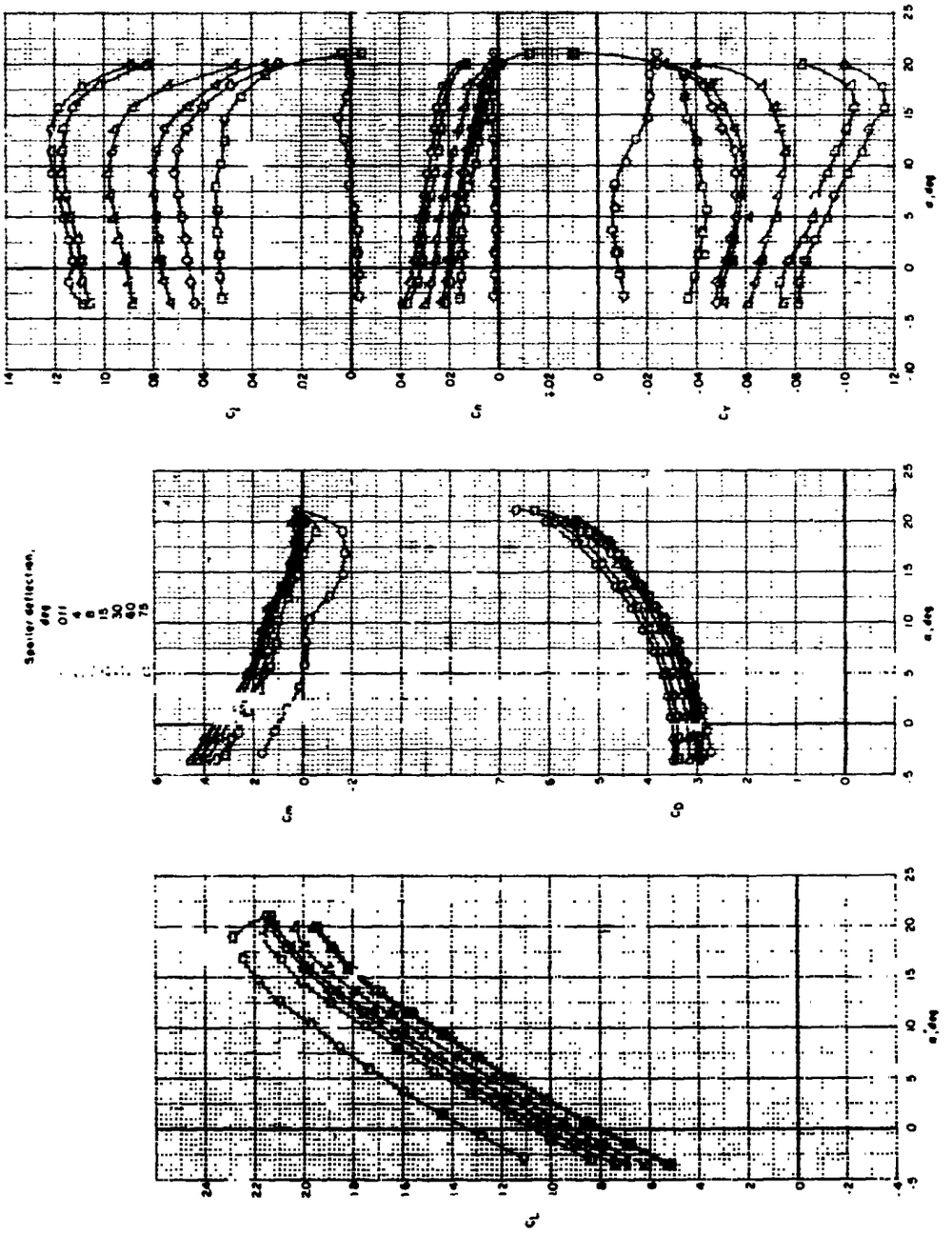

(b) $\delta_f = 50^o$; $\delta_s = 50^o$.

Figure 19.- Continued.

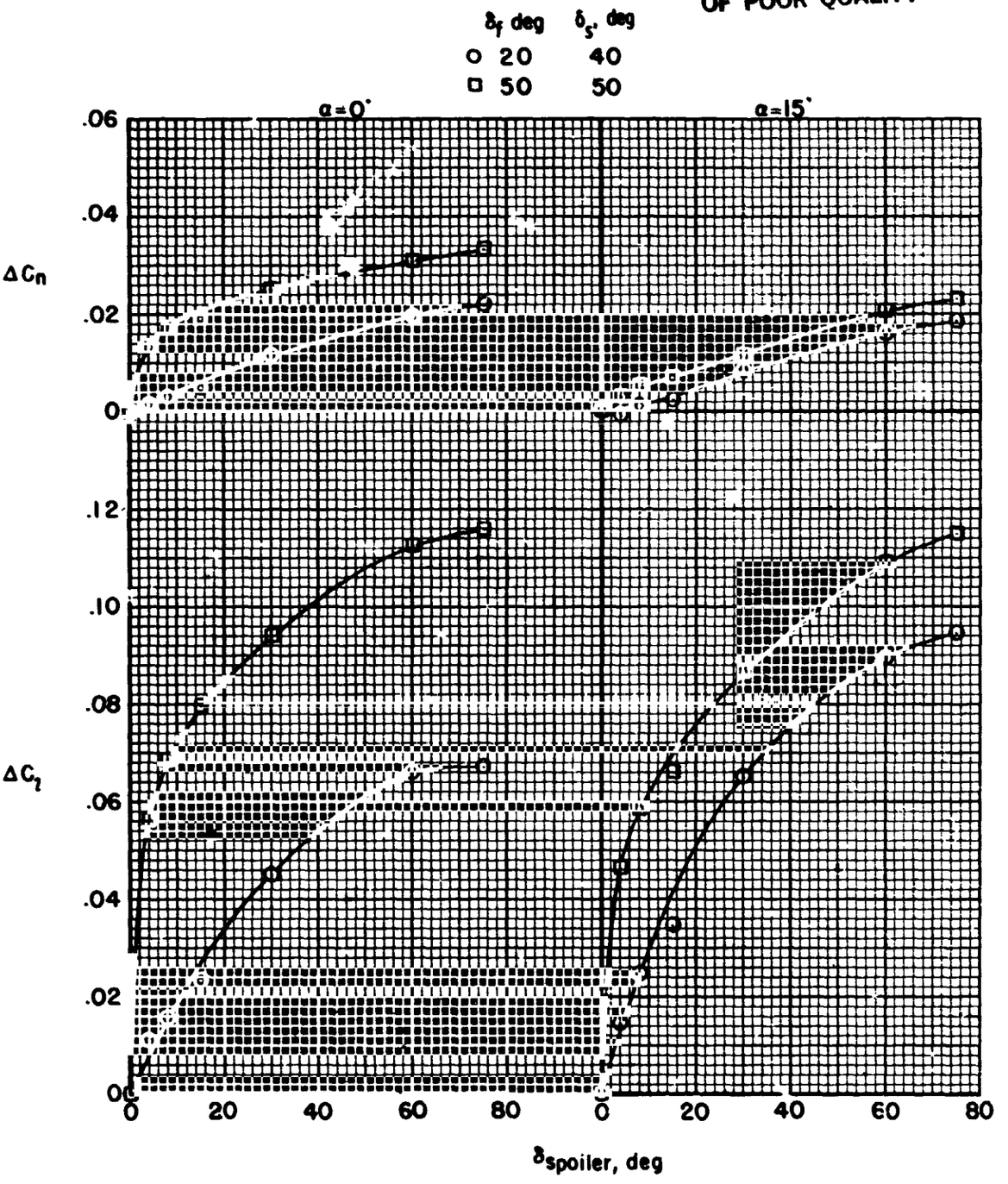

(c) $\delta_{spoiler}$.

Figure 19.- Concluded.

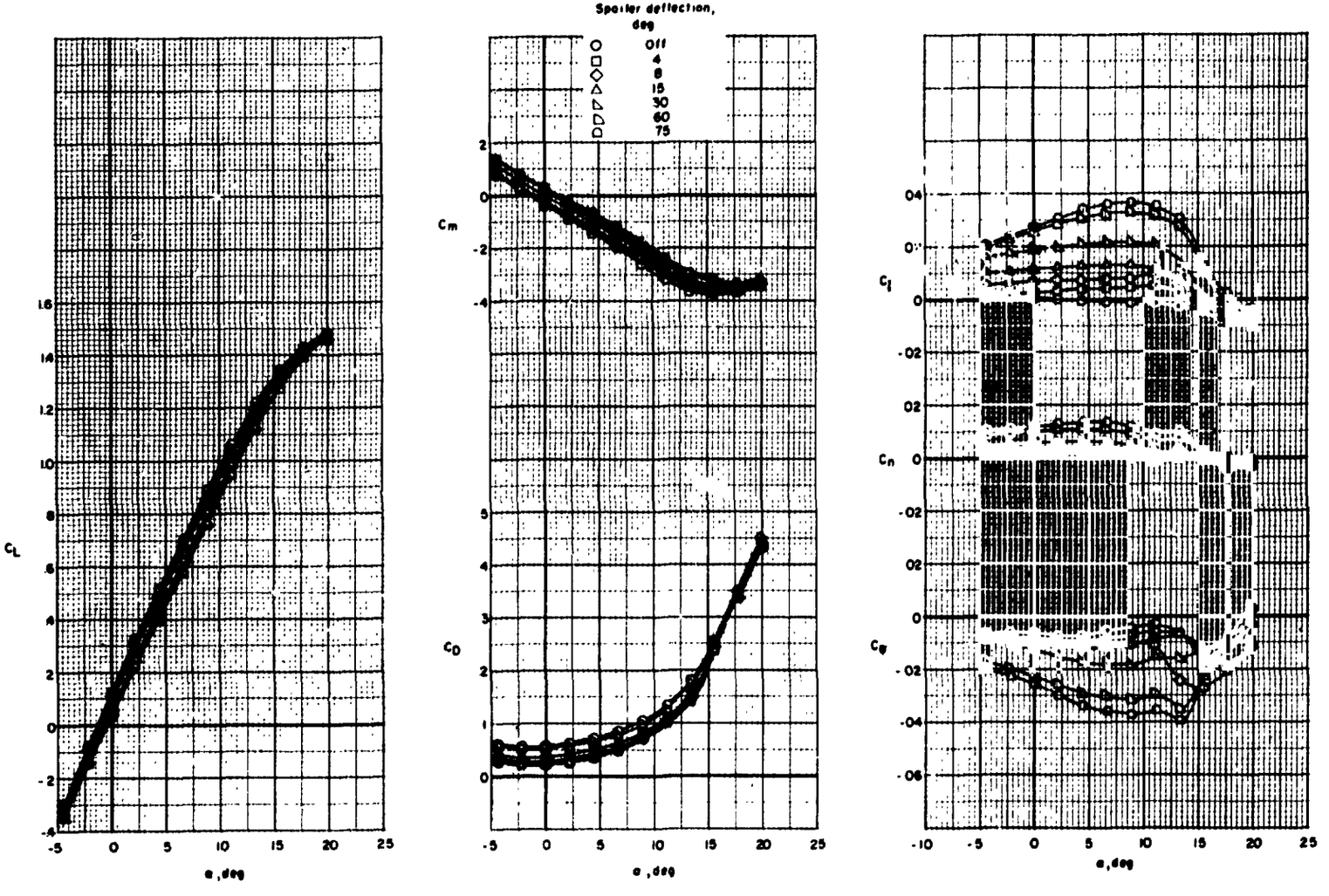

(a) $\delta_i = 0^o$; δ_s = Off; no gap with flap undeflected.

Figure 20.- Effectiveness of right wing upper surface spoiler as lateral control for several leading-edge slats and full-span flap deflections for complete model configuration with spoiler gap closed and open. $i_t = -10^o$.

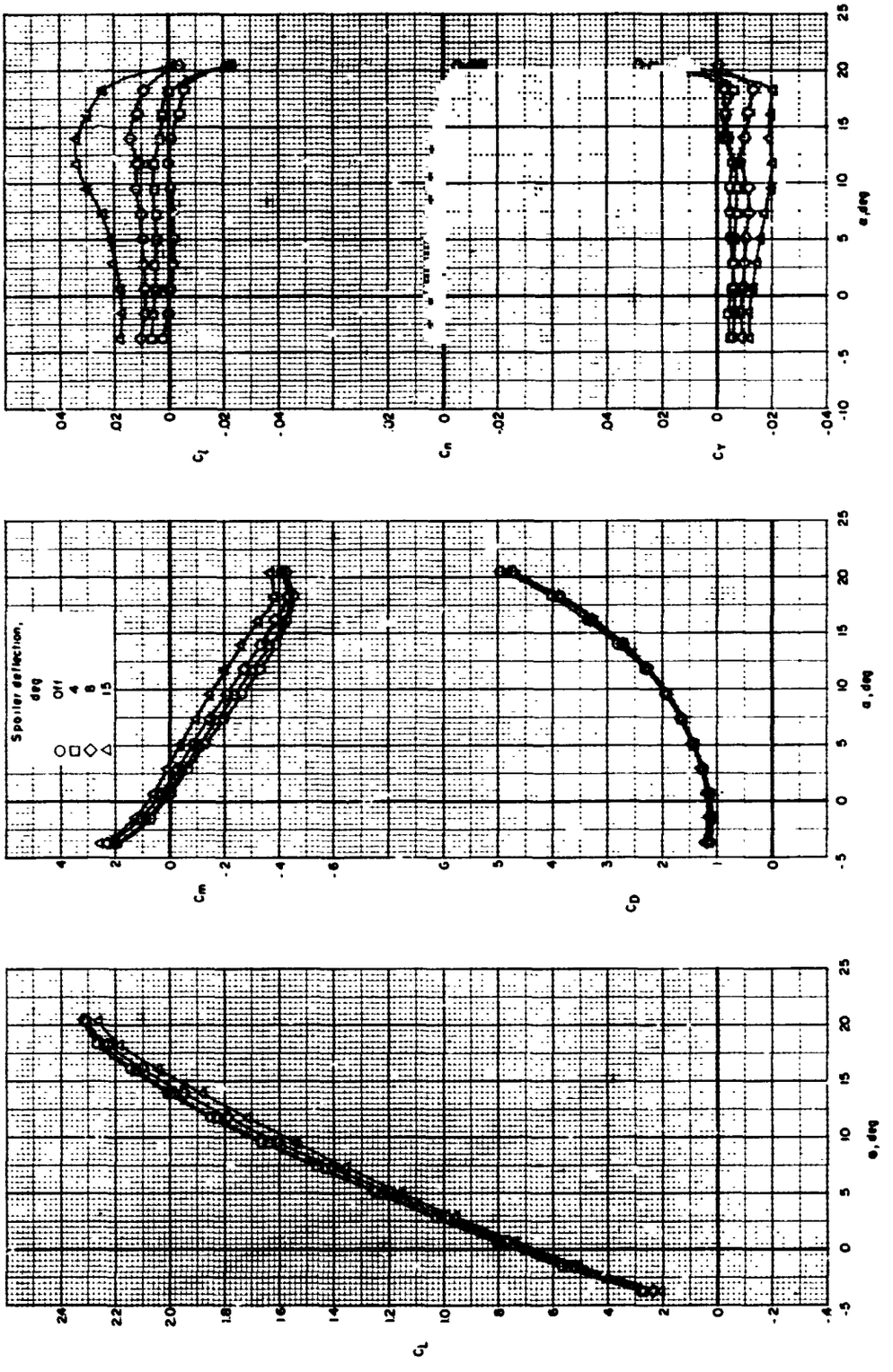

(b) $\delta_f = 20^o$; $\delta_s = 40^o$; spoiler gap closed.

Figure 20.- Continued.

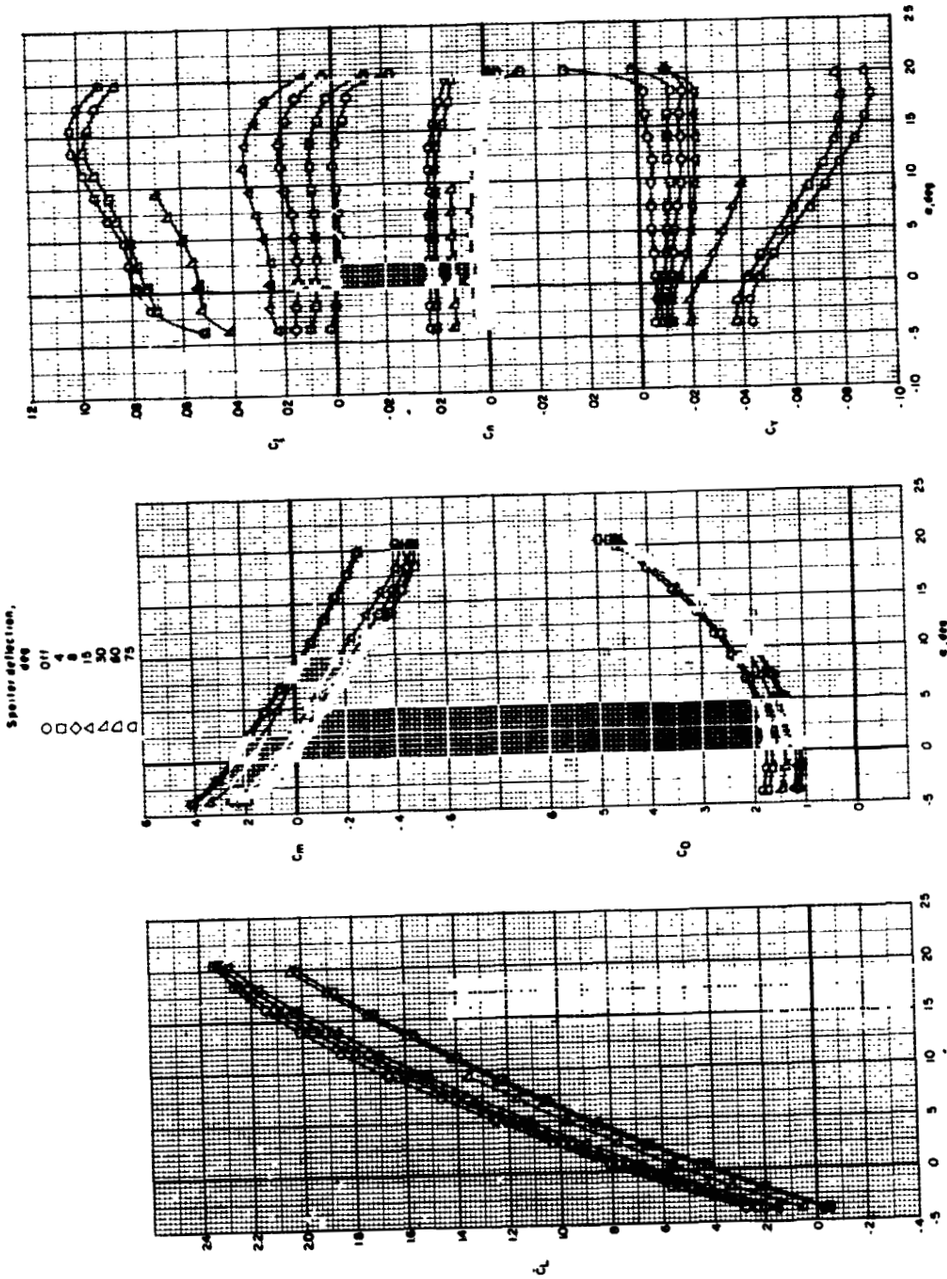

(c) $\delta_f = 20^o$; $\delta_s = 40^o$; spoiler gap open.

Figure 20.- Continued.

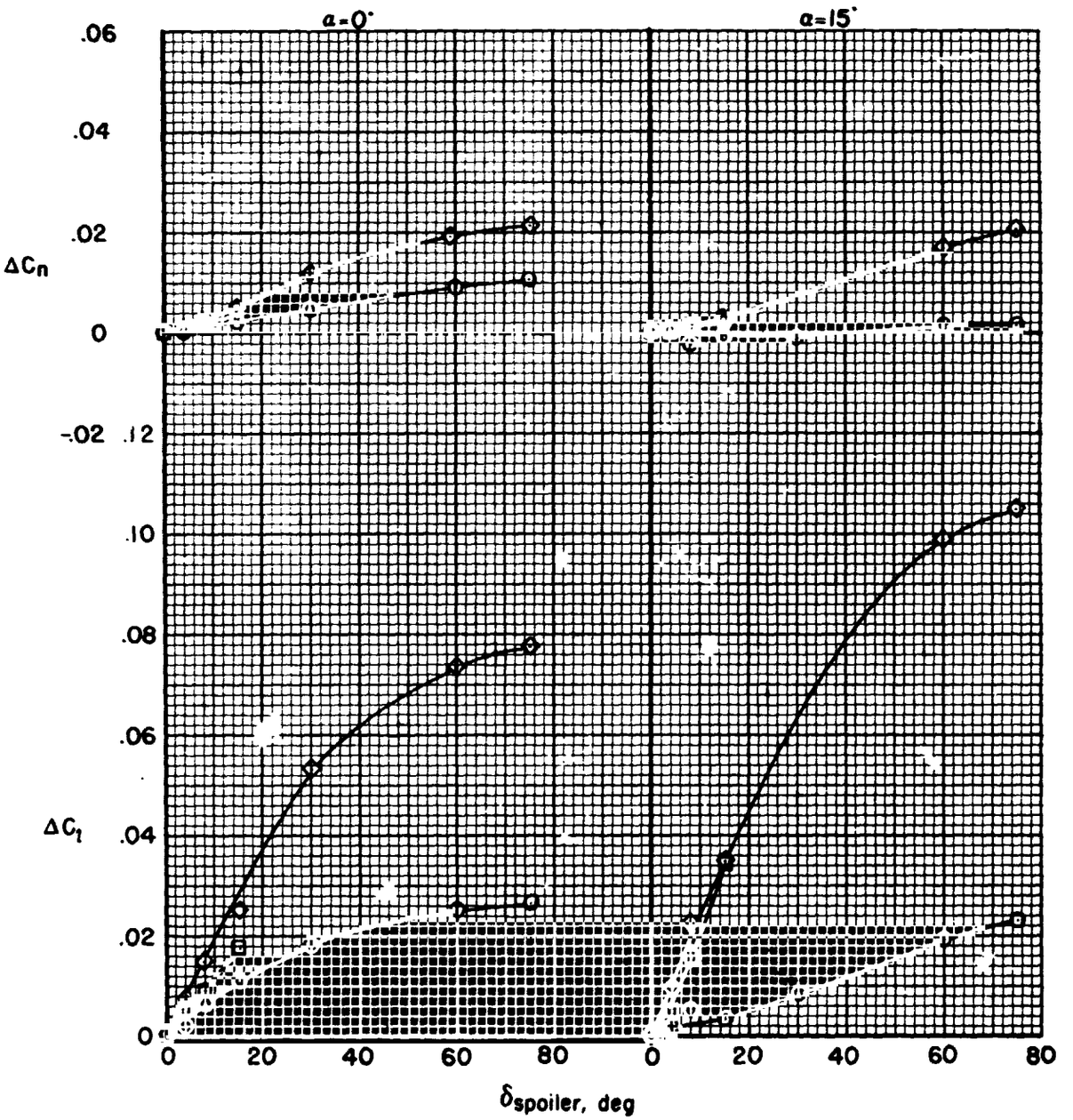

(d) $\delta_{spoiler}$.

Figure 20.- Concluded.

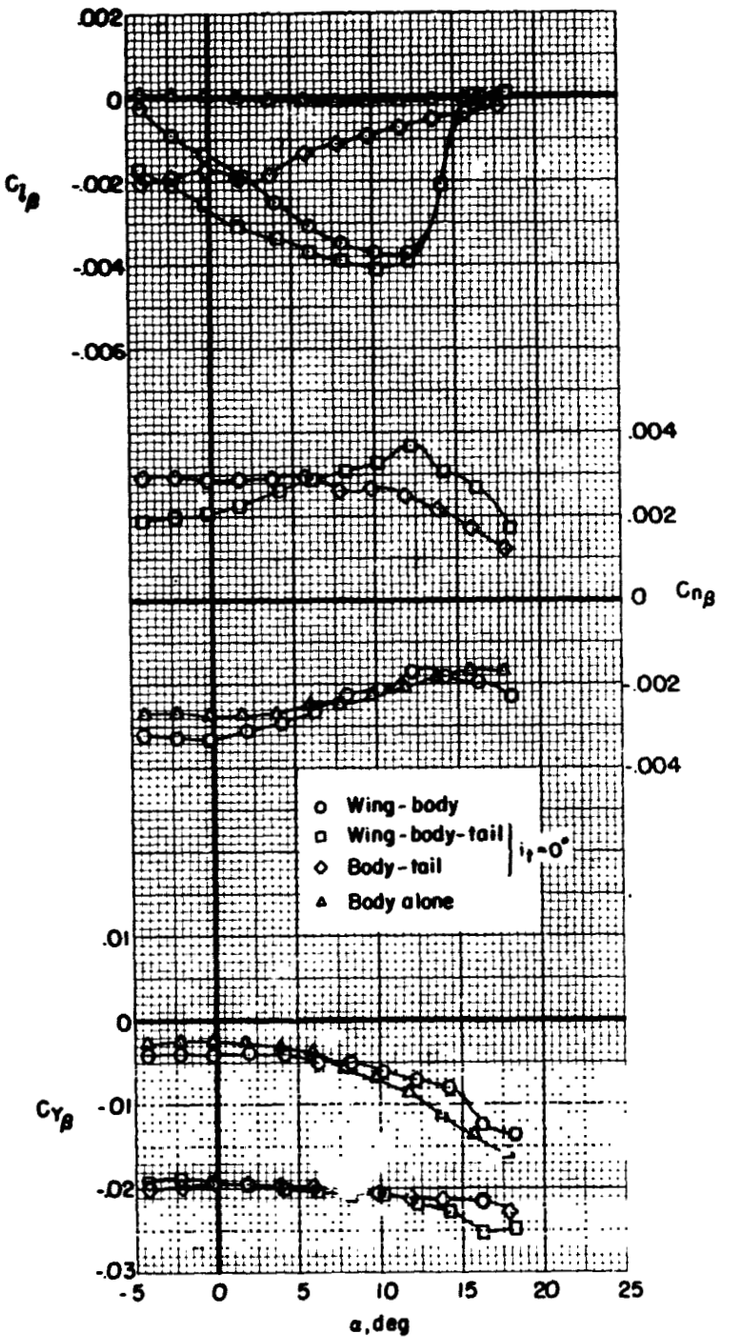

Figure 21.- Static lateral-stability derivative variation with angle of attack for various model components.

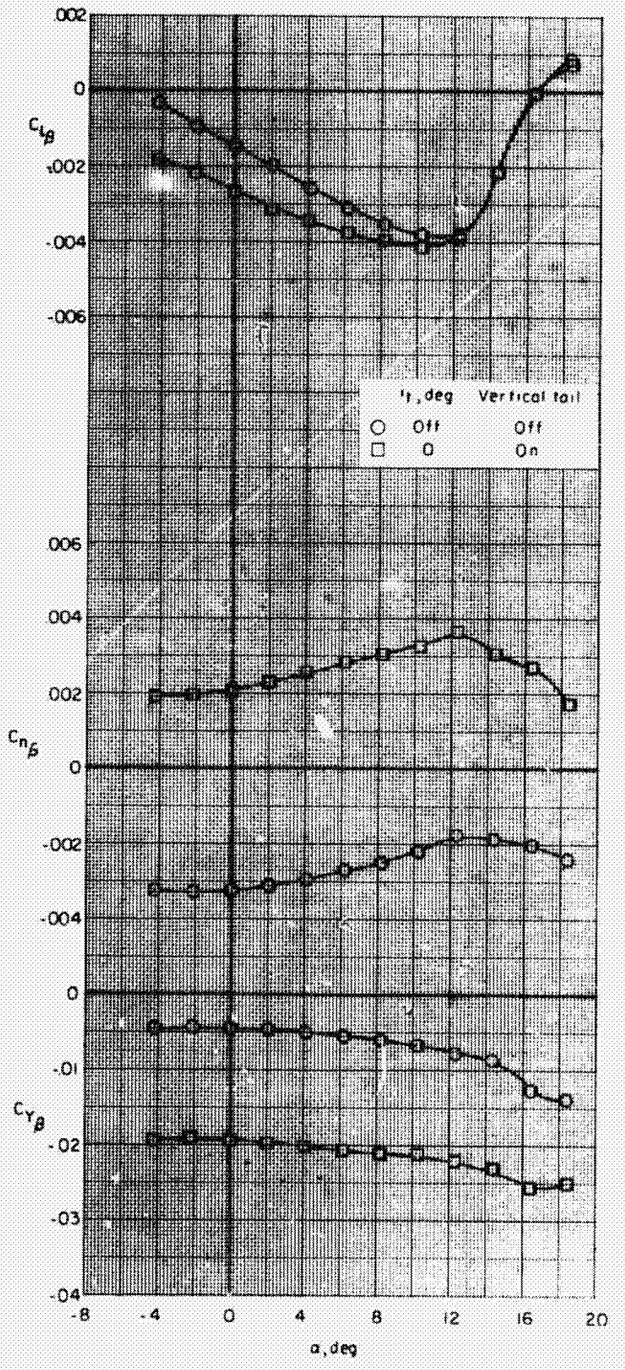

(a) $\delta_f = 0^o$; δ_s = Off.

Figure 22.- Effect of adding horizontal and vertical tails on static-lateral stability derivatives of model for several leading-edge slats and partial-span flap deflections (inboard and center).

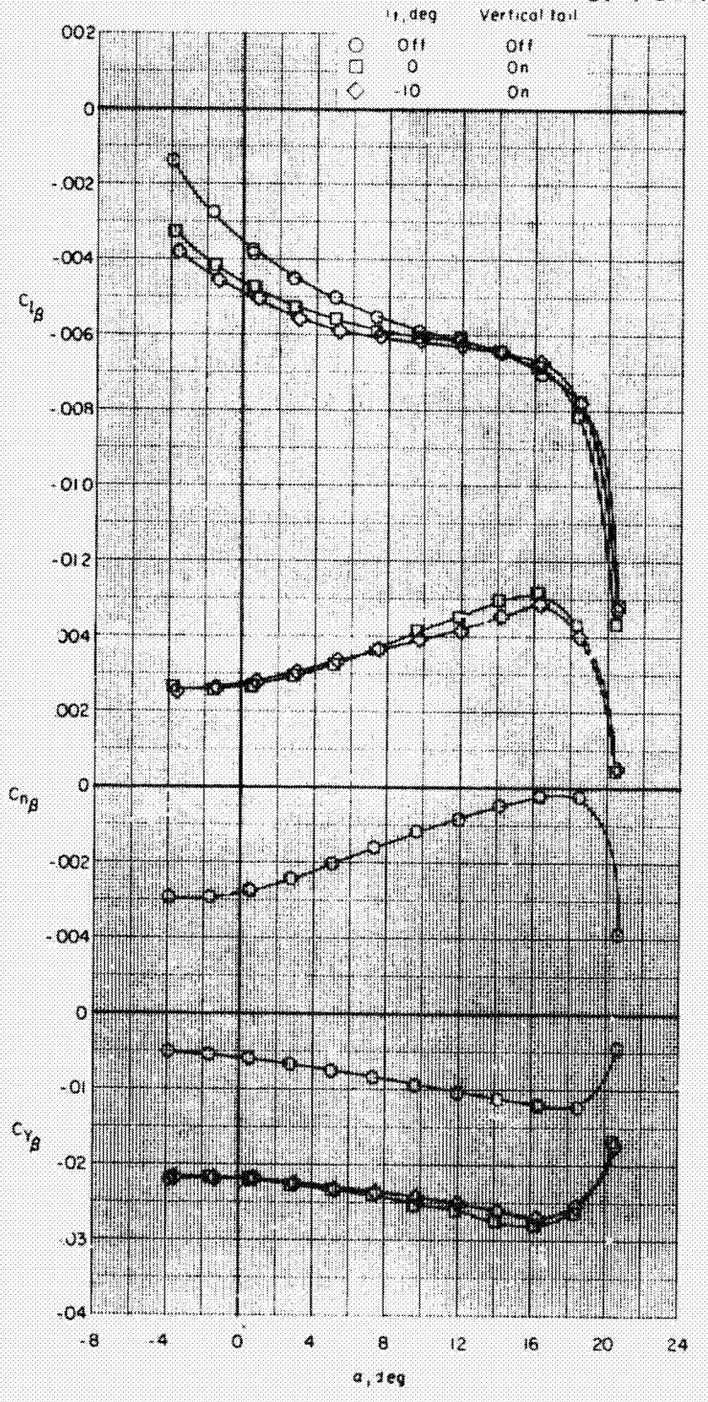

(b) $\delta_f = 20^o$; $\delta_s = 40^o$.

Figure 22.- Continued.

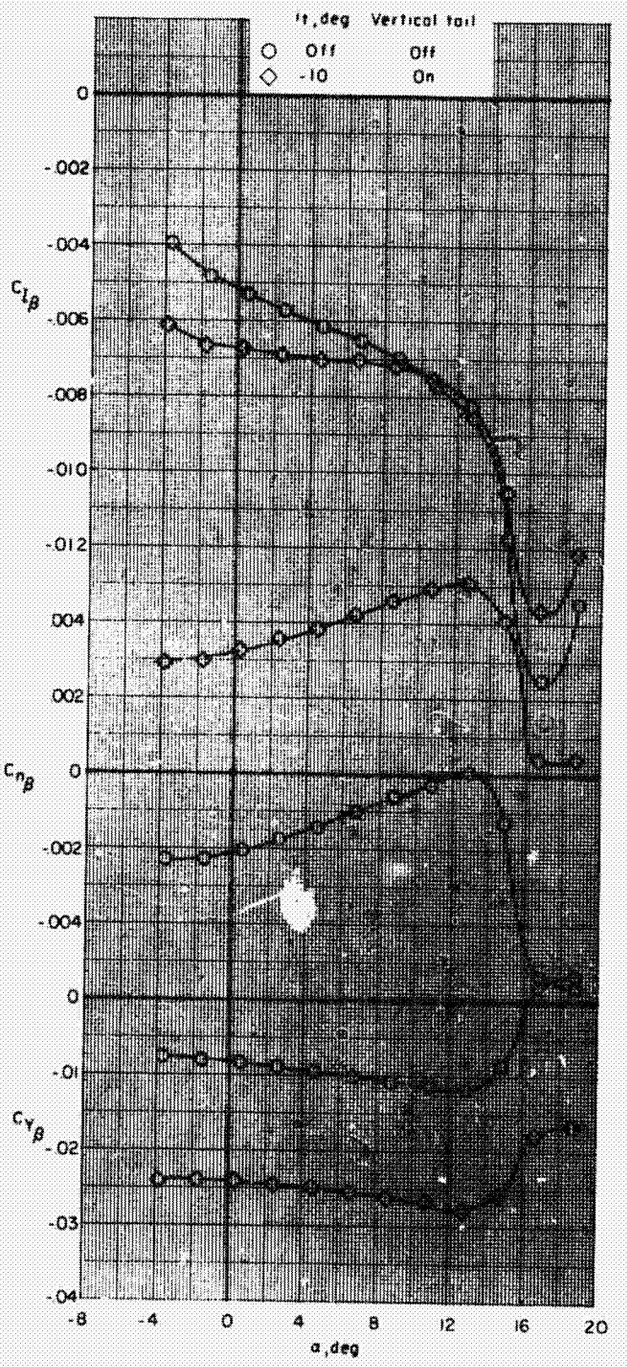

(c) $\delta_f = 30^o$; $\delta_s = 30^o$.

Figure 22.- Continued.

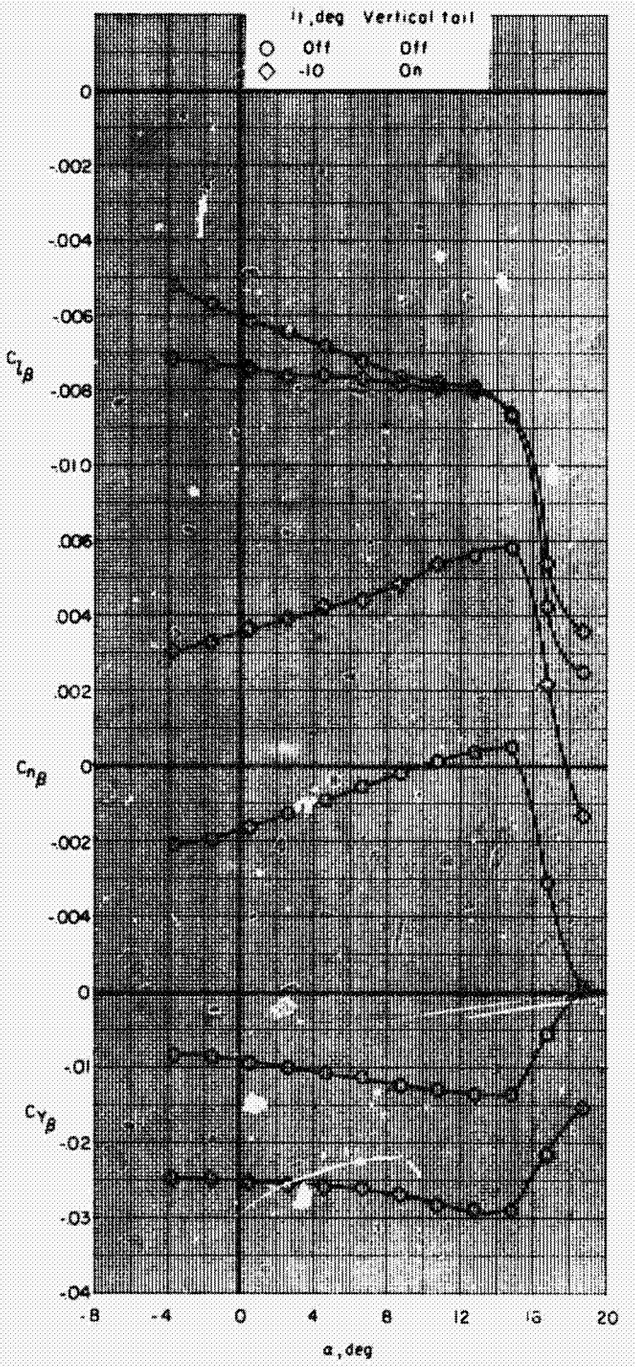

(d) $\delta_f = 40^o$; $\delta_s = 40^o$.

Figure 22.- Continued.

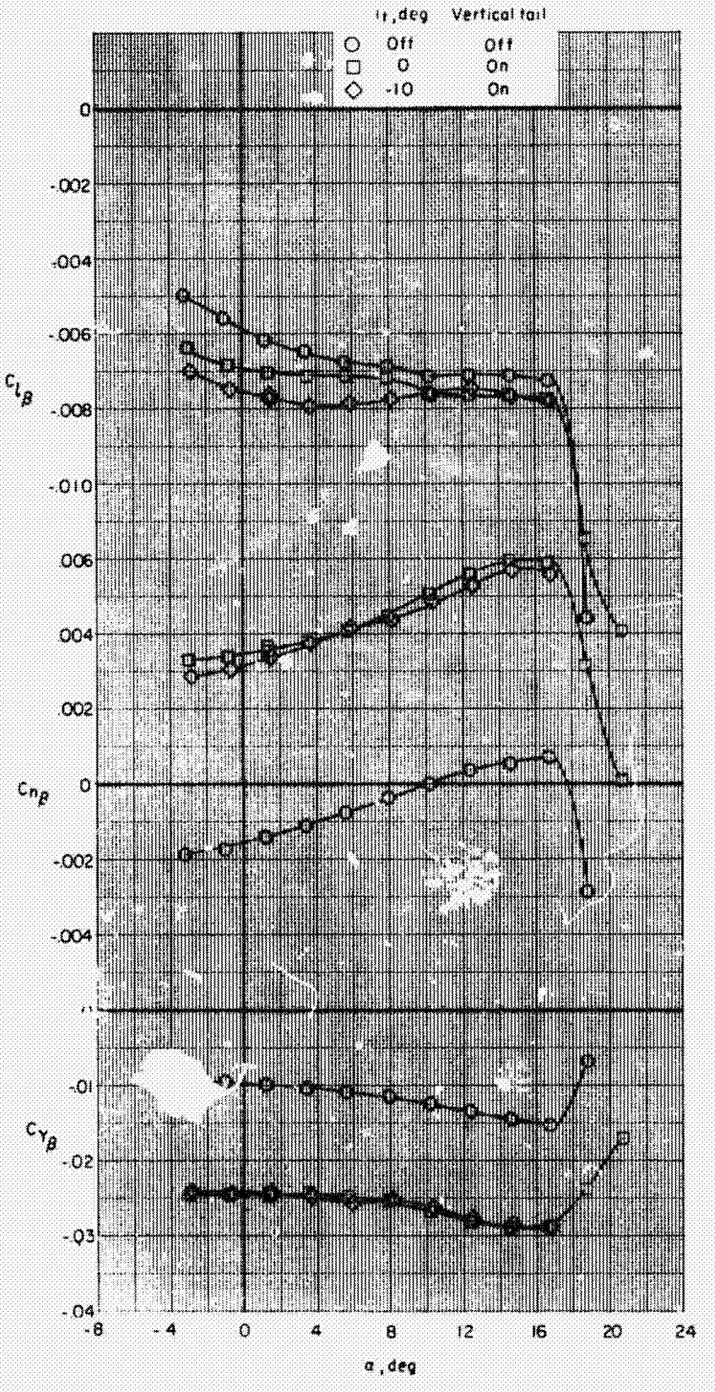

(e) $\delta_f = 45^o$; $\delta_s = 50^o$.

Figure 22.- Continued.

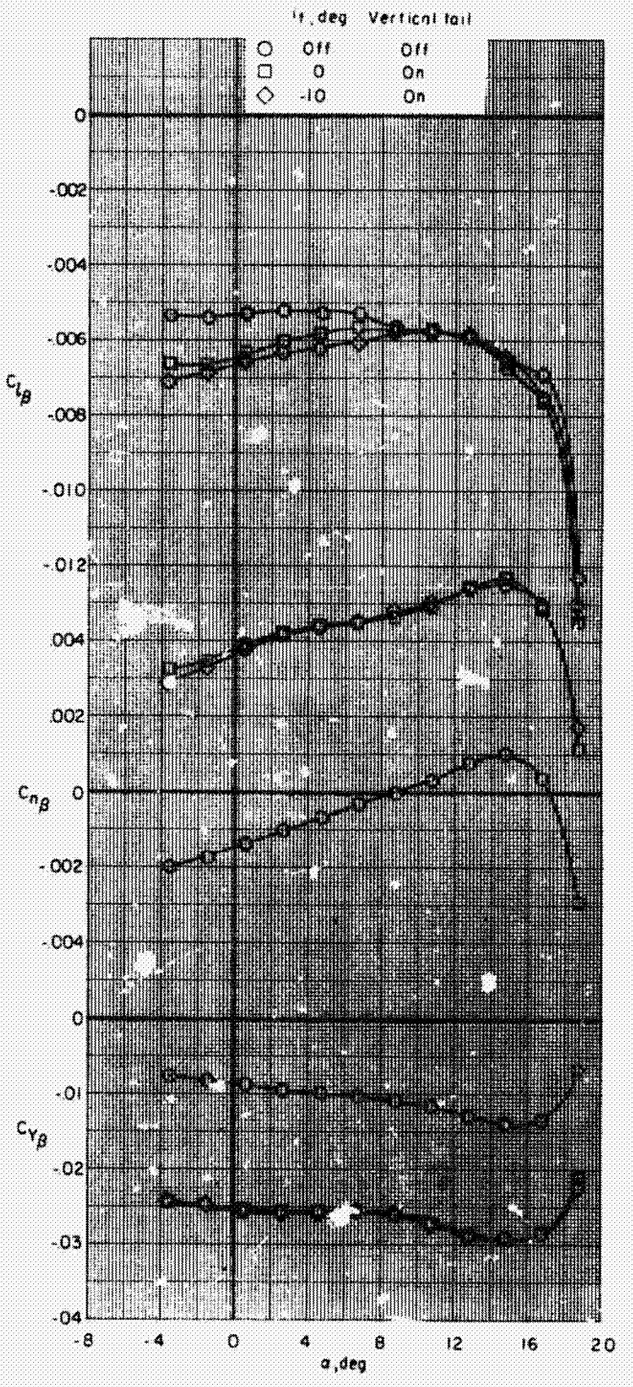

(f) $\delta_f = 50°$; $\delta_s = 50°$.

Figure 22.- Continued.

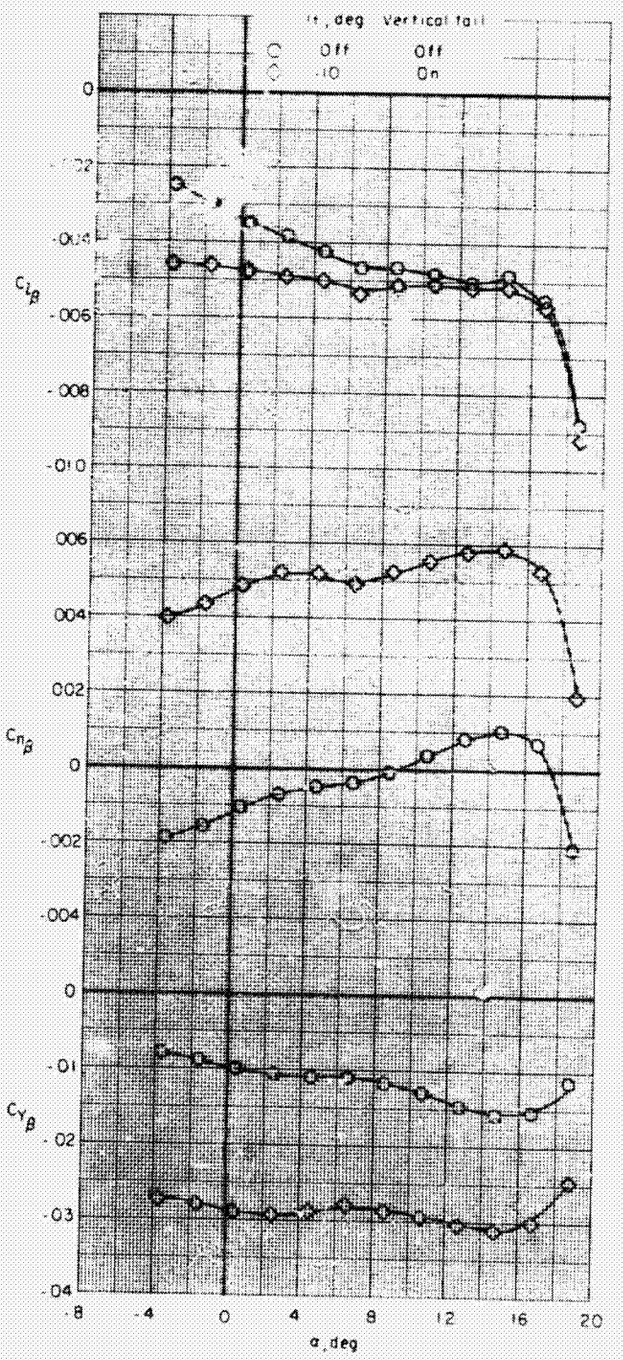

(g) $\delta_f = 60^o$; $\delta_s = 50^o$.

Figure 22.- Concluded.

C-2

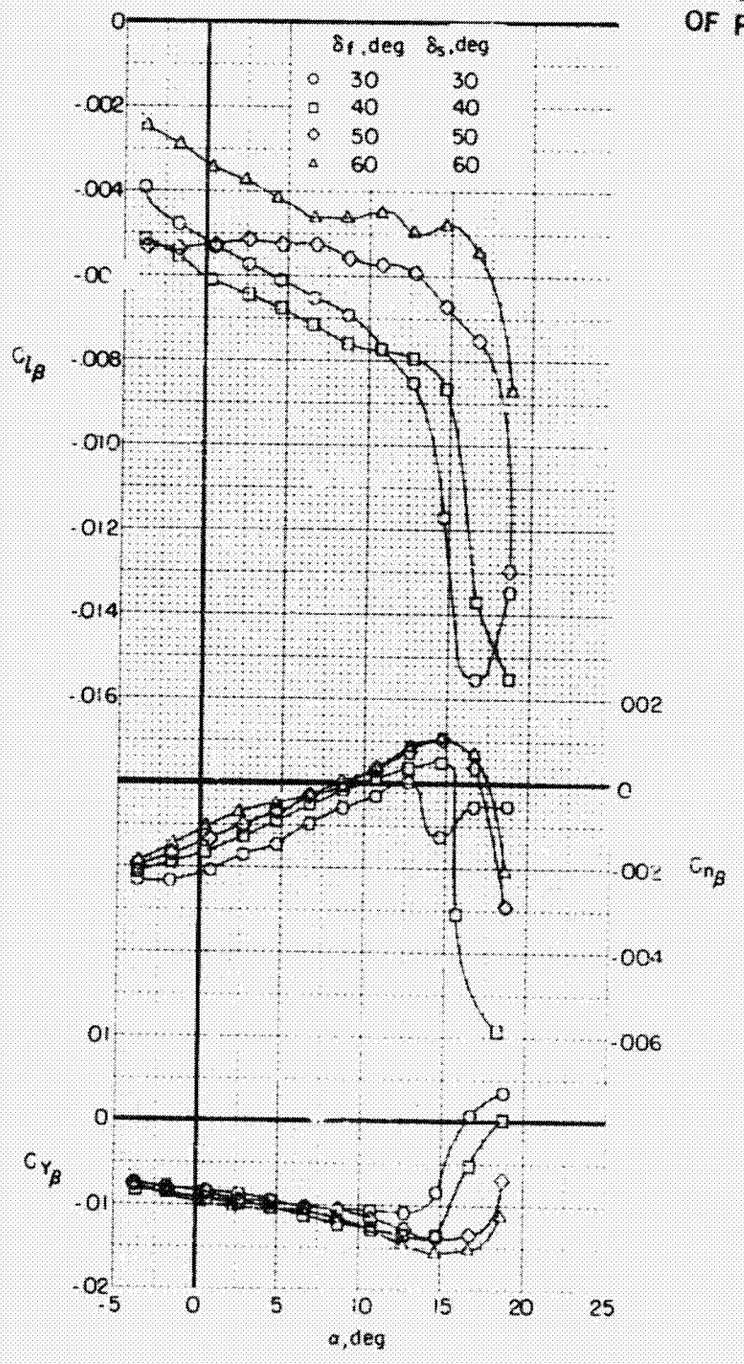

(a) i_t = Off.

Figure 23.- Static lateral-stability derivative variation with angle of attack for several flap and slat deflections. Partial-span flap deflection (inboard and center).

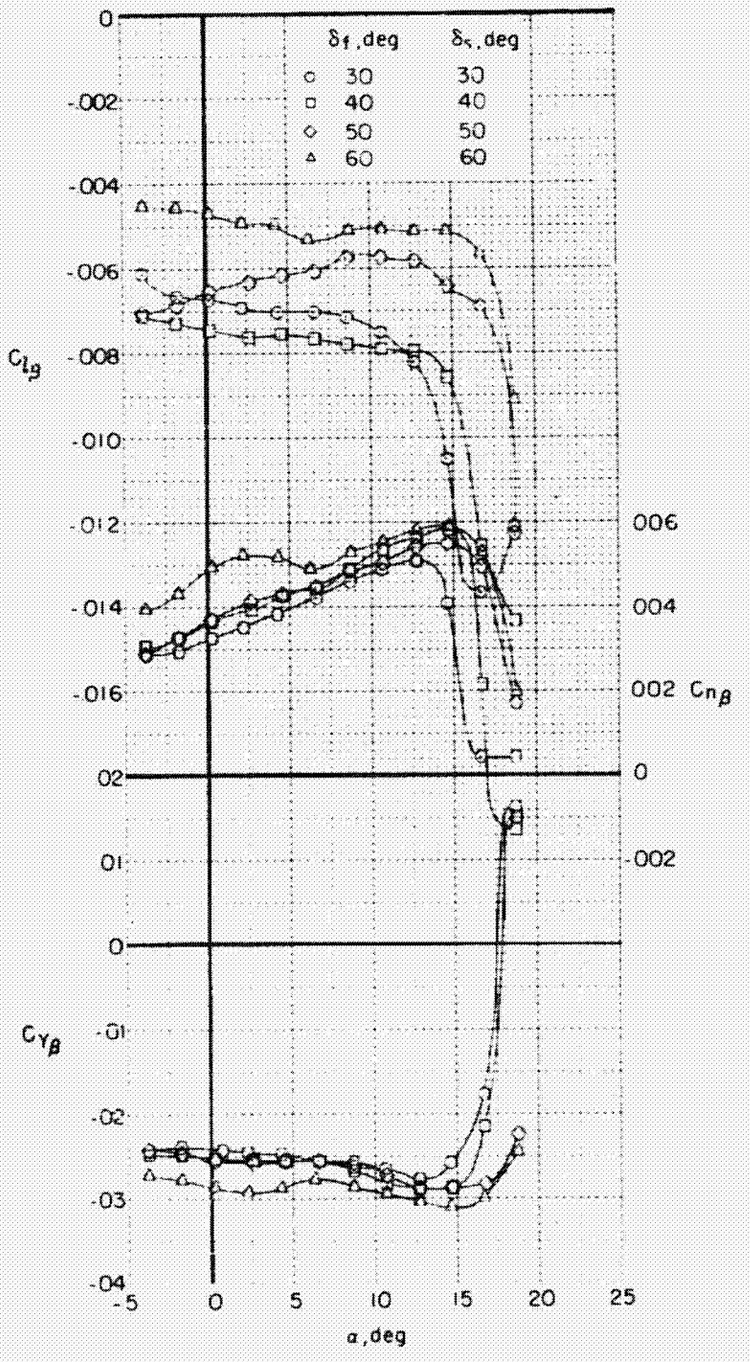

(b) $i_t = -10^o$.

Figure 23.- Concluded.

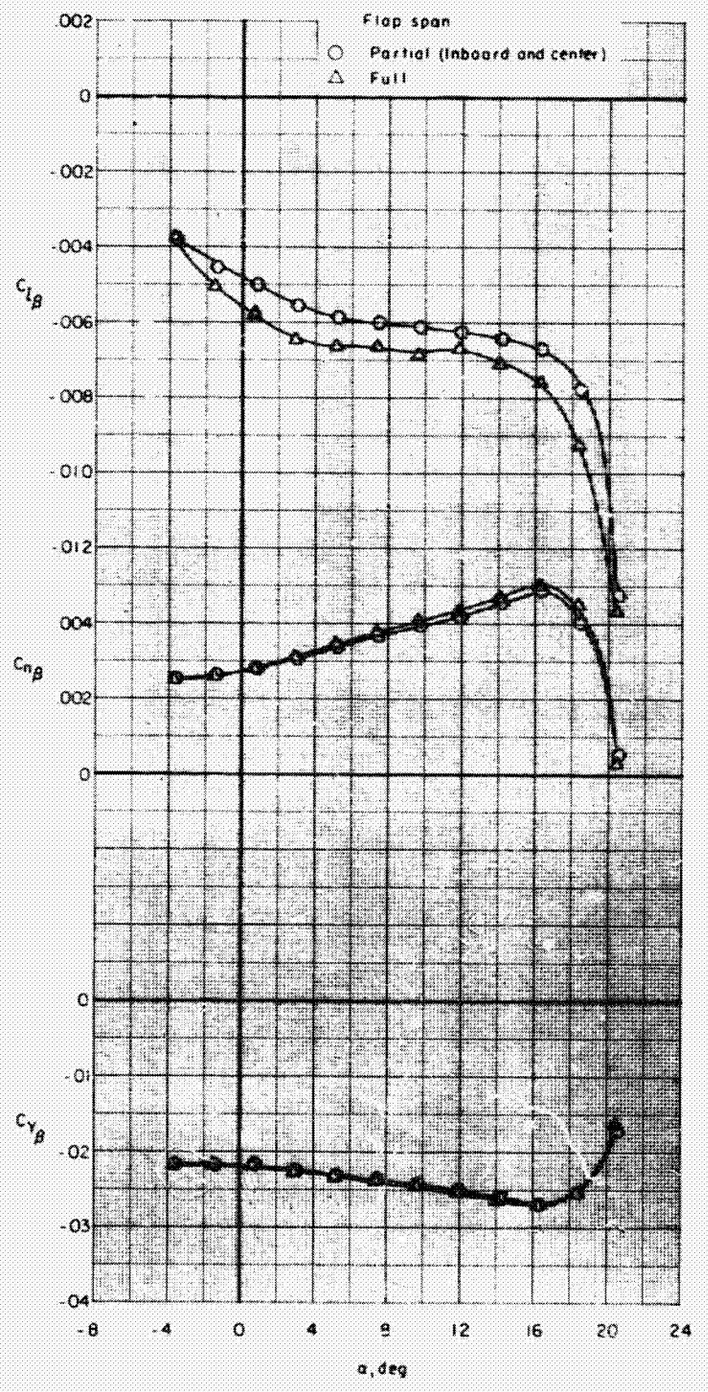

Figure 24.- Comparison of static-lateral stability derivatives for partial-span and full-span flap deflections for complete model configuration with $\delta_f = 20^o$ and $\delta_s = 40^o$, $i_t = -10^o$.

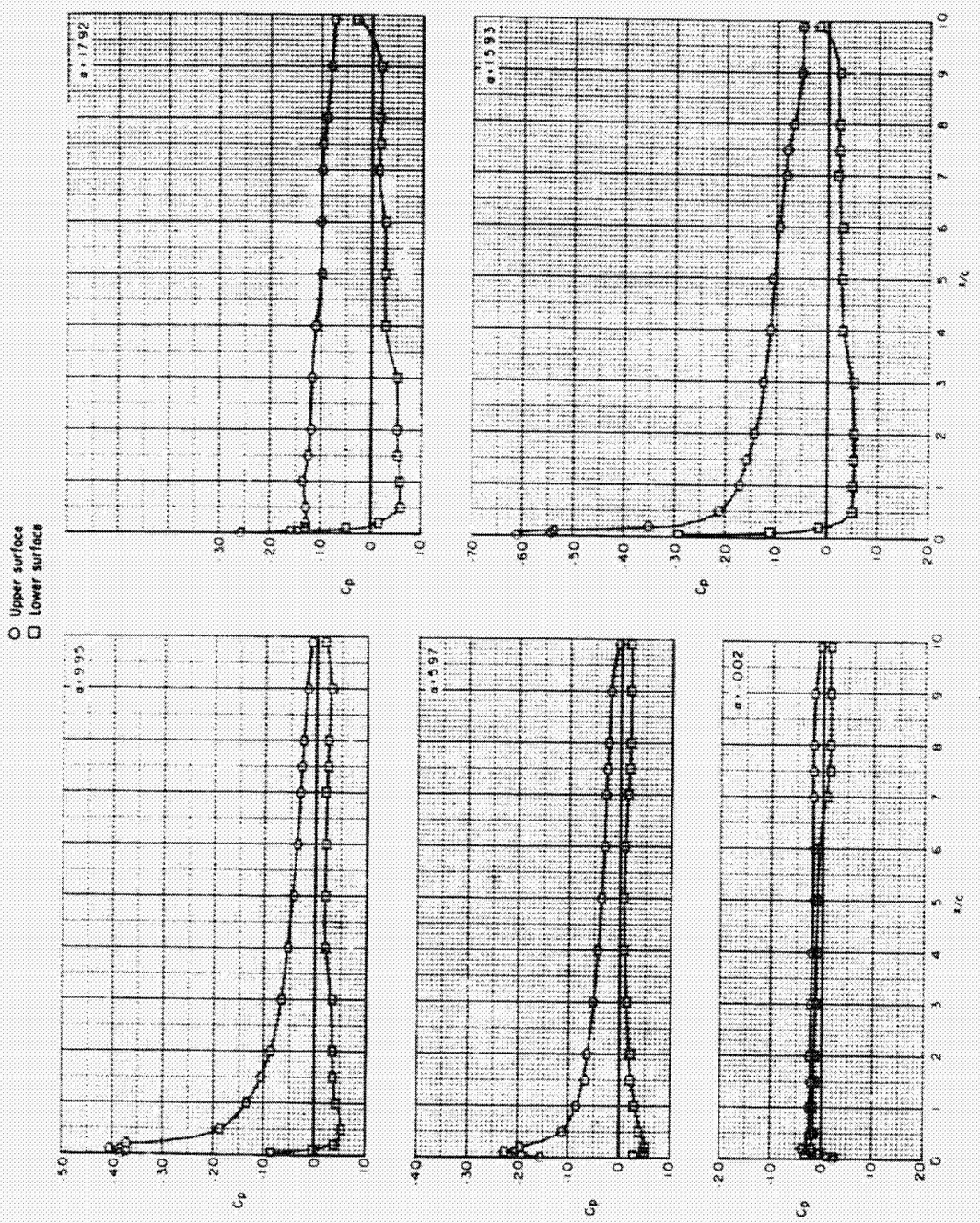

(a) Plain wing.

Figure 25.- Typical chordwise pressure distributions for plain wing and 40° deflected partial-span flap deflection (inboard and center) with various leading-edge slat deflections.

(b) Slat off.

Figure 25.- Continued.

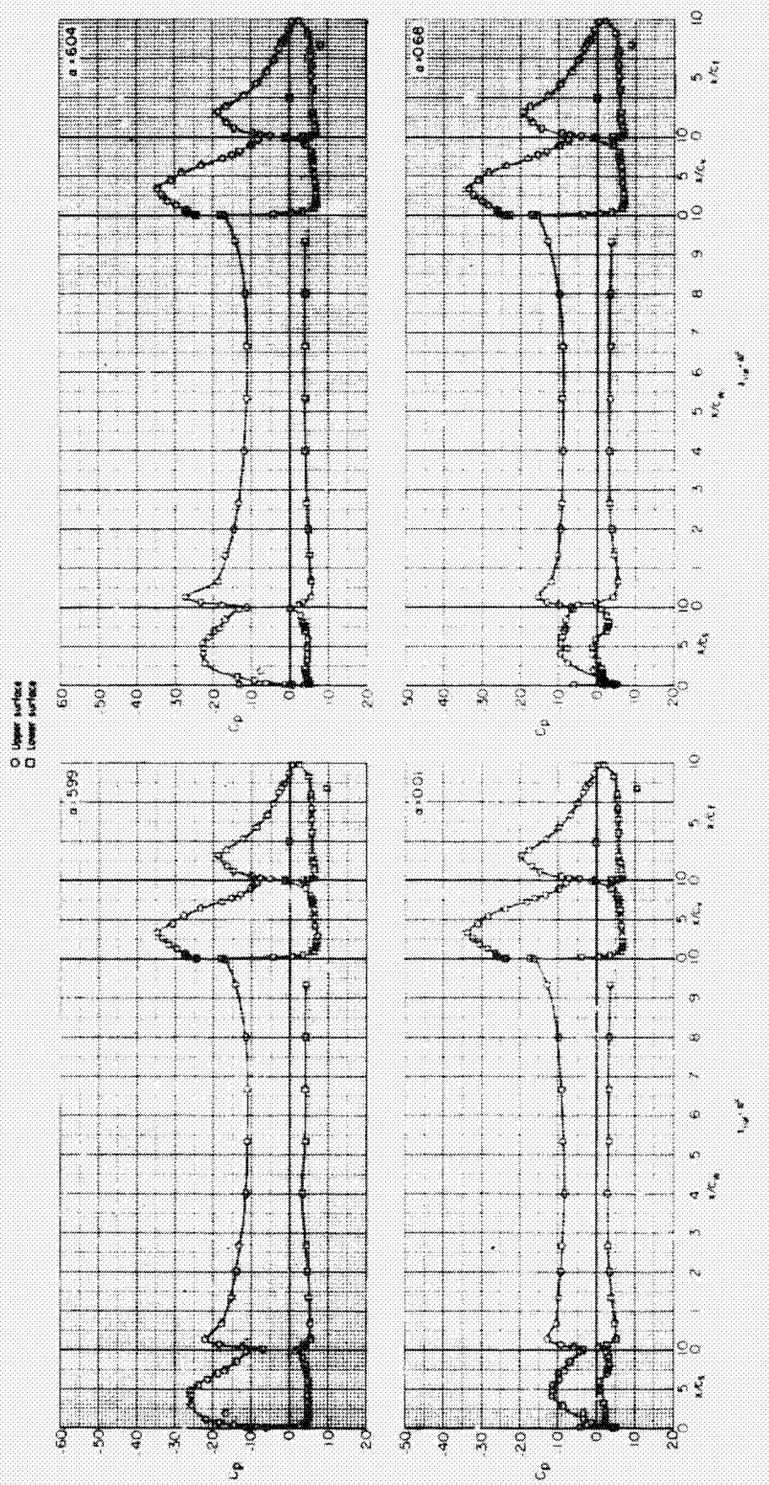

(c) Slat on.

Figure 25.- Continued.

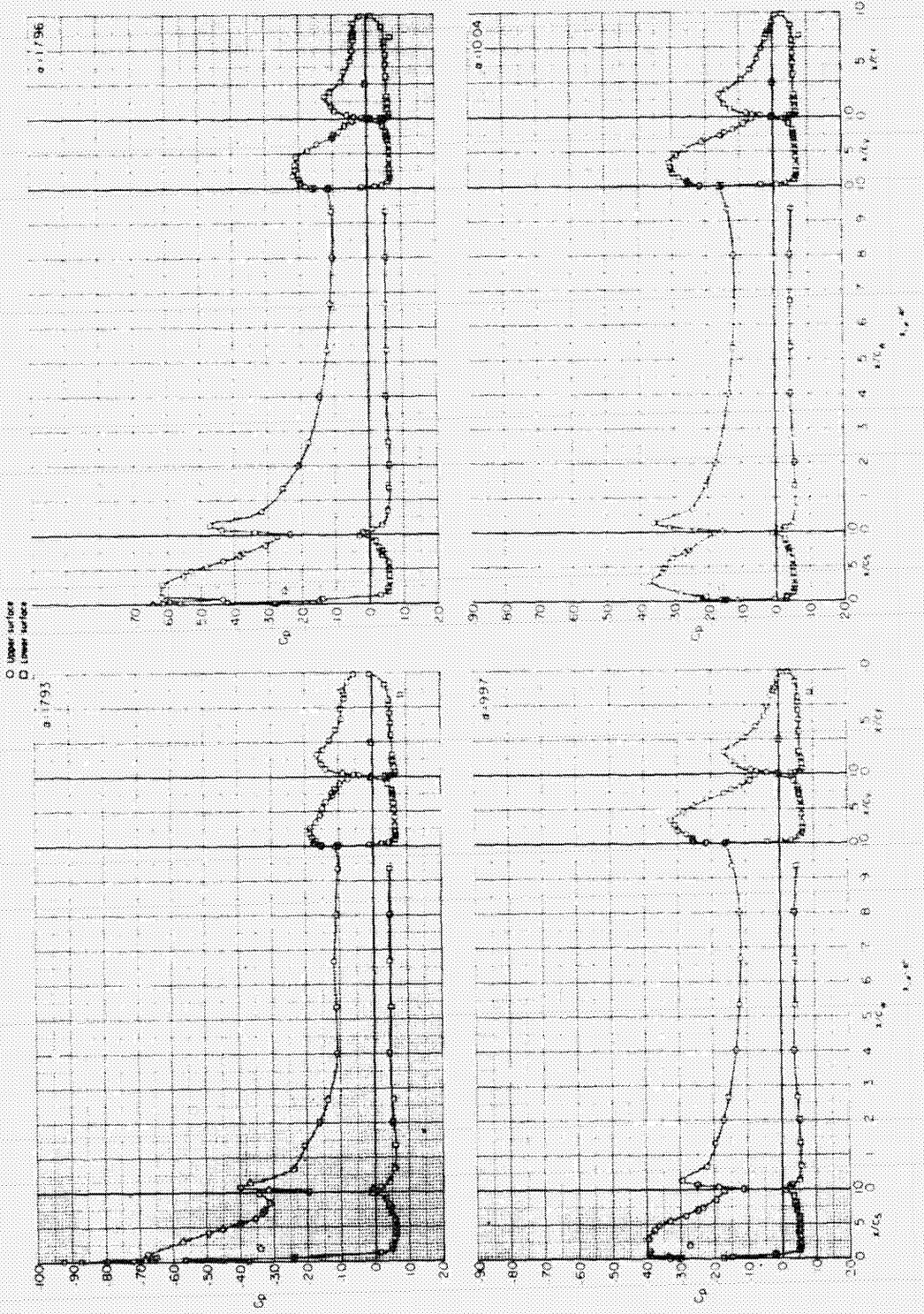

(c) Concluded.

Figure 25. - Continued.

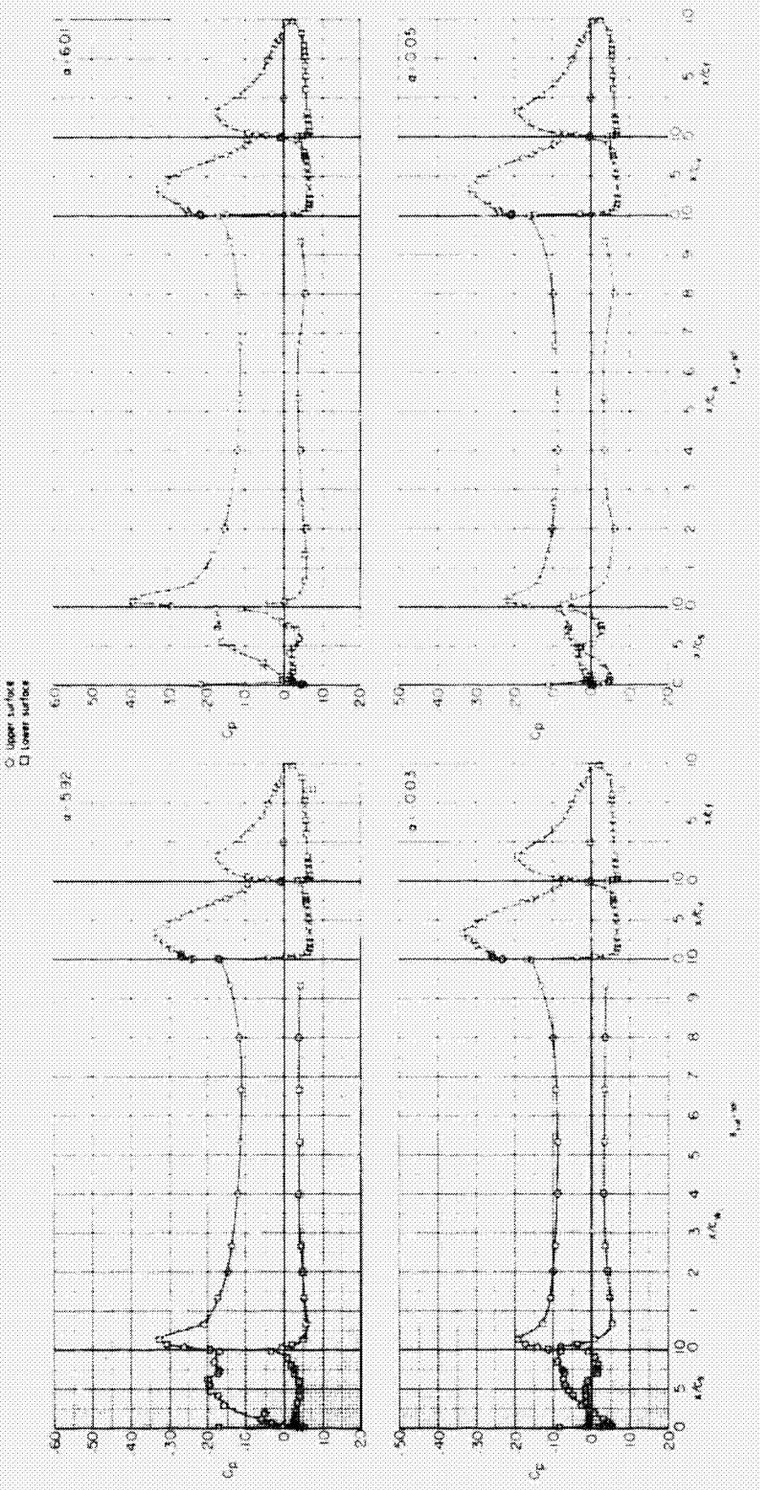

(d) Slat on.

Figure 25.- Continued.

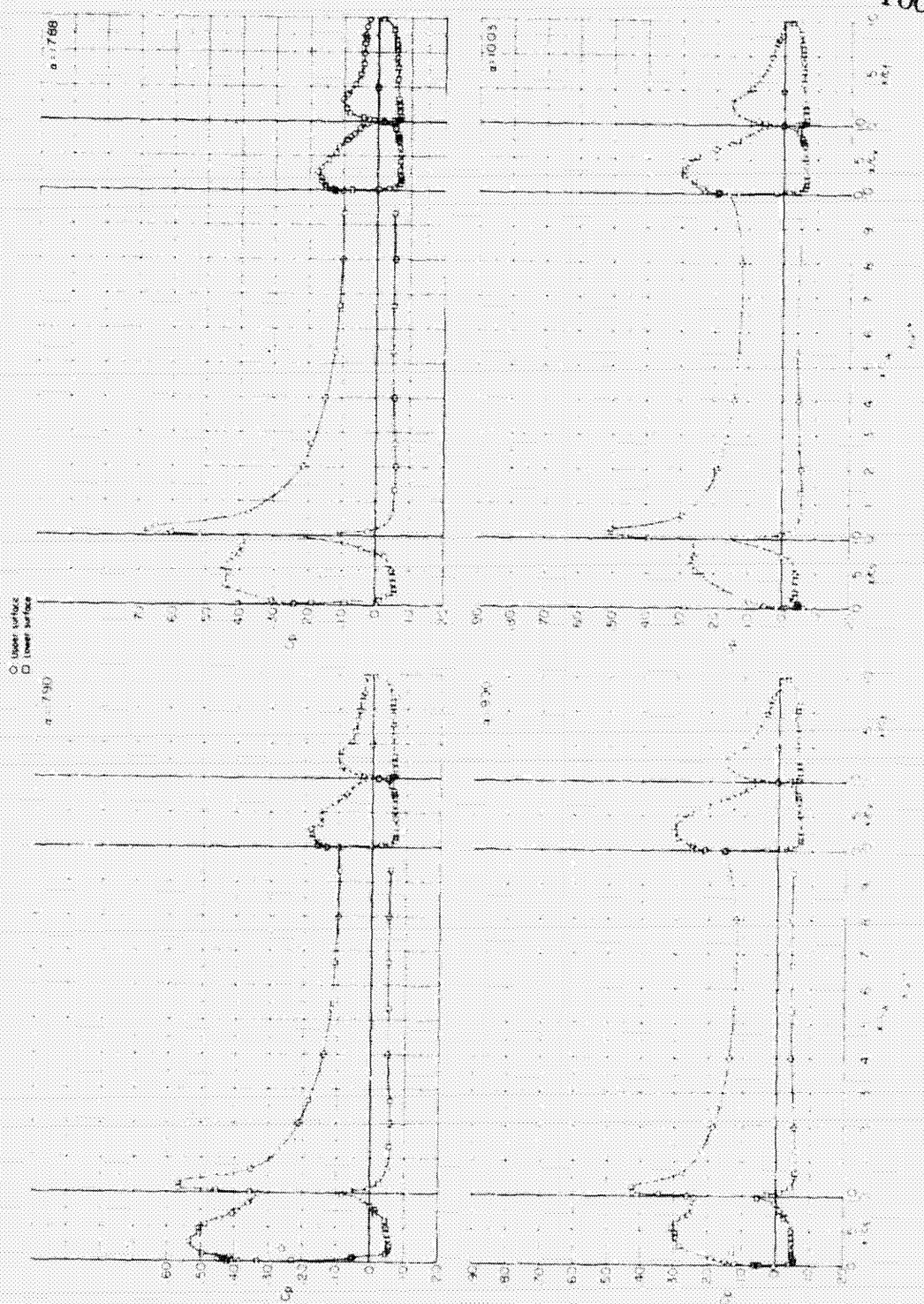

(d) Concluded.

Figure 25.- Concluded.